

**THE EFFECT OF HIP JOINT PATHOLOGY
(DYSPLASIA OF THE HIP AND
FEMOROACETABULAR IMPINGEMENT) ON THE
SPHERICITY OF THE JOINT**

A thesis submitted to the University of Manchester for the
degree of Master of Philosophy in the Faculty of Science and
Engineering.

2017

Reynol Alejandro Díaz López

School of Materials

Contents

1	Introduction	22
1.1	Overview	22
1.2	Research background	23
1.3	Objectives and methodology	24
1.3.1	Design of study diagram	25
2	Anatomy and Biomechanics of the Hip Joint	27
2.1	Introduction	27
2.2	Hip Joint Anatomy	28
2.2.1	Acetabulum	28
2.2.2	Femur	29
2.2.3	Labrum and hip joint capsule	31
2.2.4	Hip joint ligaments	32
2.2.5	Muscles	33
2.3	Bone tissue	34
2.3.1	Cortical bone	35

2.3.2	Trabecular bone	36
2.3.3	Mechanical behaviour of bone tissue	37
2.3.4	Bone Material Properties	38
2.4	Articular Cartilage	39
2.4.1	Mechanical behaviour of articular cartilage	40
2.4.2	Material properties of articular cartilage	40
2.5	Ligaments	41
2.5.1	Mechanical behaviour of ligaments	41
2.5.2	Material properties of ligaments	42
2.6	Biomechanics of the hip	42
2.6.1	Anatomical planes of the human body	42
2.6.2	Hip joint movements	44
3	Pathologies: Developmental Dysplasia of the Hip (DDH) and Femoroacetabular Impingement (FAI)	47
3.1	Introduction	47
3.2	Dysplasia of the Hip	48
3.2.1	Aetiology	48
3.2.2	Diagnosis and Symptoms	49
3.2.3	Treatment	56
3.3	Femoroacetabular Impingement	57
3.3.1	Aetiology	58
3.3.2	Pathology	58

3.3.3	Types of Impingement	58
3.3.4	Diagnosis and Symptoms	61
3.3.5	Physical Evaluation	62
3.3.6	Imaging assessment	63
3.3.7	Treatment	65
3.4	Sphericity	66
4	Development of the Finite Element models	70
4.1	Introduction	70
4.2	Modelling	71
4.2.1	3D models	71
4.2.2	Finite element models	75
4.2.3	Material properties	77
4.2.4	Loading conditions	78
4.2.5	Boundary and contact conditions	79
4.2.6	Mesh analysis	80
4.3	Model validation	82
5	Sphericity analysis normal hip joint group	84
5.1	Introduction	84
5.2	Computer models development	85
5.3	“Sphericity” quantification of the acetabulum and femoral head	85
5.3.1	Articular surfaces	85

5.3.2	Method to create the “Ideal” Sphere of the acetabulum and femoral head	87
5.3.3	Sphericity percentage	89
5.3.4	Average normalised distance	90
5.4	Centre-Edge, Tönnis, acetabular and alpha angles	93
5.5	Results	94
5.5.1	Table of results	94
5.5.2	Anatomical angles	97
5.5.3	Sphericity percentage	98
5.5.4	Asphericity of the sections	100
5.5.5	Contact area and contact pressure	101
5.5.6	Discussion	105
6	Sphericity analysis on hips suffering of Developmental Dysplasia and Femoroacetabular impingement	107
6.1	Introduction	107
6.2	Computer models development, Sphericity and anatomical angles	108
6.3	Femoroacetabular Impingement: Results	108
6.3.1	Table of results	108
6.3.2	Anatomical Angles	111
6.3.3	Sphericity percentage	112
6.3.4	Asphericity of the sections	114
6.3.5	Contact area and contact pressure	116

6.3.6	Discussion	122
6.4	Developmental Dysplasia of the Hip: Results	123
6.4.1	Table of results	123
6.4.2	Anatomical Angles	126
6.4.3	Sphericity percentage	127
6.4.4	Asphericity of the sections	129
6.4.5	Contact area and contact pressure	130
6.4.6	Discussion	135
7	Conclusions	137
7.1	Conclusions: Normal hip joints	137
7.2	Conclusions: Hips joints with cam-type Impingement	137
7.3	Conclusions: Dysplastic hip joints	138
7.4	Overall	138
7.5	Limitations	139
7.6	Future work	140

Number of words: 20,112

List of Figures

1.1	Flow chart of activities and analysis performed in this investigation.	26
2.1	Hip joint.	28
2.2	Lateral view of the pelvis bone (Modified)[20].	29
2.3	Femur	30
2.4	Structure of the thigh bone.	31
2.5	Proximal femur structure	32
2.6	Ligaments of the hip joint.	33
2.7	Structure of the bone (Modified)[9].	35
2.8	Osteon unit(Modified)[9].	36
2.9	Trabecular system of a normal hip joint.	36
2.10	Stress-strain curve of bone(Modified) [28]	39
2.11	Articular cartilage structure(Modified) [9]	40
2.12	Ligament fibre structure.	41
2.13	Human anatomical planes.	43
2.14	Flexion/extension movements. (Modified) [34]	44
2.15	Abduction/adduction movements. (Modified) [34]	45

2.16	Internal/External rotation movements. (Modified) [34]	46
3.1	Anterior-posterior radiograph of a patient suffering DDH. In this case, the left hip is affected and presents a deficient acetabular coverage of the femoral head.	48
3.2	Central-Edge (CE) angle. The location of the centre of the femoral head was define with the intersection of two perpendicular diameters of a circle fitted into the femoral head [53].	52
3.3	Vertical centre anterior (VCA) angle. a)Radiographic false profile view technique. b)VCA radiograph. c) The anterior centre edge angle (Modified) [41, 54]	53
3.4	Acetabular roof angle (Tönnis angle).	53
3.5	Acetabular angle (Sharp angle).	54
3.6	Computed tomography (CT) scan of the right hip of a patient suffering DDH. a)Transversal plane. b) Coronal plane.	54
3.7	Magnetic resonance imaging (MRI), in this image the left hip of a 57 year old female patient with mild displasya is shown. a) Coronal plane. b) Sagittal plane. Black arrows show cartilage yielding. [55].	55
3.8	Abnormal growth in bone causing FAI. (a)Femoral head-neck junction. (b) Acetabular rim.	57
3.9	Abnormal growth in bone causing FAI. (a)Normal. (b)Cam. (c)Pincer. (d)Mixer	59
3.10	Cam-type femoroacetabular impingement.	61
3.11	Cam-type femoroacetabular impingement.	61
3.12	FABER test. Left picture negative test. Right picture presents a positive test with increased distance between the exam table and knee.(Modified)[74]	63

3.13	Radiographic assessment of FAI. a)Cam-type b)Pincer-type.	64
3.14	Alpha angle on AP radiograph.	65
3.15	Radiographic assessment of FAI. a)Cam-type b)Pincer-type.	65
3.16	Distribution of Gaussian (a) and mean(b) curvatures on the acetabular cartilage surface. [6]	68
4.1	3D visualization of Normal patient 1 right hip based on DICOM image format.	71
4.2	ScanIP [®] work area. a)Segmentation tools and filters window. b)Mask list window. c)CT scan slides window. d)Mask visualization tools window. e) Transverse view window. f)Sagittal view window. g)Coronal view window. h)Fast preview window	73
4.3	ScanIP [®] threshold window. ScanIP [®] allows you to manipulate lower and upper values of the threshold. Also, it gives the option to update the visualization of the mask in real time.	73
4.4	Surface smoothing process	74
4.5	Different mask sizes of cortical bone to create trabecular bone and cartilage in ScanIP [®]	75
4.6	Boolean operation to create the cartilage geometry on Abaqus/CAE [®]	76
4.7	Boolean operation to create the cortical geometry on Abaqus/CAE [®]	76
4.8	Selection of inner edges on the bottom of femur to create a new cell. a)Edges of the hollow at the bottom of the femur part selected. b)New face created. c)Edges to create a new cell selected.	77
4.9	Bergmann's coordinate system and angles of the components.	79
4.10	Boundary conditions in the coronal plane. The green arrow on the local coordinate system shows the axis where the pelvis is allowed to move. . . .	80

4.11 (a) Meshed geometry using tetrahedral elements. (b) Tetrahedral element configuration.	81
4.12 Different mesh sizes of the femoral head cartilage.	82
5.1 Proximal femur structure and epiphyseal line. (a) Proximal femur structure and its name. (b) Concave section formed by the epiphyseal line, arrows show the starting point of the articular surface. (c) Femoral head cartilage surface partition.	86
5.2 Definition of the acetabular articular surface.	87
5.3 Visual representation of the distance of a node to the centre of the “Ideal” sphere.	89
5.4 Femoral head orientation on the: (a) transversal plane and (b) coronal plane.	91
5.5 Surface sections of the: (a) Acetabulum and (b) Femoral head	91
5.6 Surface sections of the: (a) Acetabulum and (b) Femoral head	92
5.7 Position of the node and sign asphericity	93
5.8 Table of results from subjects N1, N2, N3, and N4	95
5.9 Table of results from subjects N5, N6, N7, and N8	96
5.10 Table of results from subjects N9 and N10	97
5.11 Asphericity visualisation of subject N2. (a) Asphericity pattern of the femoral head (b) Asphericity pattern of the acetabulum (c) Asphericity range of the subject.	99
5.12 Contact pressure distribution of subject N2. (a) Sagittal view of the contact pressure pattern on the femoral head. (b) Sagittal view of the contact pressure pattern on the acetabulum.	102
5.13 (a) Asphericity of the sections on subject N3. (b) Contact pressure distribution on subject N3.	103

5.14 (a) Asphericity of the sections on subject N3 femoral head and acetabulum.	
(b) Contact pressure distribution on subject N3 acetabulum.	104
5.15 (a) Asphericity of the sections on subject N3 acetabulum and femoral head.	
(b) Contact pressure distribution on subject N3 acetabulum.	105
6.1 Table of results from subjects FAI1, FAI2, FAI3, and FAI4	109
6.2 Table of results from subjects FAI5, FAI6, FAI7, and FAI8	110
6.3 Table of results from subjects FAI9 and FAI10	111
6.4 Asphericity visualisation of subject FAI5. (a) Asphericity pattern of the femoral head (b) Asphericity pattern of the acetabulum (c) Asphericity range of the subject.	114
6.5 Contact pressure distribution of subject FAI5. (a) Sagittal view of the contact pressure pattern on the femoral head. (b) Sagittal view of the contact pressure pattern on the acetabulum.	117
6.6 (a) Asphericity of the sections on subject FAI1 femoral head and acetabulum.	
(b) Contact pressure distribution on subject FAI1 acetabulum.	118
6.7 (a) Asphericity of the sections on subject FAI4 femoral head and acetabulum.	
(b) Contact pressure distribution on subject FAI4 acetabulum.	119
6.8 (a) Asphericity of the sections on subject FAI9 femoral head and acetabulum.	
(b) Contact pressure distribution on subject FAI9 acetabulum.	120
6.9 (a) Asphericity of the sections on subject FAI6 femoral head and acetabulum.	
(b) Contact pressure distribution on subject FAI6 acetabulum.	121
6.10 Posterior asphericity on the acetabular rim of subject FAI2.	121
6.11 (a) Asphericity of the sections on subject FAI3 femoral head and acetabulum.	
(b) Contact pressure distribution on subject FAI3 acetabulum.	122
6.12 Table of results from subjects DDH1, DDH2, DDH3, and DDH4	124

6.13	Table of results from subjects DDH5, DDH6, DDH7, and DDH8	125
6.14	Table of results from subjects DDH9 and DDH10	126
6.15	Asphericity visualisation of subject DDH1. (a) Asphericity pattern of the femoral head (b) Asphericity pattern of the acetabulum (c) Asphericity range of the subject.	128
6.16	Contact pressure distribution of subject DDH1. (a) Sagittal view of the contact pressure pattern on the femoral head. (b) Sagittal view of the contact pressure pattern on the acetabulum.	132
6.17	(a) Asphericity of the sections on subject DDH1 femoral head and acetabulum. (b) Contact pressure distribution on subject N3 acetabulum. .	133
6.18	(a) Asphericity of the sections on subject DDH6 femoral head and acetabulum. (b) Contact pressure distribution on subject N3 acetabulum. .	134
6.19	(a) Asphericity of the sections on subject DDH8 femoral head and acetabulum. (b) Contact pressure distribution on subject N3 acetabulum. .	135

List of Tables

4.1	Young’s modulus, poisson’s ratio of cartilage, cortical and trabecular bone.	78
4.2	Table of mesh densities and their perspective number of elements, contact area and maximum contact pressures	82
5.1	“Asphericity” sign of the femoral head and acetabulum and the effect on surface distances.	93
5.2	Table of anatomical angles of the normal hip joint group	98
5.3	Table of overall surface “Sphericity” of the normal hip joint group.	99
5.4	Table of the sections asphericity signs of the acetabulum from the normal hip joint group.	100
5.5	Table of the sections asphericity values of the femoral head from the normal hip joint group.	101
5.6	Table of finite element analysis results of the normal hip joint group.	102
6.1	Table of anatomical angles of the FAI hip joint group	112
6.2	Table of overall surface “Sphericity” of the Femoroacetabular hip joint group.	113
6.3	Table of the sections asphericity values of the acetabulum from the femoroacetabular hip joint group.	115
6.4	Table of the sections asphericity values of the femoral head from the femoroacetabular hip joint group.	115

6.5	Table of finite element analysis results of the Femoroacetabular hip joint group.	116
6.6	Table of anatomical angles of the DDH hip joint group	127
6.7	Table of overall surface “Sphericity” of the normal hip joint group.	128
6.8	Table of the sections asphericity values of the acetabulum from the dysplastic hip joint group.	129
6.9	Table of the sections asphericity values of the femoral head from the dysplastic hip joint group.	130
6.10	Table of finite element analysis results of the normal hip joint group.	131

List of Abbreviations

3D Three-Dimensional.

AAC Anterior Acetabular Coverage.

AIT Anterior Interior Test.

AP Anterior-Posterior.

CE Centre-Edge.

CT Computed Tomography.

DDH Developmental Dysplasia of the Hip.

DDH1 Hip joint with DDH 1.

DDH10 Hip joint with DDH 10.

DDH2 Hip joint with DDH 2.

DDH3 Hip joint with DDH 3.

DDH4 Hip joint with DDH 4.

DDH5 Hip joint with DDH 5.

DDH6 Hip joint with DDH 6.

DDH7 Hip joint with DDH 7.

DDH8 Hip joint with DDH 8.

DDH9 Hip joint with DDH 9.

DICOM Digital Imaging and Communication in Medicine.

FABER Flexion-Abduction Test.

FAI Femoroacetabular Impingement.

FAI1 Hip joint with FAI 1.

FAI10 Hip joint with FAI 10.

FAI2 Hip joint with FAI 2.

FAI3 Hip joint with FAI 3.

FAI4 Hip joint with FAI 4.

FAI5 Hip joint with FAI 5.

FAI6 Hip joint with FAI 6.

FAI7 Hip joint with FAI 7.

FAI8 Hip joint with FAI 8.

FAI9 Hip joint with FAI 9.

FE Finite Element.

MRI Magnetic Resonance Imaging.

N1 Normal hip joint 1.

N10 Normal hip joint 10.

N2 Normal hip joint 2.

N3 Normal hip joint 3.

N4 Normal hip joint 4.

N5 Normal hip joint 5.

N6 Normal hip joint 6.

N7 Normal hip joint 7.

N8 Normal hip joint 8.

N9 Normal hip joint 9.

OA Osteoarthritis.

VCA Vertical-Centre-Anterior.

Nomenclature

$ASph_s$ Asphericity of the articular surface section.

E Young's modulus.

Sph Percentage of Sphericity.

\overline{AP} Vector from Point A to Point P.

ν Poisson's Ratio.

$^\circ$ Degrees.

d_i Distance of the node to the centre of the ideal sphere.

n Number of nodes.

n_T Total number of nodes in the surface.

n_s Number of nodes in the section.

r Radius of the sphere.

cm Centimeters.

mm Millimeters.

MPa Megapascal (10^6 Pascals).

N Newton.

Abstract

The shape of the hip joint components has a crucial role in the loading distribution and functionality of the hip joint. Hip joint pathologies commonly diagnosed on adults, such as femoroacetabular impingement (FAI) and developmental dysplasia of the hip (DDH) are characterized by abnormalities in the morphology of the pelvic or/and femoral bone. Surgical procedures focus on restoring the mobility or slowing the degenerative process of cartilage damage by reorienting the acetabulum or removing abnormalities from the acetabulum and/or the femur. However, in a number of cases damage appears in a different location or symptoms do not disappear. This suggests that the shape of the articular surfaces of the hip joint is affected by the hip joint pathologies.

To investigate this, anatomical angles of the hip joint were measured, finite element models were constructed, and a sphericity analysis of the femoral head and acetabulum surface was performed on thirty hip joints, 10 with cam-type impingement, 10 with DDH and 10 normal hips. Radiographic parameters were taken from CT scan data, finite element models were used to obtain hip joint contact areas and contact pressures from a one-leg-standing loading condition, and, regarding sphericity, acetabulum and femoral head surface sphericity was assessed using quantitative and visualization methods.

It was found that the femoral head was more spherical than the acetabulum in all subjects. However, the sphericity percentage of the acetabulum and femoral head from the DDH and FAI group was lower than the normal hip joint group. Furthermore, DDH and FAI group had similar values on the sphericity of the acetabulum and femoral head. We believe that the abnormal morphology of the pelvic bone and femur found in DDH and FAI subjects affects the shape of the hips, and this leads to damage on the articular surface or acetabular rim.

Declaration

No portion of the work referred to in the thesis has been submitted in support of an application for another degree or qualification of this or any other university or other institute of learning.

Copyright

1. The author of this thesis (including any appendices and/or schedules to this thesis) owns certain copyright or related rights in it (the “Copyright”) and he has given The University of Manchester certain rights to use such Copyright, including for administrative purposes.
2. Copies of this thesis, either in full or in extracts and whether in hard or electronic copy, may be made only in accordance with the Copyright, Designs and Patents Act 1988 (as amended) and regulations issued under it or, where appropriate, in accordance with licensing agreements which the University has from time to time. This page must form part of any such copies made.
3. The ownership of certain Copyright, patents, designs, trade marks and other intellectual property (the “Intellectual Property”) and any reproductions of copyright works in the thesis, for example graphs and tables (“Reproductions”), which may be described in this the sis, may not be owned by the author and may be owned by third parties. Such Intellectual Property and Reproductions cannot and must not be made available for use without the prior written permission of the owner(s) of the relevant Intellectual Property and/or Reproductions.
4. Further information on the conditions under which disclosure, publication and commercialisation of this thesis, the Copyright and any Intellectual Property University IP Policy (see <http://documents.manchester.ac.uk/display.aspx?DocID=24420>), in any relevant Thesis restriction declarations deposited in the University Library, The University Library’s regulations (see <http://www.library.manchester.ac.uk/about/regulations/>) and in The University’s policy on Presentation of Theses.

Acknowledgements

I want to express my greatest gratitude to my supervisors Professor Teresa Alonso and Professor Colin Bailey for their guidance, support and, particularly, their patience. Their experience was very helpful in the development of the research. Thank you for giving me the opportunity to be part of your team.

My deepest thanks to my advisor Dr Alan Walmsley for all his academic and personal support during my research. His encouragements and advices were always precise.

I would like to thank Prof Tim Board for his guidance and constructive comments.

My greatest gratitude to the Mexican National Council of Science and Technology (CONACyT) for the financial support provided for my postgraduate studies.

Many thanks to my family for their heart-warming support and unconditional love.

Thanks to all the great friends I met at the bioengineering department and friends I made during my studies. Thank you for your support and good times.

Chapter 1

Introduction

1.1 Overview

In human anatomy, a joint is the connection between two or more bones in the body that allows different types and range of movements. Joints can be classified depending on their function and structure. The hip joint is a synovial joint, this type of joints allow a large range of motion, are self-lubricating and can support heavy loadings.

There are several factors that can lead to the abnormal function of the joints, such as congenital deformities, abnormalities acquired by growth, extreme physical activities, and injuries. Other factors can be diseases, such as osteoporosis and osteopenia, which affect the bone mineral density.

In young adults, Femoroacetabular Impingement (FAI) and Developmental Dysplasia of the Hip (DDH) are the two most common diagnosed diseases that affect the hip joint, and if left unthreatened both can lead to early osteoarthritis. FAI occurs due to irregular morphology of the proximal femur and/or acetabulum, repetitive contact on this abnormalities by extremes of motion produces can cause damage to chondrolabral junction, leading to permanent degenerative changes. DDH is caused by an abnormal development of the femoral and acetabulum, the main characteristic of DDH is the undercoverage of the femoral head due to a shallow acetabulum or a mal-oriented acetabulum. Insufficient acetabular coverage is associated to small contact area between the acetabulum and femoral

head producing abnormal high contact pressures. It is believed that prolonged abnormal high pressures damages the articular surface of the hip joint.

To prevent complications related to these diseases, like osteoarthritis, or to avoid very invasive treatments, it is imperative to have an early diagnosis and appropriate treatment. Surgical treatments focus on restructuring the shape of the hip joint bones to allow the proper functioning of the joint, however symptoms develop again or a new lesion appears in a different location of the hip joint soft tissue. Moreover, surgeons do not take into account the topology of the articular area of the hip when planing the surgical intervention as they assume that removing/modifying the bone abnormality is the “cure” of pathomechanical diseases.

1.2 Research background

Despite the fact that it has been suggested from previous work that random “bumps” on the articular surfaces of the femoral head and acetabulum create high contact pressure [1], and that using a “Natural” shape rather than a spherical shape of the acetabulum and femoral head articular geometries give more realistic results when predicting contact stresses between the acetabulum and femoral head [2–4], the morphological structure of the hip joint articular components have been little investigated.

Sankar et al. [5] quantified the “Sphericity” of the femoral head in 37 hip joints from walking aged children suffering of DDH. Sankar et al. created a femoral head “Sphericity” score based on the largest difference between 4 radii measured from the centre of the femoral head to the edge. Gu et al.[6] created a method using reverse engineering, surface-fitting algorithms and curve surface theory to create a mathematical representation of the acetabular cartilage. Gu et al. concluded that the shape of the acetabular cartilage surface is a rotational ellipsoid, rather than a simple sphere.

1.3 Objectives and methodology

The aim of this research is to investigate the effect of pathological conditions (Dysplasia of the hip and femoroacetabular impingement) on the sphericity of the articular surfaces of the femoral head and acetabulum. To investigate this, the contact area and contact pressure of the hip joint during one-leg-standing was calculated using finite element models, and later related to landmarks to diagnose pathological hip joints, and finally it was related to the “Sphericity” of the hip joint articular components. The research project was undertaken in collaboration with Wrightington Hospital, UK. All patient information was provided by the hospital.

The following section presents the structure and content in this thesis: Chapter 2 describes the anatomical structure and function of the human hip joint. This chapter gives a description of the different structures and tissues that form the hip joint. Descriptions of bone and cartilage mechanical behaviour and material characteristics are also include. In addition, this chapter gives a description of anatomical planes and hip joint movements. The purpose of this chapter is to become familiar with medical terminology, anatomy and biomechanics regarding to the hip joint.

Chapter 3 presents the aetiology, diagnosis and treatments of two major pathologies presented on adults, Femoroacetabular Impingement and Dysplasia of the hip. In addition, a review of the latest and relevant research work regarding the effect of the femoral head and acetabular articular surfaces “Sphericity” on the biomechanics of the hip joints and its relationship with hip joint pathological conditions is presented. In this research the structural morphology of the articular surfaces of the femoral head and acetabulum is called “Sphericity”.

Chapter 4 describes the methodology used to create subject-specific geometries from Computed Tomography (CT) scans using ScanIP[®] and, the creation of assembly of the Finite Element model on Abaqus/CAE[®]. This chapter also describes mechanical properties, mesh properties, and loading, boundary and contact conditions defined to perform the finite element analysis. In addition, a description of the finite element models validation and mesh sensitivity analysis is presented.

Chapter 5, presents the procedure to assess the “Sphericity” on the femoral head and acetabulum surfaces, and describes the method to create a visualization of asphericity of the

femoral head and acetabulum surface. Additionally, this chapter describes typical characteristics of the normal hip joint group, by relating geometrical features, “Sphericity”, and the contact between the acetabulum and femoral head on normal hip joints.

Chapter 6, using the same methodology described on chapter 5, this chapter describes typical anthropometric, “Sphericity” and contact characteristics on subjects suffering of dysplasia of the hip and hips suffering from cam-type femoroacetabular impingement.

Chapter 7, presents the conclusions of the qualitative/quantitative analysis performed on the hip joint groups.

1.3.1 Design of study diagram

The flow chart in Figure 1.1 illustrates the sequence of activities and analysis performed in this investigation. 30 hips joints (10 normal, 10 dysplastic and 10 with cam-type impingement) were used for this analysis. X-rays and computer tomographies (CT) data were used to measure anatomical features of the pelvic bone and to build computer geometries of the hip joint. From frontal plane x-rays anatomical angles related to pathological conditions of the hip were measured. Computer models of the hip joints were used for “Sphericity” and finite element analysis. Results were analysed to obtain typical values from each hip joint group. Finally, representative characteristics of each group were compared and conclusions were obtained.

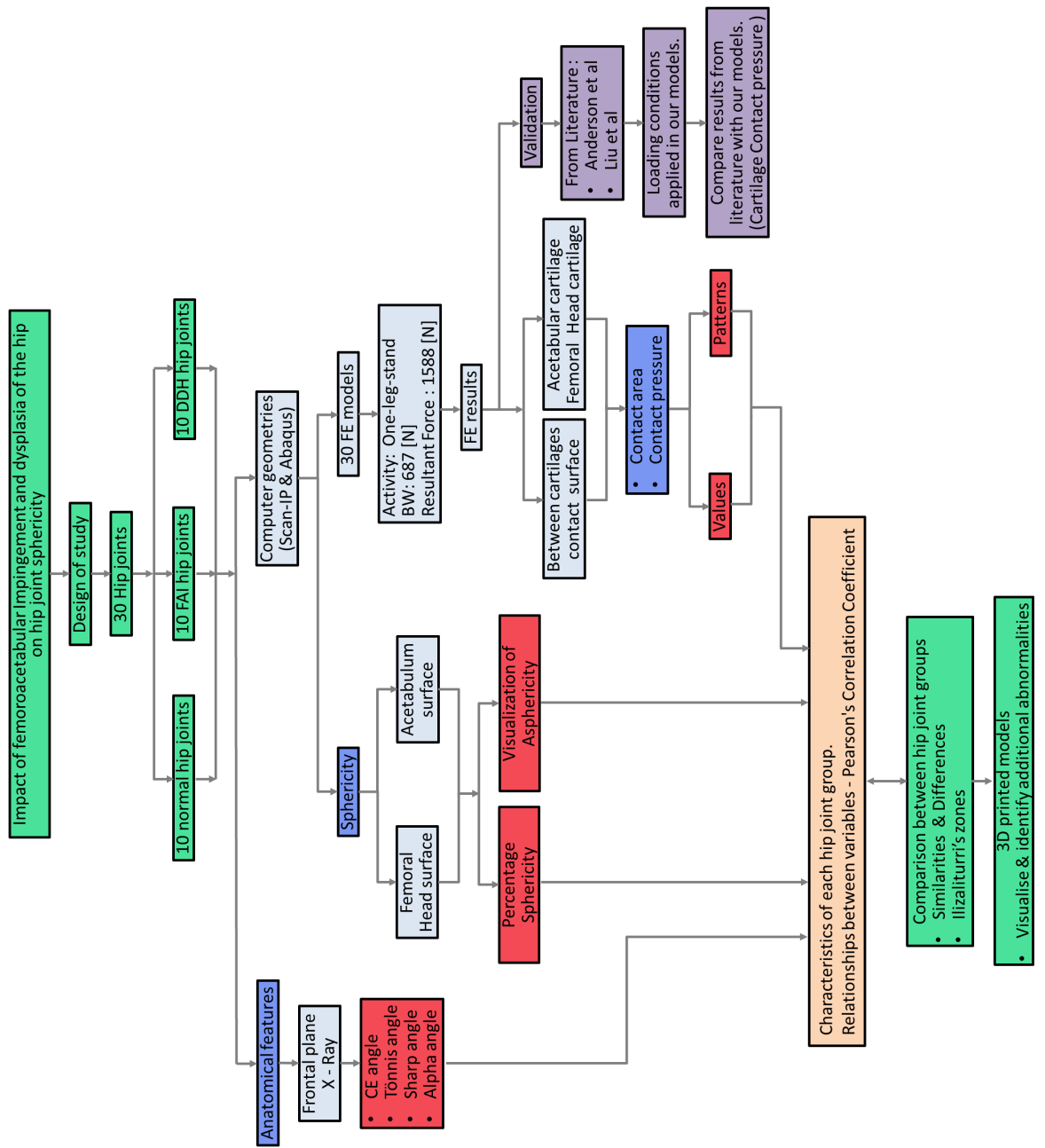


Figure 1.1: Flow chart of activities and analysis performed in this investigation.

Chapter 2

Anatomy and Biomechanics of the Hip Joint

This chapter describes the anatomy, structure and function of the hip joint with purpose of providing the medical terminology and bio mechanics of the hip joint related to this investigation. Also, a description of the mechanical behaviour and mechanical characteristics of bone and cartilage is included.

2.1 Introduction

The human body is the physical structure and material substance of a human being. The musculoskeletal system is the organ that gives the human body the ability to perform different motions throughout our daily activities. That is, the purpose of the skeletal system is to provide weight bearing support, protect internal organs and facilitate muscle action. The skeletal system is composed by bones, cartilage and ligaments and it accounts approximately 20% of body mass.[7–12]

The hip joint, also known as coxo-femoral joint, is the largest and most stable joint in the body. It allows the movement and force transmission between the torso and the lower extremities. Therefore, it is indispensable for weight transmission of the body during human motion. Ligaments and muscles in the joint help to support body weight and provides the hip joint different movements such as walking and running. Alterations to the hip can produce

abnormal stress distribution in the hip joint cartilage and bone leading to cartilage damage and arthritis. [10, 12–14]

2.2 Hip Joint Anatomy

The hip joint is formed by the head of the femur and the cupped acetabulum of the pelvis as illustrated in Figure 2.1. It is located lateral and anterior to the gluteal regions, and also it is strengthened by the acetabular labrum, muscles and the joint capsule, which contains lubricating synovial fluid. [9, 11, 15–18]

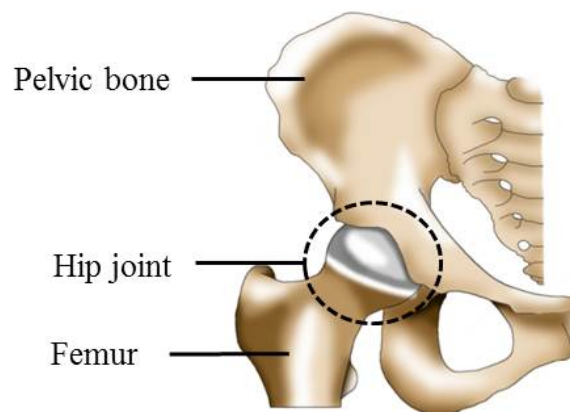


Figure 2.1: Hip joint.

The hip joint has a ball-and-socket configuration. The acetabulum being the concave surface of the configuration, deepened by the acetabular labrum and the femoral head as the convex surface forming two-thirds of a sphere.[17–19]

2.2.1 Acetabulum

The acetabulum is the cup-shaped portion of the ball-and-socket hip joint structure, located on the lateral outer surface of the pelvis. It is formed from the fusion of the ilium, ischium and pubis bones angling in the anterolateral direction as Figure 2.2 shows.[9, 10]

The acetabular cavity is covered with articular cartilage that is thicker at the edge and thickest at the top part. It faces diagonally forward, outward and downward. [10]

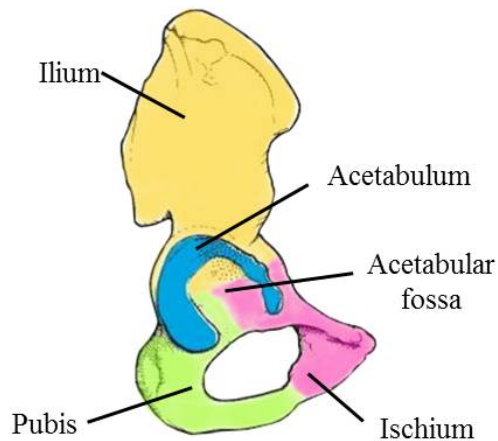


Figure 2.2: Lateral view of the pelvis bone (Modified)[20].

The acetabulum has a smaller diameter than the femoral head when the hip joint is not loaded. The acetabular cavity deforms about the femoral head when the hip joint is subjected to a load. [9, 10, 19]

A malaligned acetabulum does not cover the femoral head properly, commonly causing dislocation and osteoarthritis. Geometrical parameters, such as centre-edge angle and acetabular ante version angle, are used to describe how much coverage the acetabulum provides to the femoral head. The centre edge angle measures the extent to which the acetabulum covers the femoral head in the frontal plane, while the acetabular ante version denotes how much the acetabulum surrounds the femoral head within the horizontal plane.[10, 18, 21]

2.2.2 Femur

The Femur, or thighbone, is the closest bone to the centre of the body of the lower limb. It is the largest, heaviest and strongest bone in the human body. The femur bone transmits the body weight from the pelvis to the upper end of the tibia. It posses a long shaft and two expanded extremities.

The proximal part of the femur articulates with the pelvis throughout the acetabulum and it consists of the femoral head, fovea capitis, femoral neck and a greater and lesser trochanter. Furthermore, the trochanters server as site for muscle attachment and assists

with the abduction movement of the hip. Figure 2.3 illustrates the proximal femur anatomy. [10, 17]

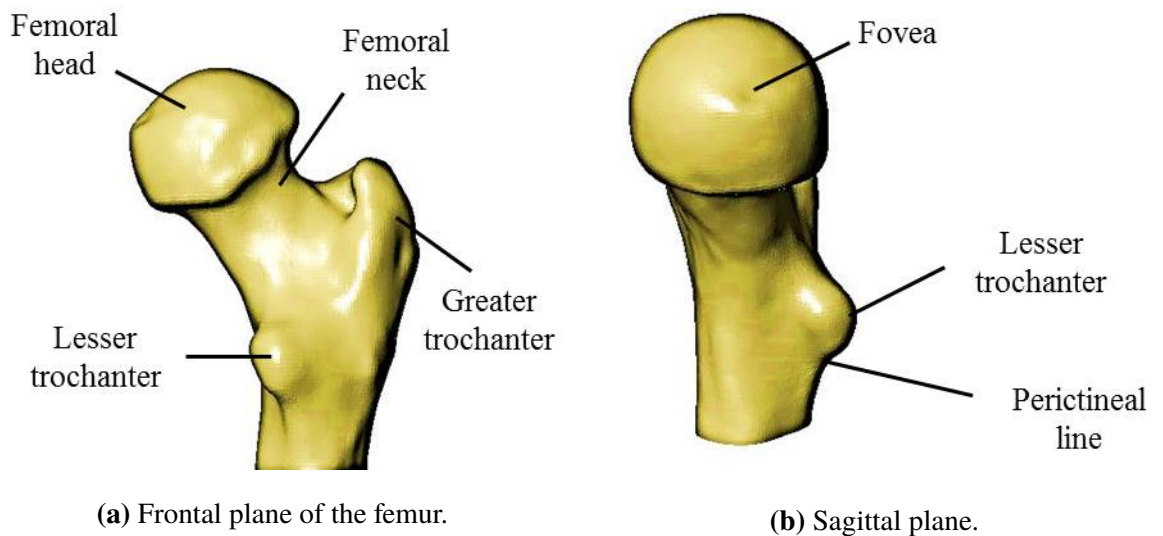


Figure 2.3: Femur

Long bones of the human have their own descriptive terminology. The femur can be divided into diaphysis, metaphysis, and epiphysis. On the proximal femur, the metaphysis consists of the trochanters, femoral neck and the body, and the proximal epiphysis is composed only by the femoral head. [12]

During childhood, between the diaphysis and epiphysis, there is an epiphyseal plate of cartilage which is replaced by an epiphyseal line when bone growth is completed on adulthood. Figure 2.4 illustrates the structure of the femur.[12]

Femoral Head

The femoral head is the ball component of the ball-and-socket configuration of the hip joint. It faces upwards, medially and forwards. The articular surface is covered by hyaline cartilage except for a pit presented in the lower centre, called fovea capitis. It is thickest on the medial-central surface surrounding the fovea, where the ligament teres attaches, and thinnest toward the edge of the head. In a normal hip joint, the centre of the femoral head coincided with the centre of the acetabulum.[10, 12, 19]

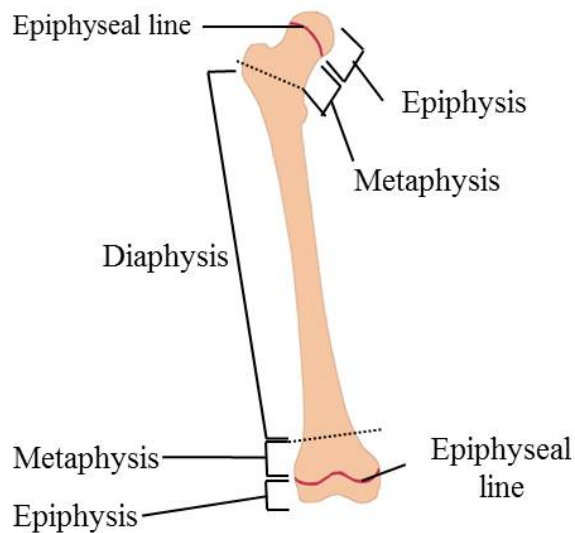


Figure 2.4: Structure of the thigh bone.

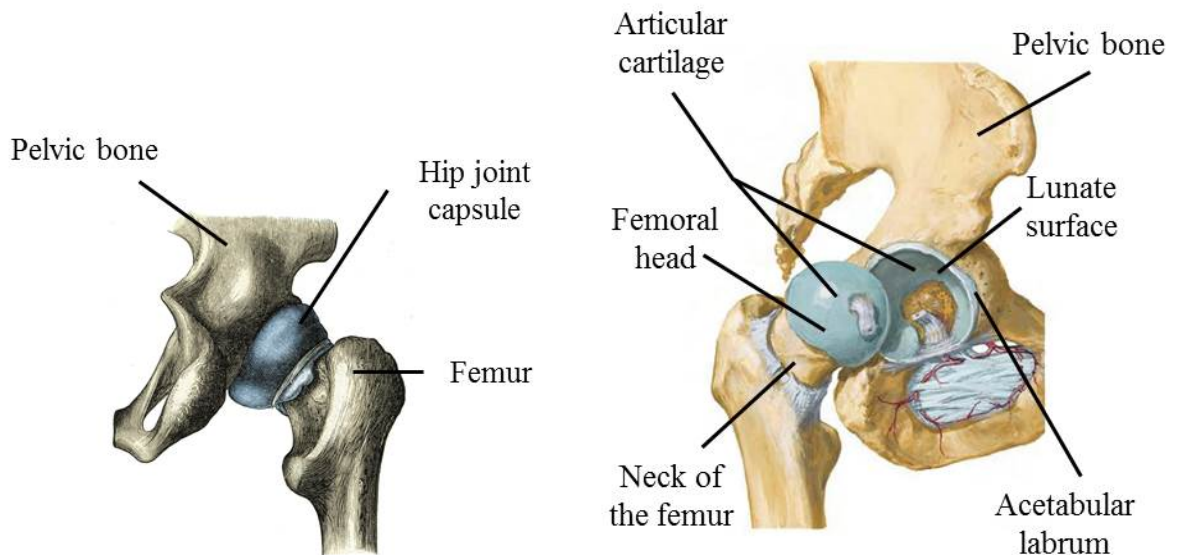
Femoral Neck

The femoral neck connects the femoral head to the shaft and it is approximately 5cm long. In healthy patients, it forms a 125° angle with the shaft, this angle helps to maintain a congruent articulation within the hip joint and to keep away the femur from the body. The femoral neck is, on its posterior surface wide, concave and smooth, while tight and curved in the anterior surface. [10, 17, 19]

The angular relationship between the femoral neck and the femoral shaft plays an essential role in the proper function of the hip joint. Abnormal angles shift the alignment between the acetabulum and the femoral head, altering the hip movements and the impact forces applied to the joint by the upper body. [19, 21]

2.2.3 Labrum and hip joint capsule

The acetabular labrum is a fibrocartilaginous lip that encircles and deepens the acetabulum. The acetabular labrum itself is essential for the proper functions of the hip joint, it prevents the femoral head to dislocate in extremes of motion and is thought to act as a seal to prevent loss of interstitial fluid. Figure 2.5a illustrates the lateral view of the hip joint opened exposing the acetabular labrum.[10, 19]



(a) Hip joint capsule (Modified)[15]

(b) Lateral view of the hip joint opened (Modified)[22]

Figure 2.5: Proximal femur structure

The hip joint is surrounded by the hip capsule which is an important stabiliser of the joint. It attaches directly to the perimeter of the acetabulum, above the acetabular labrum. The capsule is made up of longitudinal and circular fibres. Circular fibres form a collar surrounding the femoral neck, while the longitudinal fibres travel along the neck and carry blood vessels. Moreover, three ligaments enforce the outer surface of the capsule and serve to stabilise the hip joint as well. Figure 2.5 illustrates the hip joint capsule.[9, 10, 15, 19]

2.2.4 Hip joint ligaments

Three ligaments are found on the external surface of the hip capsule. These ligaments are iliofemoral, pubofemoral, ischiofemoral. The iliofemoral ligament lies in the anterior part of the joint and attaches from the pelvis to the femur. It is a ligament of considerable strength and allow the human body to maintain posture for large periods of time without muscular fatigue. The pubofemoral ligament is attached to the pubic bone and merges inferolaterally with the capsule and the iliofemoral ligament. This ligament prevents the overabduction of the hip joint. The ischiofemoral is a triangular ligament and attaches on the posterior part of the acetabulum and to the ischium to the femur. This ligament blends with circular fibres

of the capsule giving support to the posterior aspect of the hip capsule. Figure 2.6 illustrate external ligaments of the hip joint. [9, 15, 19]

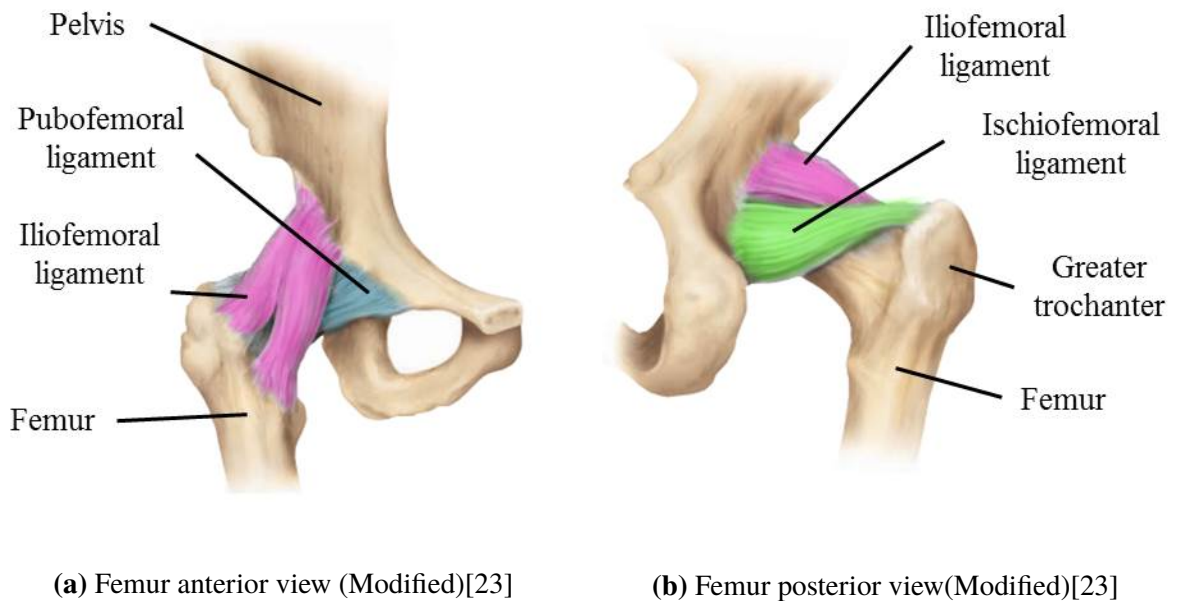


Figure 2.6: Ligaments of the hip joint.

Finally, there is the ligament teres which connects the head of the femur to the acetabulum and it is located inside of the joint. This ligament supports little or no loads, however it serves as an important conduct to supply blood to the head of the femur. Figure 2.5(b) illustrates a lateral view of the hip joint opened where ligament teres can be seen.[9, 15, 19, 23]

2.2.5 Muscles

Hip Joint muscles are responsible for providing protection to the joint and distinct types of movement. Additionally, muscles help to stabilise and support the body weight during locomotion. These muscles enable flexion-extension, abduction-adduction and rotational movements.[9, 12, 23]

Muscles at the hip joint are divided into anterior, posterior and medial groups. The iliacus, rectus femoris, Sartorius, Psoas major and pectinous are anterior muscles that perform flexion movement. Hip joint extensors muscles are the semitendinosus, semimembranosus, gluteus maximus and biceps femoris. Abductor muscles include tensor fascia lata, gluteus maximus, medius and minimus. The hip joint adductor muscles are

pectineus, gracilis, adductor longus, brevis and magnus. The muscles are gluteus maximus, obturator internus and externus, piriformis, gemellus superior and inferior, and the Quadratus femoris.[9, 12, 19, 24]

2.3 Bone tissue

The bone tissue is a calcified and complex connective tissue characterised by its composition that forms most of the skeletal system. It has a complex structure that grants the bone the capacity to modify its structure and shape according to the mechanical demand and location within the skeleton. Furthermore, bone has the essential function to provide mechanical support to the body and protection for vital organs. [7, 15]

Bone tissue consist of cells, osteocytes, and organic and extracellular fibres and ground substance. Also, it has a high content of inorganic material in form of mineral salts, which combine intimately with the organic structure. The inorganic part of the bone gives to the bone great stiffness and strength. On the other hand, the organic component grants the bone its flexibility and resistance. Its compositions varies according to body location, function, dietary, presence of disease, age and sex of the person.[7, 10, 15]

In addition to the protective role and supporting roles, bone serve as a storage for essential minerals in the body, especially calcium, and proteins. Additionally, most of the water can be found in the organic matrix around the collagen fibres and ground substance.[10, 15]

There are four type of cells that form the bone tissue: osteogenic cell, osteoblast, osteocyte and osteoclast. Each cell type is a specialized form of the same basic cell type that has transformed to its mature or functional form. [9, 10]

Bone tissue configuration allows osteocytes to swiftly detect strain and send signals to each other facilitating bone remodelling. Thus, bone tissue is considered a dynamic tissue that has an excellent capacity to repair itself and alter its properties in response to load demand.[7, 10]

At a microscopic level bone forms: Woven and lamellar bone. Woven, or non lamellar bone, is considered the immature bone and is characterised by the presence of collagen fibres.

This type of tissue can be found in the embryo, in the new born, fracture callus, growing bone and in the beginning of the fracture healing process. The other type of osseous tissue, lamellar bone, is a more mature bone in which the collagen fibres are organised in parallel layers called lamella.[10]

At a macroscopic level, bone is classified in two types of osseous tissue: Cancellous (Trabecular) and cortical (Compact). Cortical bone forms the outer shell of the bone, whereas the trabecular is found within the outer shell of the bone. Both type of tissues are found in most bones of the human skeletal system. Figure 2.7 illustrates trabecular and cortical bone in the proximal femur.[7, 10, 15]

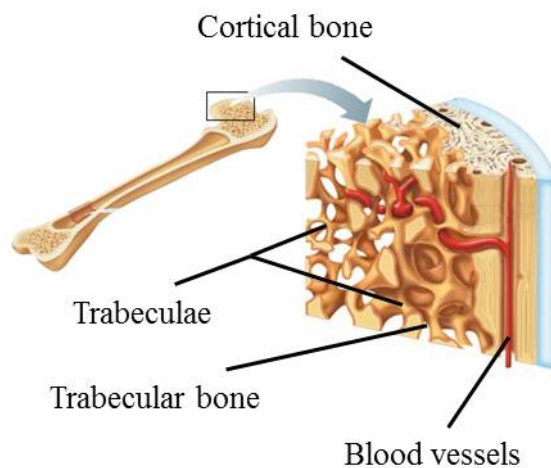


Figure 2.7: Structure of the bone (Modified)[9].

2.3.1 Cortical bone

Cortical bone tissue has a dense structure and constitute up to 80 percent of the skeleton. It nearly has no space between its hard components. Also, cortical bone forms the outer shell of all bones and it withstands the stresses produced by the body movement. [7, 10, 13, 25]

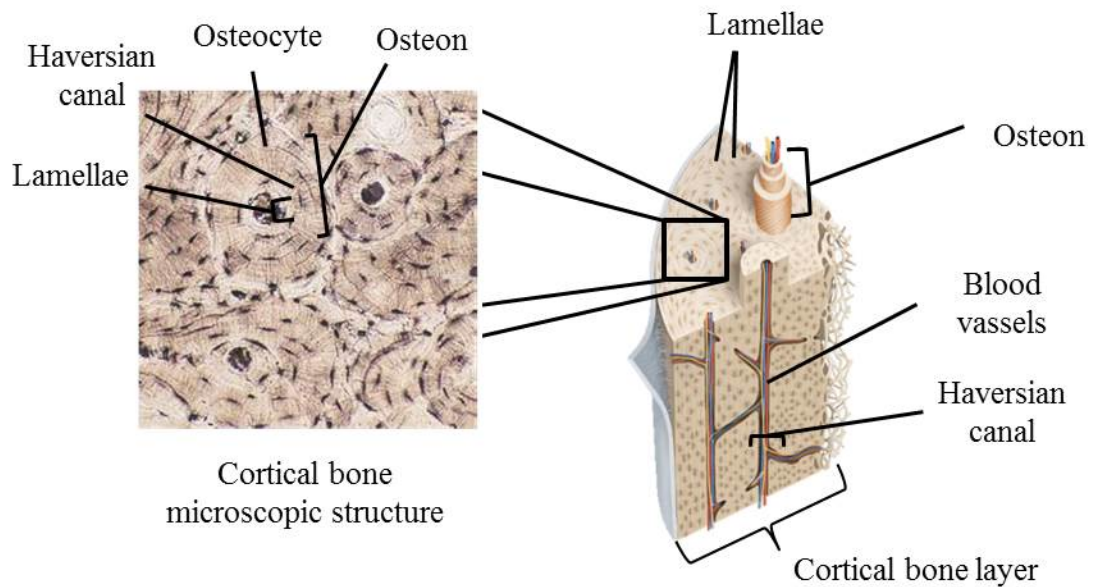


Figure 2.8: Osteon unit(Modified)[9].

The basic structural unit of the compact bone is the Osteon, also known as Harvesian system. At the centre of each system there is a small channel called haversian canal which contains blood vessels and nerve fibres. The osteon consists of concentric mineral layers, lamellae, surrounding the central canal. Furthermore, along each layer are small cavities containing osteocytes. Figure 2.8 illustrates the structure of the Osteon. [9, 10, 23]

2.3.2 Trabecular bone

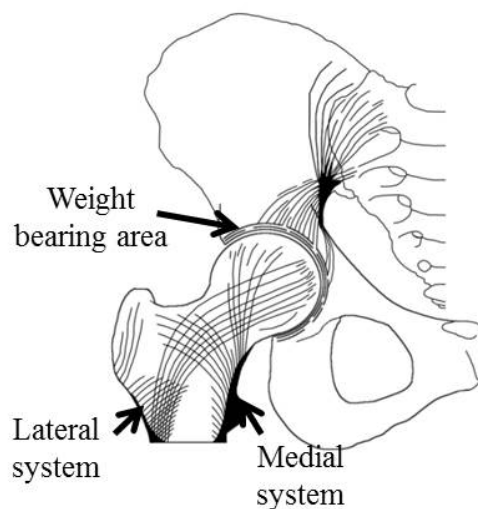


Figure 2.9: Trabecular system of a normal hip joint.

Trabecular bone represents the remaining 20 percent of the skeleton but occupies a larger volume than cortical bone. Trabecular, or cancellous, bone is composed of thin rods, called trabeculae. The loose trabecular bone helps to dissipate and distribute the energy coming from loads on the joints during daily activities.[7, 10, 13]

The main difference against cortical bone, is that trabecular bone is a more porous than cortical bone structure. Trabeculae are oriented precisely along load lines, this feature permits the bone to resist and transfer loads without breaking, as illustrated in Figure 2.9. [7, 10, 13]

2.3.3 Mechanical behaviour of bone tissue

Bone tissue most important characteristics are stiffness, flexibility and toughness. Bone can be described as a two-phase composite material, composed by inorganic and organic materials. The inorganic phase provides to the bone hardness and stiffness, while the organic phase, constituted by collagen and ground substance, provides its flexibility and toughness.[10–12]

Even though cortical and trabecular bone are formed from the same material they present different mechanical behaviour, mainly because they differ in their porosity. Cortical bone due to its compact property it is stiffer and supports higher stresses than trabecular bone, but exhibits lower strain before failure. In the other hand, trabecular bone is more flexible, yielding up to 50% before yielding. [7, 10, 11]

Moreover, the mechanical properties of bone also depends on the type of load applied, in relation to the orientation of its trabecular system of the bone. Additionally, trabecular bone properties are determined by secondary factors such as density, location and function.[8, 10, 19, 25–27]

Bone behaves anisotropically because it exhibits different mechanical properties according to the loading axes, this is caused because its structure is different in the transverse and longitudinal directions. Also, bone exhibits more brittle or more ductile behaviour depending on its age and the rate which it is loaded.[8, 10, 19, 25–27]

2.3.4 Bone Material Properties

Bone material properties, such as strength and stiffness are determined by factors such as material composition, bonding between its components and microscopic arrangement. In the other hand, structural parameters depend on the bone geometry and anatomic location.[8, 10, 19, 26, 27]

Since bone is anisotropic material, strength and stiffness are dependent on the orientation and the type of loading which the bone structure is subjected to. Bone is stronger when the loading is applied longitudinally than transversally, in contrast, in terms of loading conditions, bone can support higher loads when is subjected to compressive loading than tensile modules. Furthermore, bone presents a more ductal-to-brittle transition depending on the strain rate that is subjected to.[8, 10, 19, 26, 27]

Stiffness represents how elastic a material is and it is measured by the elastic modulus of the material, or Young's modulus (E), which is the slope of elastic region in the stress-strain curve of the material.[8, 19, 27]

The stress-strain curve represents the behaviour of a material when is subjected to different magnitude loadings. Stresses are considered the intensity of a load is applied, or force, per unit area that develops on a plane surface within a structure in response to externally applied loads. Strains in change in dimension, or deformation, that results within a structure in response to externally applied loads. Figure 2.10 shows a characteristic stress-strain curve of bone.[8, 10, 19, 26–28]

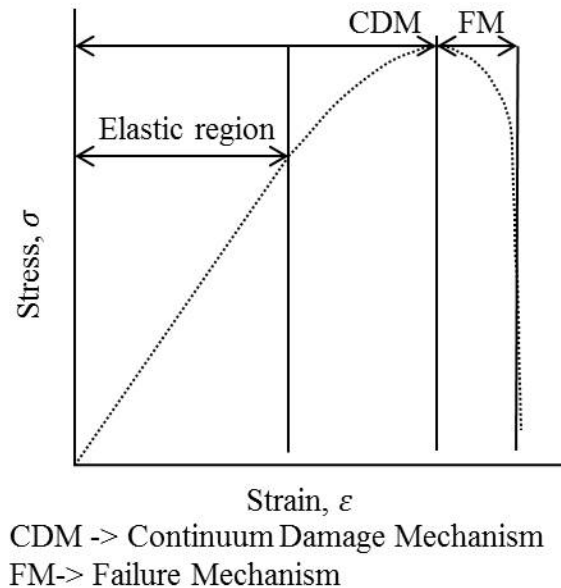


Figure 2.10: Stress-strain curve of bone(Modified) [28]

2.4 Articular Cartilage

Articular cartilage is a major component of synovial joints. It is composed of type II collagenous fibres and chondrocytes assembled together in a solid firm gel. Its mechanical properties, extremely low coefficients of friction, high strength and flexibility allows bone movement against each other without damage and pain. Figure 2.11 illustrates the articular cartilage structure.[7, 8, 10, 19, 27]

Both components of the ball-and-socket configuration of the hip joint are covered with a layer of hyaline cartilage. The acetabulum is covered with a horseshoe-shaped layer of articular cartilage, its thickness on a healthy adult hip joint ranges from 1.2mm to 2.3mm. The head of the femur is completely covered with a regular layer of hyaline cartilage except where the fovea capitis femoris is, ranging from 1.0mm to 2.3mm thick.[7, 8, 10, 27, 29–31]

Cartilage can be either flexible or very strong and resistant depending on the type of cartilage. Different types of cartilage can be found, the most important are hyaline cartilage, elastic cartilage and fibrocartilage.[7–10, 27]

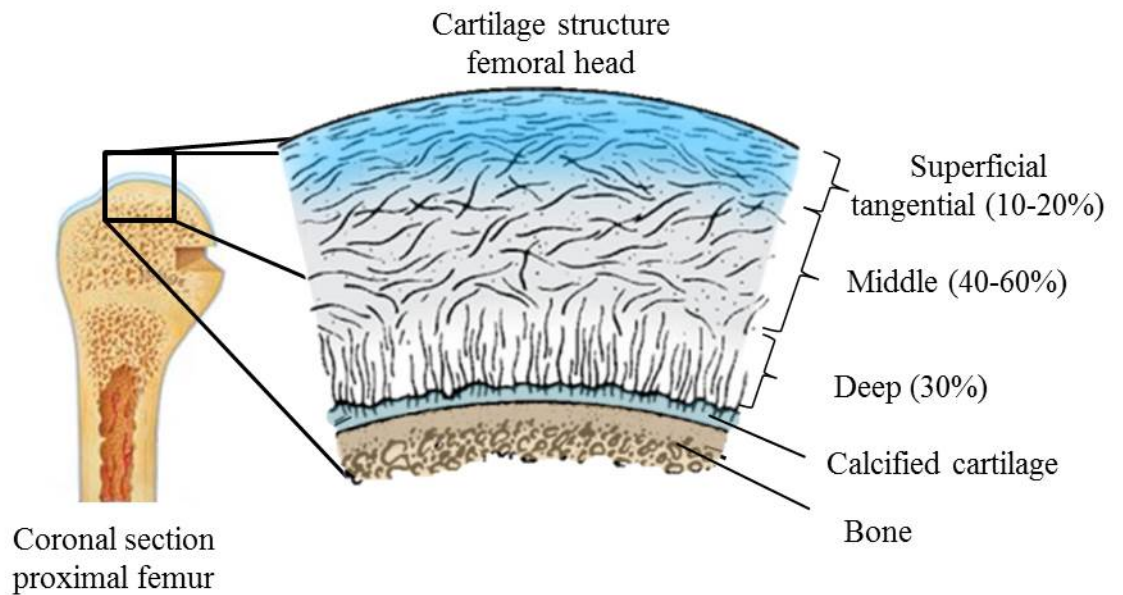


Figure 2.11: Articular cartilage structure(Modified) [9]

2.4.1 Mechanical behaviour of articular cartilage

In articular cartilage, the mechanical behaviour is determined by the type of loading subjected to. Under compressive loads the performance of the cartilage depends of the flow of the interstitial fluid, while, the movement of the collagen fibres determines the shear behaviour. Under tension, articular cartilage presents anisotropic properties since collagen fibres are stronger and stiffer within superficial areas. [7, 10, 14, 16]

2.4.2 Material properties of articular cartilage

Articular cartilage is considered a viscoelastic composite material formed of a solid cell matrix and collagen fibres and an inorganic solution made of water with salts and proteins. The anisotropy property comes from the inhomogeneous distribution of the collagen fibres. As many other fibrous tissues, articular cartilage tends to stiffen with increasing strain when the strain becomes larger.[7, 10, 14, 16]

If the molecular configuration of collagen is altered the tensile properties of the articular cartilage will be damage. This is a significant factor in the early events that leads to the development of osteoarthritis.[7, 10, 14, 16]

2.5 Ligaments

Ligaments in the skeletal system are fibrous connective tissue which attach one bone to another across the joints. Ligaments help to guide joint movement and provide mechanical stability. Ligaments are mainly composed of collagen, elastin fibres and proteoglycans. Ligament fibres are generally nearly arranged parallel to resist tensile forces.[7, 10, 14, 16]

Ligaments in the hip joint surround the articular capsule, also known as capsular ligaments. The hip joint has a small intra-capsular ligament called ligament teres which helps with motion and stability.[8, 10, 32, 33]

2.5.1 Mechanical behaviour of ligaments

Ligaments are viscoelastic, ductile and flexible structures. These mechanical properties allow ligaments to natural movement of the bones to which are attached to, while at the same time are strong and stiff to provide resistance to external forces and unexpected motions. Ligaments can modify their behaviour in response to the mechanical demand, in consequence the tensile strength increases during normal and excessive loading and it is reduced in repose. Figure 2.12 illustrates the ligament structure in repose and under tension. [8, 10, 32, 33]

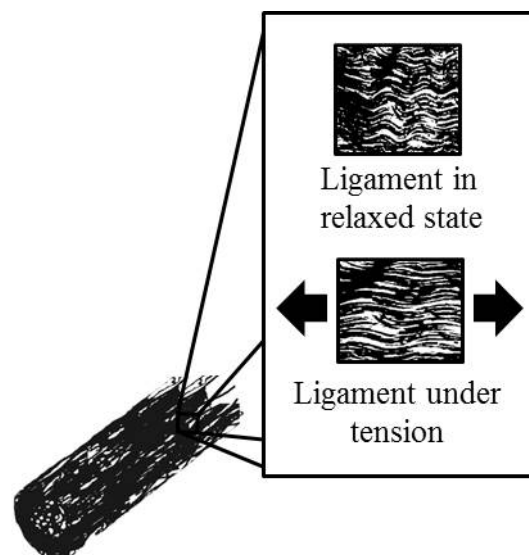


Figure 2.12: Ligament fibre structure.

2.5.2 Material properties of ligaments

Material properties of the ligaments are determined by its biomechanical properties and its micro-structural organisation, orientation and interaction of its components. Its material properties are expressed in the behaviour of its stress-strain curve.[8, 32, 33]

2.6 Biomechanics of the hip

Hip joint plays an important role in the human locomotor system as its primary function is to support body weight and to transmit forces between the trunk and lower limbs. The ball-and-socket configuration provides the hip joint a wide range of motion and great stability. In consequence, in order to study the position and movement of the human body a reference system is use and defined in relation to a neutral position.[8, 10, 13, 14, 19, 27, 33]

2.6.1 Anatomical planes of the human body

In human anatomy three planes and three axes are used to transect the human body in order to describe anatomical structures, position and movement direction of the limbs. Both planes and axes origins at the centre of mass of the human body. Anatomical planes and axes are shown in Figure 2.13.[8, 10, 14, 19]

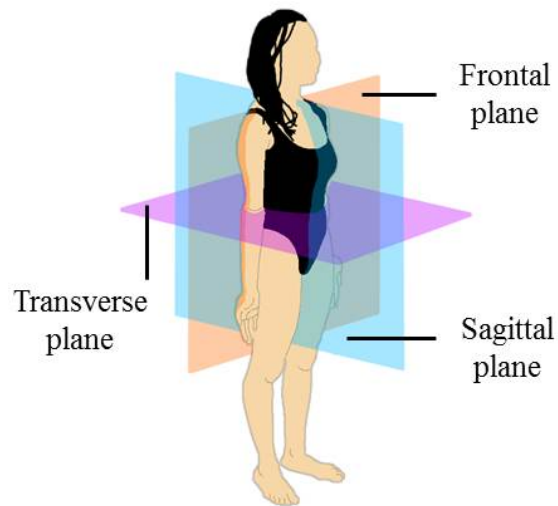


Figure 2.13: Human anatomical planes.

Sagittal plane

The sagittal plane, also known as lateral, is perpendicular to the ground. It separates the body in two halves, right and left. The sagittal plane is formed by the anteroposterior axis and longitudinal axis.[8, 10, 14, 19]

Coronal plane

The coronal plane, also known as frontal plane is perpendicular to the ground and is formed by the mediolateral and longitudinal axes. It separates the human body in anterior and posterior. Also, it defines fewer movements of the whole body in relation with the mass centre.[8, 10, 14, 19]

Transverse plane

The transverse plane, also known as axial or horizontal, is parallel to ground and it is formed by mediolateral and anteroposterior axes. It separates the body in upper and lower sections.[8, 10, 14, 19]

2.6.2 Hip joint movements

The hip joint is capable of performing locomotion in all anatomical planes. This variety of movements is possible because of the range of rotation of the joint. Limitations on the hip joint are related to structure, material and quantity of its connective tissue. The hip joint is capable of performing flexion-extension, abduction-adduction and rotation movements.[8, 10, 14, 19]

Flexion-Extension movement

Flexion-extension movement refers to forward and backward motion of the hip joint as shown in Figure 2.14. Hip flexion is limited by the tight contact with abdominal wall and it has a range of motion nearly 0° to 140° . Whereas, in extension the range of motion is smaller, ranging from 0° to 30° . [8, 10, 14, 19]



Figure 2.14: Flexion/extension movements. (Modified) [34]

Abduction-adduction movement

Abduction-adduction in the hip joint motion takes place in the frontal plane are the motions that move the limb away from or towards the centre of the body as shown in Figure 2.15. The range of abduction movement ranges from 0° to 30° in a neutral position, yet then hip is

partially flexed can reach up to 90° . Adduction has a range of 0° to 25° and it is limited with opposite limb.[8, 10, 14, 19]

Rotational movements

Rotations can be internal and external. These movements involve moving the entire lower extremity, including the foot, around its vertical axis. Its range of motion reach up to 50° , if the hip is flexed it reaches up to 90° .[8, 10, 14, 19]



Figure 2.15: Abduction/adduction movements. (Modified) [34]

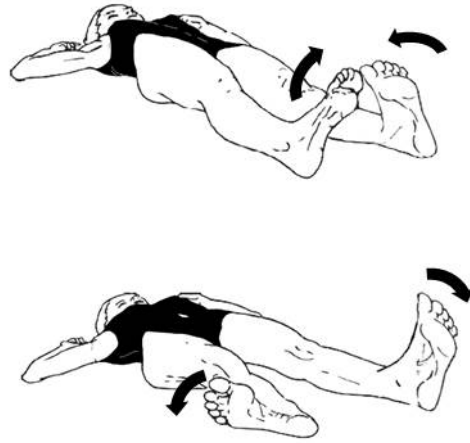


Figure 2.16: Internal/External rotation movements. (Modified) [34]

Chapter 3

Pathologies: Developmental Dysplasia of the Hip (DDH) and Femoroacetabular Impingement (FAI)

3.1 Introduction

The hip joint is essential for the normal functioning of the human body, its function is to support a great proportion of the body weight during daily activities and is fundamental to the proper movement of the body. [9, 13, 15]

The hip joint is frequently subjected to loads, therefore if undergone to improper development, repeatedly traumas and prlonged wear it can lead to pathological conditions in the hip joint. Hip pain is a common cause for medical complaint and is present in different diseases and in patients of all ages and sexes.[9, 13, 15]

In this chapter, two of the most common hip joint disorders Developmental Dysplasia of the Hip and Femoroacetabular Impingement, which are normally diagnosed in young-adult patients, are described.[21, 35–40]

3.2 Dysplasia of the Hip

The Developmental Dysplasia of the Hip (DDH) is a common condition that refers to a wide range of disorders, ranging from a fixed dislocation at birth to asymptomatic acetabular dysplasia in adults. Other terms for describing DDH make reference to the results of physical examination or anatomic abnormalities, such as instability, subluxation and dislocation. Regarding to dysplasia, it refers to the abnormal development of bone or soft tissue.[21, 37, 38, 41–44]

The main attribute of the DDH is the poor acetabular coverage of the femoral head due to a mal-oriented acetabular articular surface, DDH can affect bones and soft tissues. DDH in adults/adolescent is not usually diagnosed until symptoms develop, however it may have been present since birth and childhood. Figure 3.1 illustrates a dysplastic hip where it can be seen typical radiographic characteristics of DDH. [21, 37, 43]

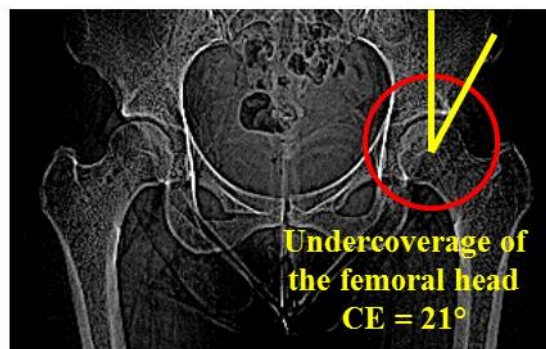


Figure 3.1: Anterior-posterior radiograph of a patient suffering DDH. In this case, the left hip is affected and presents a deficient acetabular coverage of the femoral head.

3.2.1 Aetiology

The exact aetiology of DDH is unknown, it is believed that different genetic and environmental causes can contribute to DDH. Furthermore, such factors can be divided into

two groups: Internal and external. Internal factors consider the morphological structure of the components of the hip joint and the joint itself, for example: decreased resistance of the hip to dislocation, shallow acetabulum and connective tissue laxity. Whereas external factors consider lifestyle and environmental conditions, such factors can be breech presentation, multiple pregnancy and infant position.[21, 37, 45–47]

A typical and adequate development of the acetabulum depends on the epiphyseal development of the triadiate cartilage and the development of the individual ossification centres of the pubis, ilium and ischium which are the common physis of the acetabulum. During this development the acetabulum deepens stimulated by the spherical femoral head. If this interaction is absent or alterations take place, the acetabulum fails to properly develop causing atrophy on the cartilage or leads to Developmental Dysplasia of the Hip.[21, 37, 45–47]

Another factor to consider on the occurrence of DDH is female gender and breech positioning. The left hip is more frequently affected since is associated with the intrauterine position of the left hip and the relative position of the sacrum of the mother at moment of birth. Neuromuscular disorders, as cerebral palsy or Larsen's syndrome, may cause an abnormal development of the hip in children, however these cases are not classified as DDH. Most of the factors can be presented on childhood, but some patients may present symptoms of DDH until adulthood and it is usually related to acetabular malformation. Furthermore, the incident varies in different ethnic groups, which North American and caucasian eastern Europe populations have the most elevated incidence (0.5%) with a predominant female distribution. [21, 37, 45–47]

It is difficult to conclude that DDH is a consequence of only genetic factors of the population. It is necessary to also take into account cultural practices, obstetric care and life style of the patient. [45, 46]

3.2.2 Diagnosis and Symptoms

Developmental Dysplasia of the Hip changes with age and so does diagnosis. A full history of the patient including age and occupation, must be considered to underlie the feasible pathology. In new born babies, a clinical examination, such as Ortolanis and Barlow tests, is

used to diagnose DDH. Dysplasia in children is commonly associated with dislocated, subluxated and unstable hip joints. However not all children may present clinical signs after birth. Furthermore, dysplasia in adulthood is associated with acetabular malformation.[21, 37, 45–50]

It is possible to diagnose dislocation and subluxation through clinical examination. However, occasionally it is necessary to use imaging tools, especially in adults. Imaging tools used for diagnosis on adults are radiography, computed tomography and magnetic resonance imaging. [21, 37, 38, 45–48, 50]

Ultrasound imaging is used to see internal soft tissue. In consequence, ultrasound scans are only used on new-borns up to 5 months babies, when bones are still cartilaginous. Ultrasounds are also important during the treatment of DDH on babies. [43, 48]

Radiography

Radiography imaging is helpful in patients older than 5 months old, when the ossification of bones has progressed adequately to allow the proper visualisation of bone structures. The most used view on the diagnosis of DDH is the Anterior-Posterior (AP).[21, 38, 43, 46, 50, 51]

The clinical diagnosis of the DDH in adults is performed by using radiological parameters that can be measured on radiographs. Moreover, some radiological parameters are used to assess features of the hip joint morphology, such as the acetabular coverage. The most common radiological angle used in diagnosis of DDH is the Centre-Edge (CE) angle, which measures the lateral acetabular coverage. Following, the Vertical-Centre-Anterior (VCA) angle which assess the anterior acetabular coverage. Other angles related to DDH are the acetabular roof angle (Tonnis angle) and the Sharp angle.[21, 38, 43, 46, 50, 51]

Radiological parameters

Radiological parameters are the measurements and angles taken from radiographies to describe the morphology of the hip joint. The following radiological parameters are commonly used to diagnose DDH on a patient: Centre-edge (CE) angle,

Vertical-centre-anterior (VCA) angle, acetabular roof angle and acetabular sharp angle.[21, 38, 43, 46, 49, 51]

Central Edge angle

The centre-edge angle, also known as Wiberg angle, is an angle formed between a vertical line crossing the centre of the femoral head and another line connecting the centre of the femoral head with superior border of the acetabulum as shown in Figure 3.2. The CE angle is used to assess the lateral acetabular coverage and, also, it is used to distinguish normal and dysplastic hips. According to literature, a normal CE angle in both men and women ranges from 25° to 45°. Being less than 25° considered as pathological. [21, 38, 43, 46, 49, 51, 52]

Vertical Centre anterior angle

The vertical-centre-anterior (VCA) angle evaluates the anterior acetabular coverage. The VCA angle is formed between a vertical line crossing the centre of the femoral head and a line crossing from the centre of the femoral head to the anterior acetabular sourcil as shown in Figure 3.3. The VCA angle is also known as Lequesne angle. VCA angle ranges from 25° to 45° on normal hips, where an angle less than 25° is considered as abnormal. In a hip joint radiography, a sourcil is the thickening of subchondral acetabular bone.[21, 38, 43, 46, 51, 52]

The VCA angle is usually used for describing the anterior acetabular coverage. However, the anterior coverage can be measured directly in the sagittal plane using CT scans. This radiological parameter is called anterior Acetabular Coverage (AAC).[21, 38, 43, 46, 51, 52]

Acetabular roof angle

The acetabular roof angle of Tönnis is used to describe the structural stability of the hip joint. It is formed by a horizontal line crossing the lowest point of the acetabular sourcil and a line from the lateral border of the acetabular sourcil as shown in Figure 3.4. The normal range of the Tönnis angle is from 0° to 10°. A value smaller than 0° indicates the likelihood

of Femoroacetabular Impingement, whereas a value greater than 10° may indicate structure instability.[21, 38, 43, 46, 51, 52]

Acetabular Angle

The acetabular angle, also known as sharp angle, is used to describe the morphology of the acetabulum. It is formed by a horizontal line that connects the inferior point of the pelvic teardrop and another line that connects the lateral edge of the acetabulum with the inferior tip of the pelvic teardrop. Teardrop refers to the end-on projection of a bony ridge running along the acetabular fossa as shown in Figure 3.5.[21, 38, 43, 46, 51, 52]

The normal range of the acetabular angle is between 33° and 38° . Angles below 33° are not common and might not require medical intervention. Whereas angles greater than 38° are considered abnormal and should be clinically attended.[21, 38, 43, 46, 51, 52]

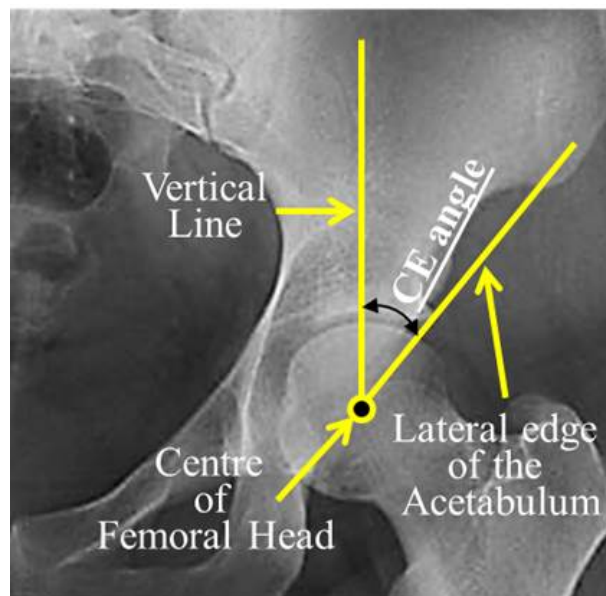


Figure 3.2: Central-Edge (CE) angle. The location of the centre of the femoral head was define with the intersection of two perpendicular diameters of a circle fitted into the femoral head [53].

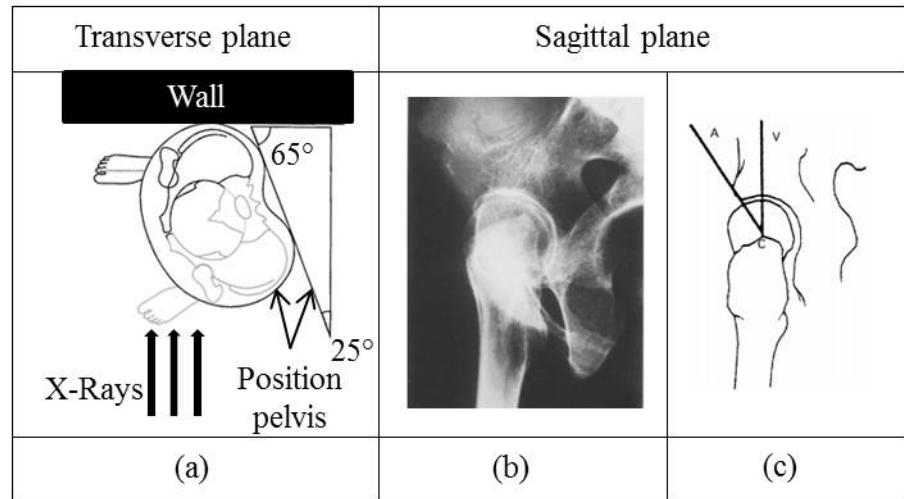


Figure 3.3: Vertical centre anterior (VCA) angle. a) Radiographic false profile view technique. b) VCA radiograph. c) The anterior centre edge angle (Modified) [41, 54]

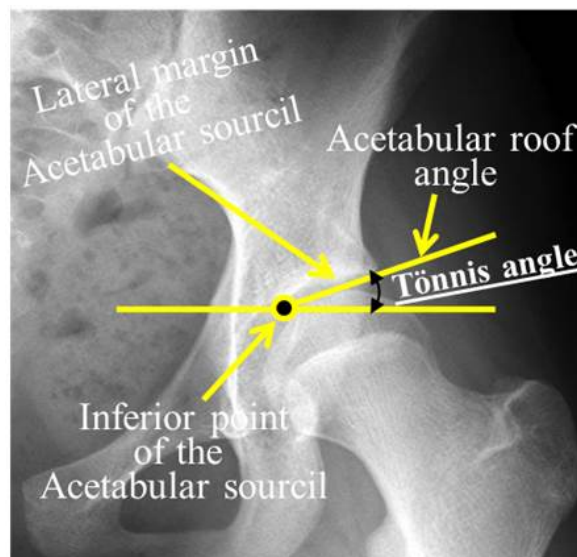


Figure 3.4: Acetabular roof angle (Tönnis angle).

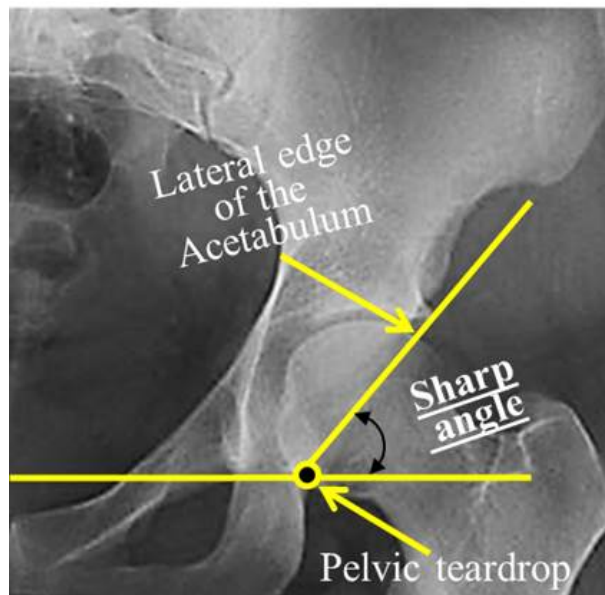


Figure 3.5: Acetabular angle (Sharp angle).

Computed tomography

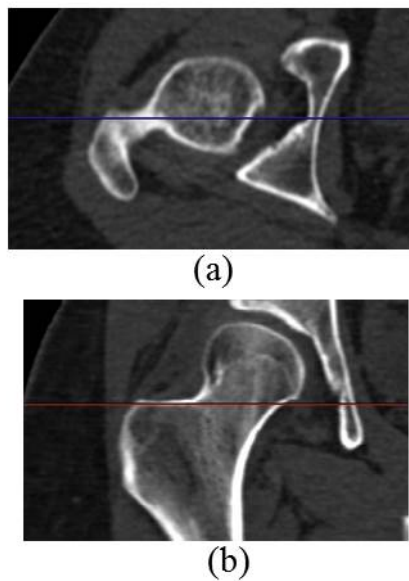


Figure 3.6: Computed tomography (CT) scan of the right hip of a patient suffering DDH. a) Transversal plane. b) Coronal plane.

The computed tomography (CT) scans are used to diagnose disease and help with preoperative planning. CT scans help to assess the hip joint congruity and study radiological parameters in three planes. Also, CT scans provide good details about the osseous structures

of the patients and its format facilitates image processing to generate Three-Dimensional (3D) models, used for further analysis and studies.[21, 37, 38, 43, 46, 51, 52]

Magnetic resonance imaging

Magnetic Resonance Imaging (MRI) presents similar characteristics to CT scans but with a greater quality imaging. MRI provides better soft tissue detail that can help to evaluate its condition. this imaging tool makes possible to study articular cartilage and identify joint congruity. MRI, along with CT scans, can be used for diagnostic and preoperative planning.[21, 37, 38, 43, 46, 51, 52]

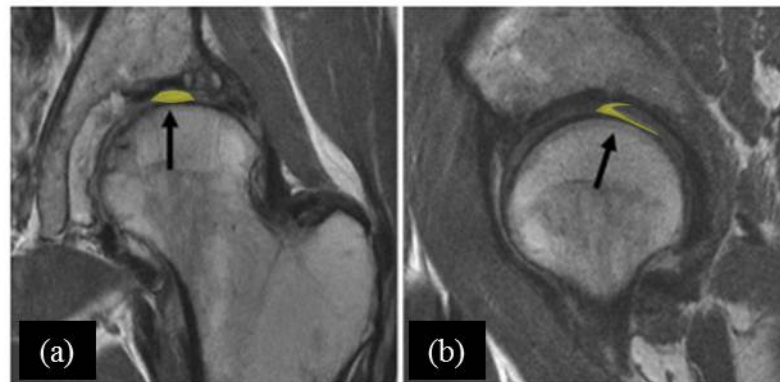


Figure 3.7: Magnetic resonance imaging (MRI), in this image the left hip of a 57 year old female patient with mild dysplasia is shown. a) Coronal plane. b) Sagittal plane. Black arrows show cartilage yielding. [55].

Average values of anatomical parameters

In 2013 Laborie et al. [52] did an analysis of the radiological parameters related to dysplasia of the hip in a population of 2011 (841 males, 1170 females) 19 year old Norwegians. For each gender, he calculated the average and standard deviation of the following angles: the Sharp's angle, the Tönnis angle, and the CE angle of Wiberg. Laboire et al. [52] found that the average values of the Sharp angle were $40.7 \pm 3.52^\circ$ for females and $38.8 \pm 3.49^\circ$ for

males. The Tönnis angle was $5.84 \pm 4.9^\circ$ for females and $5.64 \pm 4.8^\circ$ for males. And finally, the CE angle of Wiberg for females and males was $31.0 \pm 6.1^\circ$ and $32.1 \pm 6.1^\circ$, respectively. The aim of the study was to define new gender-specific standards to assess the characteristics of the hip joint. [52]

3.2.3 Treatment

Treatment of DDH can be classified into non-surgical and surgical. Non-surgical treatment such as Pavlik harness and closed reduction are usually used in children, which redirects the femoral head into the acetabulum to allow the proper development of the hips. In adults, non-surgical treatments are mainly changes in their lifestyle such as weight loss and changes in their daily routine.[21, 37, 38, 43, 46, 51, 52]

If non-surgical treatments fail to relocate the hip or symptoms are still present, a surgical procedure is needed. Osteotomies are surgical treatments for correcting the DDH. The purpose of this procedure is to reduce the excessive loading area on the acetabulum by increasing the contact area.[21, 37, 38, 43, 46, 51, 52]

Pelvic osteotomies

Pelvic osteotomies have been developed to correct and slow the degenerative process of DDH. There are two types of osteotomies: reconstructive and salvage osteotomies.[21, 38, 43, 56]

On reconstructive osteotomies, surgeons reorient the acetabulum according to the femoral head. After the osteotomy the femur keeps the hyaline cartilage. For this procedure, it is important that patients hip joint is congruent. Reconstructive osteotomies examples are: [56].

- Single(Salter) Innominate osteotomy
- Double (Sutherland and Greenfield) Innominate osteotomy
- Triple (Steel) Inominate osteotomy
- Spherical or Rotational (Wagner) Acetabular osteotomy
- Tönnis Juxta-Articular Triple osteotomy

- Bernese (Ganz) Periacetabular osteotomy

Salvage osteotomies give additional support to the femoral head using the hip capsule. In these cases the femur does not articulate with the hyaline cartilage, but with the fibrocartilage. When patients have incongruity of the femoral head and acetabulum, or they present degenerative changes, salvage osteotomy should be used. The shelf arthroplasty and Chiari Medial displacement osteotomy are two examples of Salvage osteotomies. [56]. However, the success of the treatment of DDH highly depends on early diagnosis and correct treatment. Previous work and literature show that DDH is the principal cause of Osteoarthritis.

3.3 Femoroacetabular Impingement

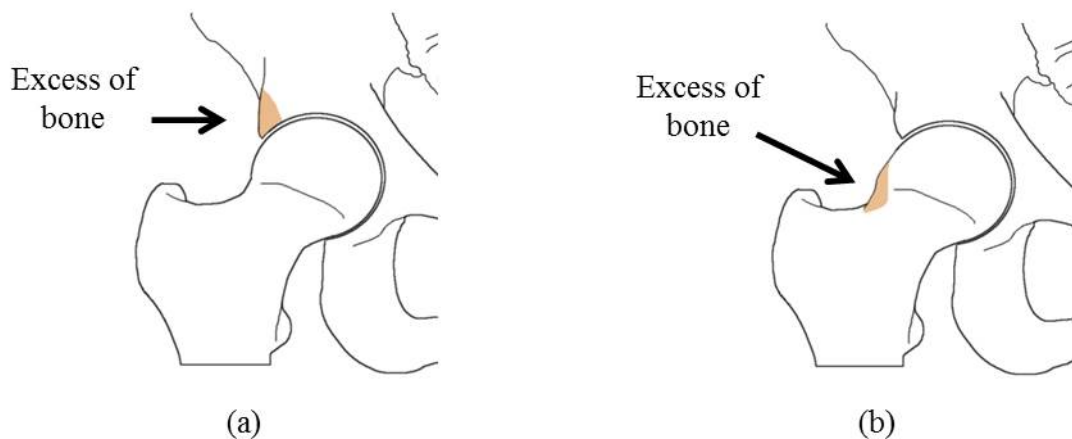


Figure 3.8: Abnormal growth in bone causing FAI. (a) Femoral head-neck junction. (b) Acetabular rim.

Femoroacetabular Impingement, FAI, is a condition characterized by defects on the pelvic/femoral bone rather than a disease. FAI refers to the abnormal contact between the proximal femur and acetabular rim produced by atypical morphologic features as shown in Figure 3.8. Frequent abnormal contact can result to progressive degenerative damage in the hip joint soft tissue, if left untreated can cause the development of Osteoarthritis (OA).

Proper diagnosis of FAI and adequate future treatments are important in slowing the degenerative process, a misdiagnosis or delayed diagnosis can lead to complications such as OA or even inappropriate surgical treatments. [39, 40, 57–64]

3.3.1 Aetiology

Currently, the exact aetiology of FAI remains unknown. It is believed that stresses produced by sports, trauma during development and/or genetic factors represent the main reasons for abnormalities in the femoral epiphysis. Moreover, distortion of the hip joint structure after a pelvic osteotomy, post-traumatic and iatrogenic deformities, such as dysplasia, femoral retroversion can also lead to FAI. [39, 57–61, 63, 65, 66]

3.3.2 Pathology

The current concept of FAI was postulated by Ganz et al.[58] as developmental abnormalities in the hip joint caused by a pathomorphology in one or both bones of the hip joint. These anatomic abnormalities reduce the space between the femoral neck junction and acetabular rim, resulting in range of motion injuries, on acetabular rim and labrum, hip pain and eventually arthrosis. Additionally, FAI can occur in a normal shaped hip as a consequence of an extreme rate of motion. [39, 65–67]

The most frequent location for femoroacetabular impingement is within the antero-lateral and supero-anterior area of the joint and the most critical motion is internal rotation during flexion. [58, 65–67]

3.3.3 Types of Impingement

In FAI, the femoral head remains well-centred, but freedom of movement is limited by the presence of an offset at the femoral head-junction or excessive acetabular deepness.

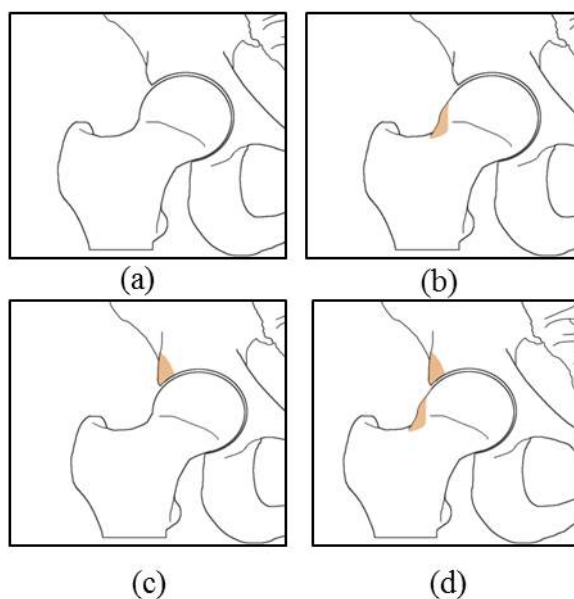


Figure 3.9: Abnormal growth in bone causing FAI. (a)Normal. (b)Cam. (c)Pincer. (d)Mixer

Two type of FAI mechanisms have been identified, based on intraoperative observations of the injuries. Cam-type impingement is caused by a malformation at the femoral epiphysis that produces and outside-in delamination of the acetabulum. Pincer-type impingement is caused by a local or general overcoverage of the acetabulum. However, only a few patients present isolated FAI abnormalities, approximately 86% of patients present both pathomorphologies. Figure 3.9 shows the normal shape of the hip joint and the three different types of femoroacetabular impingement.[39, 57–61, 63, 65]

Cam-type Impingement

Cam-type impingement characteristics are a dysplastic “bump” at the head-neck junction, a synovial herniation pit, and a “pistol-grip” deformity, which may be developmental or posttraumatic. These non-spherical extensions of the head are frequently the result of an abnormality of the capital femoral epiphysis and are covered by hyaline cartilage. Deformities are commonly found on the anterior-superior and lateral region of the femoral head at. This type of impingement is more common in young athletic men around 30 years old.[39, 58, 59, 61, 65, 68, 69]

The cam mechanism occurs when the non-spherical extension of femoral head or the off-set between the neck and head of the femur, forcibly enters into a normal morphological

acetabulum. Normally, the junction between the neck and head of the femur has a concave configuration. In cam-type impingement this area is flattened or convex.[39, 58, 59, 61, 65, 68, 69]

It has been hypothesized that cam-type FAI is the result from the development of an asymptomatic slipped capital femoral epiphysis causing a defective elongation of the femoral common physis between greater trochanter and femoral head, and as consequence leading to a reduction in the concavity of the femoral head-neck junction.[39, 58, 59, 61, 65, 68, 69]

Cam-type pathomechanical process is more common in young athletic males and commonly occurs during flexion of the hip. As the hip is flexed a shear stress appears at the labral cartilage junction where the “pistol grip” deformity presses against the labrum. As a consequence of the shear forces damage can occur on the acetabular cartilage and/or on the labrum or bone region, gradually leading to a detachment of the labrum. Furthermore, repetitive impingement between bones can cause osteophyte formations to more serious problems on the affected area. Figure 3.10 shows the reduced range of motion caused by the cam-type mechanism in the hip. joint.[39, 57–61, 63, 65]

Pincer-type Impingement

In Pincer-type impingement, contact frequently occurs on the antero-superior region of the femoral epiphysis as in cam-type impingement, however in this case it is a consequence of the abnormal acetabular shape. As in cam-type impingement its aetiology is not well-defined, although it is associated with some disorders such as slipped capital femoral epiphysis, acetabular retroversion or post-traumatic dysplasia which can lead to acetabular overcoverage. Active female patients around 40 years old are the most common patients to have a pincer-type impingement.

Unlike cam-type, pincer impingement produces damage in a very restricted area of the hip, only a small area of the acetabular rim is affected. However, repetitive impacts on the labrum produce damage and ossification in the soft tissue, leading to progressive increase of femoral head coverage. Figure 3.11 shows a pincer-type mechanism, the acetabular rim presents an excessive acetabular coverage which reduces the range of motion.[39, 57–60, 63,

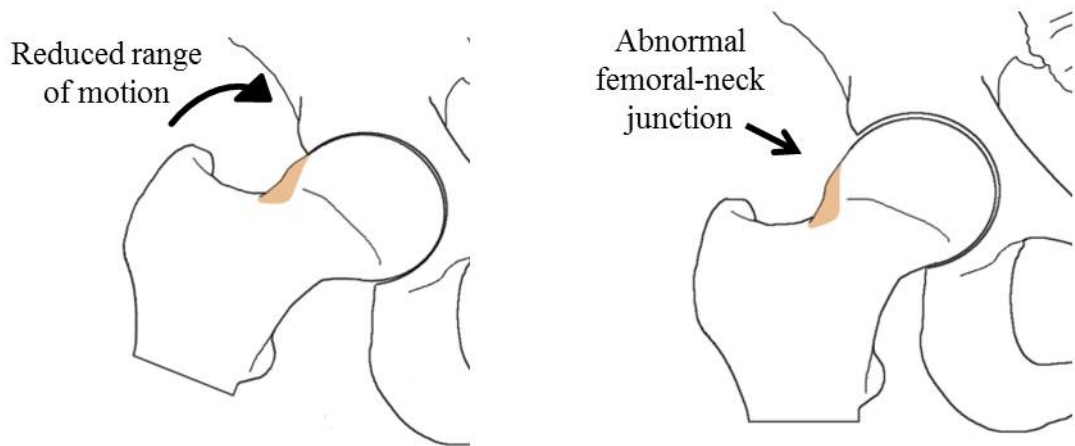


Figure 3.10: Cam-type femoroacetabular impingement.

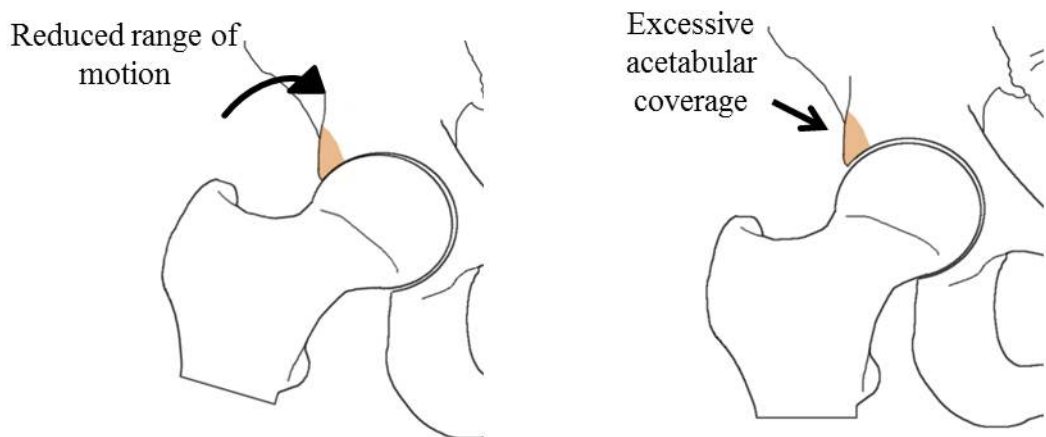


Figure 3.11: Cam-type femoroacetabular impingement.

3.3.4 Diagnosis and Symptoms

Patients with FAI regularly presents with groin pain with hip rotation and often start after a minor trauma, also, patients are aware of their limited hip mobility before symptoms appear. Patients histories report intermittent pain that increases with athletic activities, prolonged

sitting and prolonged walking. [39, 40, 58, 59, 65, 70]

The initial phase of symptoms are stiffness in the groin region or in the anterior side of the thigh and instability while flexing the hip further than 90 degrees. As symptoms develop, movements that require flexing the hip towards the trunk with internal rotation become more uncomfortable from patients.

3.3.5 Physical Evaluation

All patients presenting hip are subjected to a systematic physical examination to assess possible causes of groin pain. Physical inspection includes, standing position, passive and active range-of-motion and specialized tests for FAI.[39, 40, 58, 59, 65, 70–72]

The two most common test used to diagnose FAI are, the Anterior Interior Test (AIT) and the Flexion-Abduction Test (FABER).

Anterior impingement test

The anterior impingement test requires the examiner to flex the hip to 90° gently, followed by a forced adduction and internal rotation. The final position recreates the position that can lead to impingement bringing the femoral neck-head junction close to the antero-inferior region of the acetabulum. AIT outcome can be positive or negative based on the pain signals of the patient. A positive result is considered when pain is experienced during the test. Negative result is considered in absence of pain.[39, 40, 58, 59, 65, 71–73]

FABER Test



Figure 3.12: FABER test. Left picture negative test. Right picture presents a positive test with increased distance between the exam table and knee.(Modified)[74]

FABER test induces posterior impingement by bringing the hip into a flexed, abducted, and externally rotated position and applying a downward force perpendicularly to the leg, as is shown in Figure 3.12. A positive result is defined if distance between the lateral aspect of the knee and the examination table is greater compared to the unaffected hip or a positive result can be also be defined if a sharp sudden pain is present during examination. [58, 73, 74]

3.3.6 Imaging assessment

Plain film radiography is the primary imaging procedure to diagnose any abnormality of the bones. Radiographic assessment for FAI consist of a standard anterior-posterior (AP) plain radiograph of the pelvis and a cross-table lateral radiograph of the affected hip. For cam-type impingement the common bump deformity is frequently seen in an AP pelvis view, because non-spherical extensions of the femoral head are commonly located on the anterior region. Rim ossification and acetabular retroversion can also be seen on the anterior edge of the acetabulum. Figure 3.13 shows Cam-type and Pincer-type FAI in antero-posterior view radiographs. [39, 40, 58, 59, 65, 71–73]

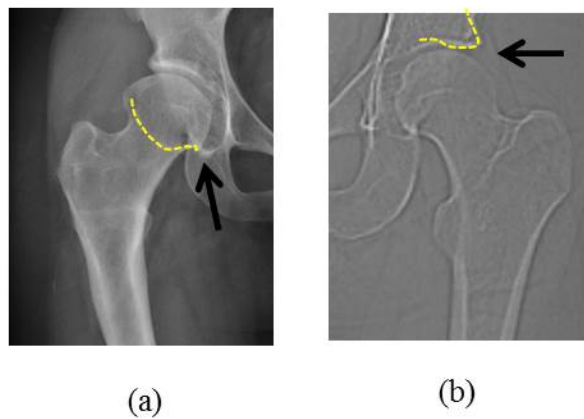


Figure 3.13: Radiographic assessment of FAI. a)Cam-type b)Pincer-type.

On Cam-type FAI, bone deformities on the femoral head can be assessed on AP plain films by the Alpha angle and it is defined as the angle between a longitudinal line to the femoral neck from the centre of the femoral head and a line where the contour of the femoral head surpasses the radius of the femoral head and it is recommended to be measure on an axial oblique view in order to have a proper view of the femoral head-neck junction, as Figure 3.14 shows. [75]

However, Laborie et al. [76] reported that 35% of asymptomatic males had signs of FAI on frontal plain film radiographs, and concluded that plain X-rays can not properly localize abnormalities on the femoral borderline or antero-superior abnormalities. Currently, magnetic resonance imaging (MRI) is the most helpful method in diagnosing labral pathologies and assisting in further detailing subtle deformities. Although MRI aids in preoperative planning, it is not part of the routine procedure to asses FAI owing to concern about radiation exposure in young patients.[72, 73, 75–78]

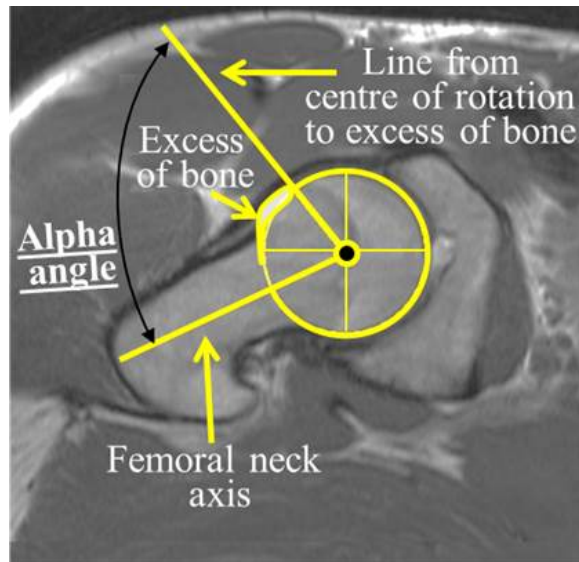


Figure 3.14: Alpha angle on AP radiograph.

3.3.7 Treatment

Treatment procedures for patients with FAI should begin with conservative management, which includes modification of all activities that may have an impact on impingement, particularly restricting activities that require extreme hip motion and high loading on the hip. Additionally, early treatment includes anti-inflammatory medications administration, to reduce pain and swelling, and physiotherapy.[39, 58, 59, 65, 72]

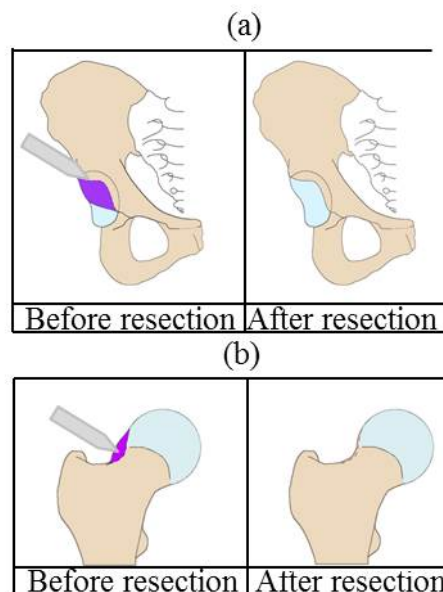


Figure 3.15: Radiographic assessment of FAI. a)Cam-type b)Pincer-type.

Definitive surgical intervention is indicated if pain is persistent in young patients despite attempts at conservative treatments. The surgical procedure focuses on improving the clearance for the proper movement of the hip joint and reducing the impact of the femur against the acetabular edge.

Osteochondroplasty focuses on improving the space for the movement of the hip by removing the bone abnormality from the acetabular rim or/and the femur that causes impingement, thus reducing the impact of the femur against the acetabular edge. The type of treatment performed is determined primarily by the bone abnormality that causes FAI.[39, 58, 59, 65, 72, 79]

In pincer-type impingement, the over coverage of the acetabulum on the femoral head is modified. In cam-type impingement, the range of motion of the femoral head-neck is optimized by increasing the removing the aspherical part of the femoral head-neck junction. Osteochondroplasty for hip impingement is carried out by open surgical or arthroscopic procedures. As Figure 3.15 shows.[39, 57–61, 63, 65, 79]

3.4 Sphericity

In general, research studies regarding Femoroacetabular Impingement and Dysplasia of the hip focus on the diagnosis, epidemiology, treatment and surgical procedures. FAI and DDH have been also investigated from a mechanical point of view with the purpose to understand the mechanical impact of these abnormalities and new surgical procedures on the hip joint. Currently, multidisciplinary research techniques and new technologies combined with experimental work have allowed researches to investigate unsolved issues regarding FAI and DDH. However, there is still a lack of studies that provide information how anatomical features affect the biomechanical behaviour of the hip joint.

Imaging methods and 3D models have been proposed as diagnosis for DDH and FAI. Wyss et al. [80] evaluated the effectiveness of using MRI images to predict clinical symptoms regarding to FAI. In this study, physical examination results are compared with MRI measurements of the hip joint on two subject groups, an asymptomatic patient group and patients diagnosed with FAI. It was found that internal rotation of the hip measured at

90° had a strong correlation with the space between the femoral neck and the acetabular rim. [80]

Li et al.[81] developed a software package that was capable of measuring different radiological parameters related to DDH using 3D hip models generated from patients CT scans. This package was also capable to perform virtual surgeries on the 3D models. Beaulé et al. [82] developed a non-invasive method to study FAI. In this study, measurements of the alpha angle on FAI symptomatic patients and a control group were compared. The alpha angle is defined by a line from the centre of the femoral head to the point where the cortical cortex exceed the radius of the femoral head and a line extended through the axis of the femoral neck. [81, 82]

Armiger et al. [83] developed an automatized procedure to diagnose DDH. Armiger developed an algorithm based on MATLAB® that uses CT data from patients and automatically creates a 3D model and measures radiological angles regarding to DDH. Other studies, such as Chen et al.[84] and Tan et al.[85], used 3D segmentation tools for diagnosis of DDH and preoperative planning to correct DDH. [83–85]

Regarding mechanical studies, many experimental and numerical researches have taken place in order to investigate stress distribution, contact area and contact pressure in hip joints. FAI studies focus on the range of motion and, the stress distribution of bone and soft tissue where the bone abnormalities are located. While DDH studies focus on the stress distribution, contact area and contact pressure of the articular surface of the hip joint.

Although, many studies have analysed the geometry of the hip joint and how affects contact area, contact pressure between the acetabulum and femoral, and also the stress distribution on the hip joint. To date, just a few studies have quantified and analysed the effect of the shape of the acetabulum and femoral head on the biomechanical behaviour of the hip joint. Sankar et al.[5] quantified the “sphericity” of the femoral head in a series of children suffering with DDH. Sankar et al. calculated an average of the femoral head sphericity of 85.2 ± 5.5 , they also found a significant variability in the “roundness” of the femoral head. Sankar et al. concluded that the femoral head in walking aged children with DDH is dysplastic and usually “aspherical”, also their results suggest that DDH affects the morphology of the acetabulum and femoral head. [5]

Gu et al.[6] presented a method to create a mathematical representation of the acetabular cartilage using reverse engineering techniques, surface-fitting algorithms and mathematical curve surface theory. Gu et al. created 3D triangulated mesh surfaces of 25 acetabula by using a 3D laser scanner. The gaussian curvature and mean curvature at each point were calculated and presented as shown in Figure 3.16. The results showed that the shape of the acetabular cartilage was not theoretically spherical but rather rotational ellipsoidal. Furthermore, the highest surface-fitting error was seen in the roof area of the acetabular cartilage.

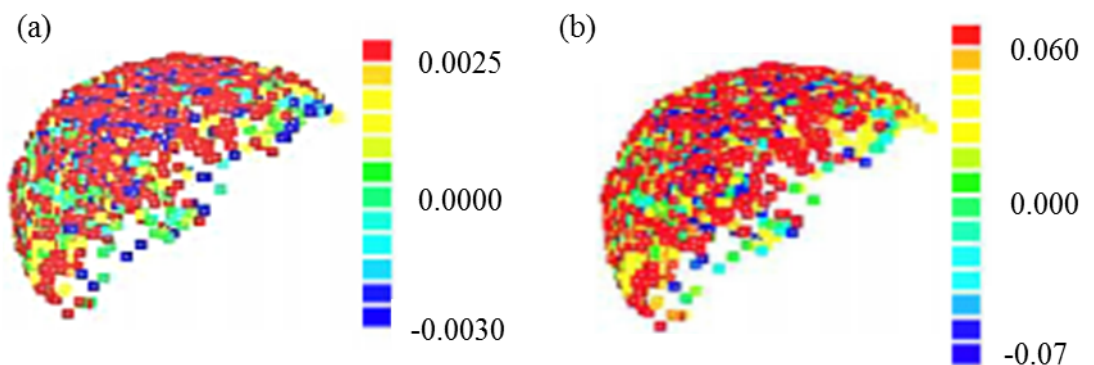


Figure 3.16: Distribution of Gaussian (a) and mean(b) curvatures on the acetabular cartilage surface. [6]

Afterwards, Gu et al. [4] used the results obtained on [6] to create 3 finite element models to investigate the role of the non-spherical acetabular cartilage in the biomechanics of the hip joint. From a healthy volunteer CT image data a model with the original shape of the acetabular cartilage was created, other two models had the acetabular cartilage shape replaced by the rotational ellipsoid and the other one had the acetabulum replaced by a sphere. Results showed that the shape of a healthy acetabular cartilage surface contributed to the optimal contact stress, as the model with rotational ellipsoid surface showed more consistent results to the natural shaped acetabulum than the sphere shaped. [4]

In order to study the influence of the anatomical parameters corresponding to different hip joint pathologies and the sphericity of the hip components, numerical models are a very useful tool as they allow to measure contact patterns, angles and positions of anatomical landmarks

and to obtain coordinate data of the hip joint geometries. The following chapter describes the process to construct a computer model of the hip joint from CT scan data; computer models were used for finite element and “Sphericity” analysis.

Chapter 4

Development of the Finite Element models

4.1 Introduction

Currently, there are few procedures to quantify and study the articular surface and its effect on dysplastic and healthy hip joints. This research focuses on the shape of the acetabulum and femoral head in healthy patients and patients with dysplastic and cam-type impingement. As discussed in the previous chapter, protuberances on the articular surface of the hip joint significantly affects the bio mechanical behaviour of the hip joint. In order to investigate if the typical pathological characteristics of bone in dysplastic hips and in hips suffering from cam-type impingement affects the articular surface of the joint , 3D models were built from CT data of 30 hip joints(10 normal hips, 10 dysplastic hips and 10 suffering from femoroacetabular impingement) and were undertaken to a “Sphericity” and finite element analysis simulating a one-leg-standing position to obtain contact area and contact pressure values and pattern.

4.2 Modelling

4.2.1 3D models

For this research, subject-specific hip models for each hip were developed. The models were constructed from CT scans using ScanIP[®] (Simpleware Ltd, version 4.2). ScanIP[®] is a cross-sectional image based modelling, it provides several image processing tools for visualization, segmentation and edition of specific regions on 3D surfaces.

On this research, CT scans had a Digital Imaging and Communication in Medicine (DICOM) image format, which is a widely used protocol to store medical images. This format can be imported to ScanIP[®] to create 3D surfaces. Every set of CT scan of each subject differed on resolution, size, frequency, and position of the slices, for this reason it was very important to have a good knowledge of anatomy, in order to properly identify hip bone structures. In such manner, 3D geometries could be constructed as accurate as possible. Figure 4.1 shows a 3D visualization of a normal patient using CT scan data from a DICOM image format.[86]

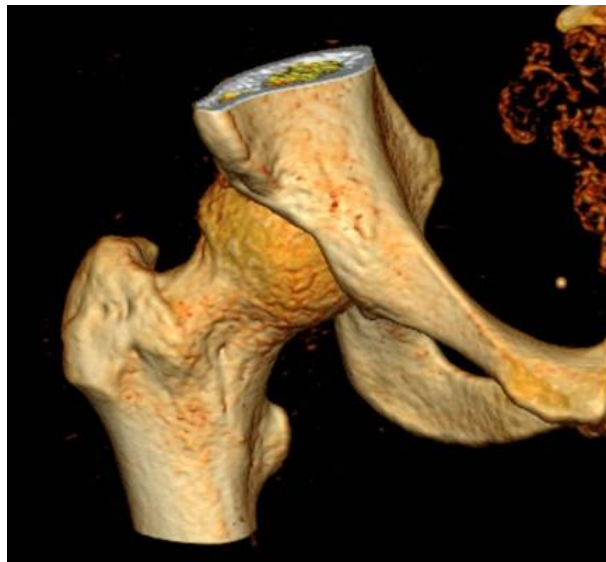


Figure 4.1: 3D visualization of Normal patient 1 right hip based on DICOM image format.

Each CT scan has a variable number of cross-sectional images depending on the scanned body part, space between slices and size of the patient. Consequently, a greater number of images indicates less space between each image, thus providing a more accurate geometry.

In order to have adequate results, for this research models constructed required an average of 200 slices. CT scan images are presented on greyscale and show all tissues inside the body according to the density of the material. Bone is well defined but not cartilage and soft tissue, in consequence cartilage geometry cannot be constructed using CT scans. Furthermore, pixel grey scale values are defined by the density of the material, bone tissue presents a white colour while soft tissue presents a clear/dark grey.[86]

ScanIP[®] reads the DICOM images and displays each of them in a transverse, coronal and sagittal planes, and also provides to the user a 3D preview of the surface as Figure 4.2 shows. ScanIP[®] provides a reference frame using cartesian coordinates, with the axis X, Y, Z, corresponding to the axis of the human body. The software also provides to the user the option to align or rotate the geometry. It also has the option change coordinate system. The assigned coordinate system is maintained during export of the model and preserved throughout further analysis processes. On this research, coordinate system is based on the axis of the human body.[86]

Based on the greyscale, ScanIP[®] takes pixel values within the threshold predefined by the user and constructs a layer called “mask”. ScanIP[®] names CT scan images as background, mask layers are presented in top of the background to facilitate edition of the mask. This process is called “segmentation”. Threshold value were defined to select only pixels in cortical bone.[86]

ScanIP[®] provides to the user different segmentation and morphological filters. The segmentation tool called “Paint” allows to merge and split segments in a mask, by selecting of just an individual pixel, this tool is very useful when working on complex geometries. [86]

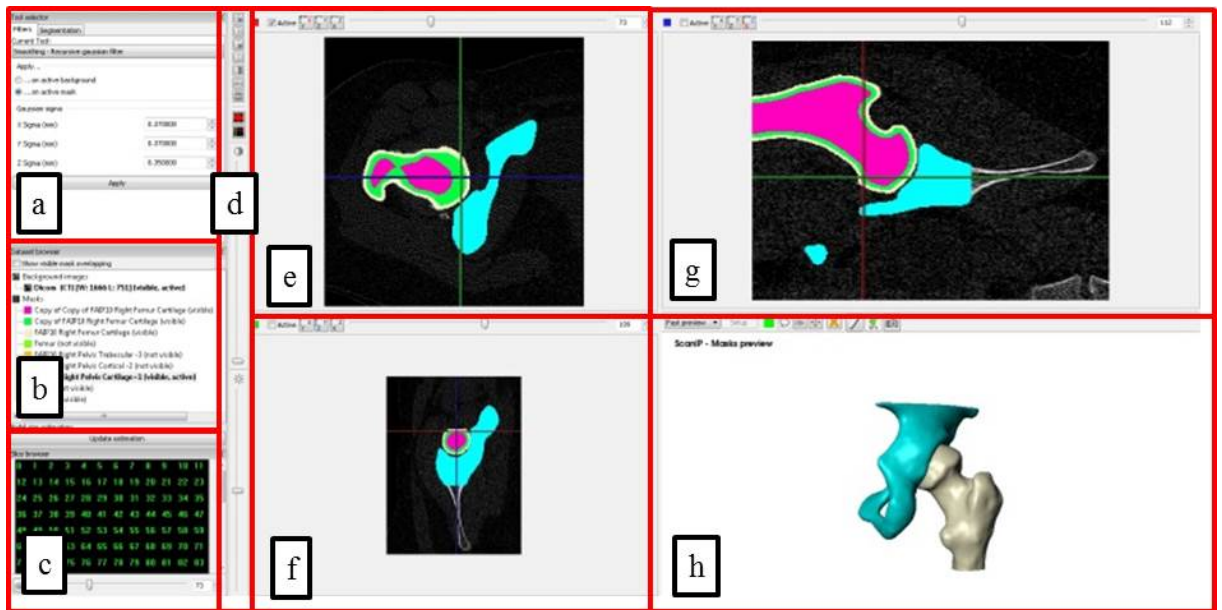


Figure 4.2: ScanIP® work area. a) Segmentation tools and filters window. b) Mask list window. c) CT scan slides window. d) Mask visualization tools window. e) Transverse view window. f) Sagittal view window. g) Coronal view window. h) Fast preview window

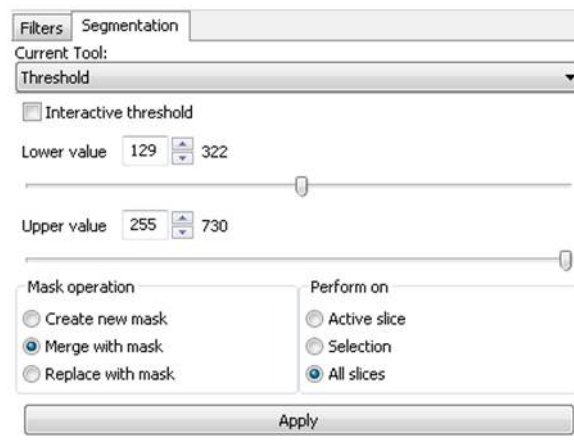


Figure 4.3: ScanIP® threshold window. ScanIP® allows you to manipulate lower and upper values of the threshold. Also, it gives the option to update the visualization of the mask in real time.

Morphological filters are applied in the colour masks to improve geometries surfaces after segmentation. First, a “binarisation” filter is applied to assign a binary value to pixels to the mask in order to eliminate the connection between the mask and the background, and to homogenize the mask itself. Afterwards, a “smoothing-recursive Gaussian” filter is applied

two times to refine contours of the surfaces as shown in Figure 4.4.

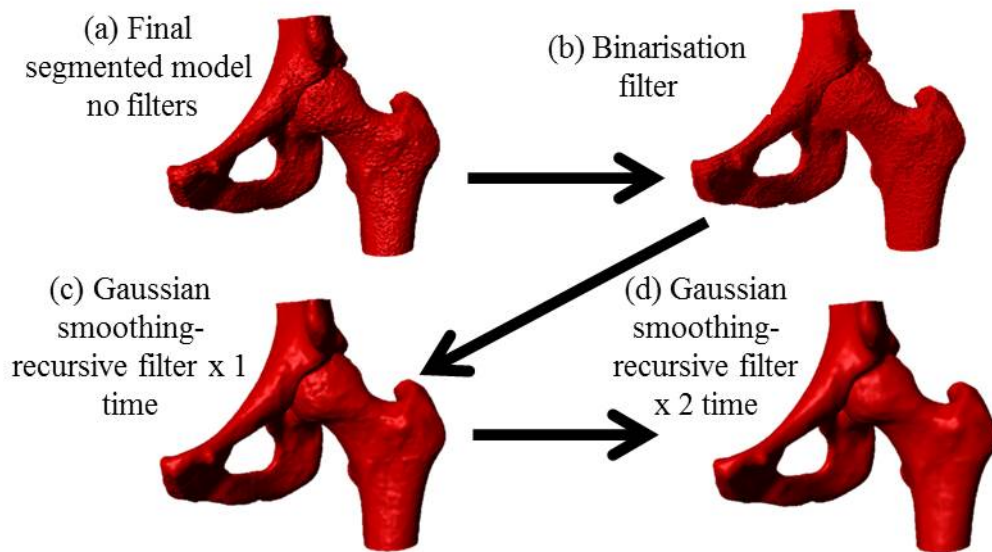


Figure 4.4: Surface smoothing process

After creating the cortical bone, trabecular bone and cartilage surfaces were constructed using morphological filters in ScanIP[®]. In order to create different tissues, masks with different colours were used. Afterwards, morphological filters were applied to variate the size of surface. In order to achieve the trabecular surface, an “erode” filter was applied to the segmented cortical bone. As its name implies, this filter erodes the segmented mask to get a new segmented mask but thinner than the previous mask.

Cartilage surface was constructed in a similar manner, but the morphological filter “dilate” was used instead. This filter expands the segmented mask to create a new thicker segmented mask. Figure 4.5 shows segmented trabecular bone, cortical bone and cartilage.

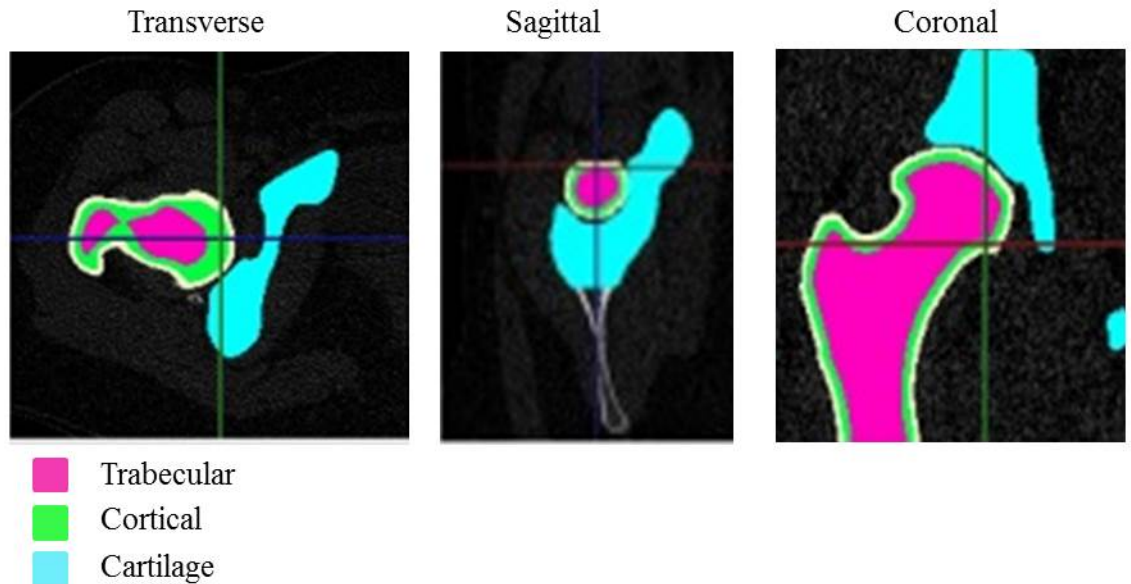


Figure 4.5: Different mask sizes of cortical bone to create trabecular bone and cartilage in ScanIP®.

4.2.2 Finite element models

Geometries used in finite element and sphericity analysis were generated in ScanIP®. 3D surfaces from ScanIP® were exported as (*.igs) files. This process converts 3D surfaces into surface models conformed by triangular geometric entities. A maximum of 5000 triangles per part was used on each part as this was the maximum number of triangles permissible on the computer system.

Afterwards, (*.igs) files were imported into the “part module” of Abaqus/CAE®. In Abaqus/CAE® boolean operations were performed to construct cortical and cartilage models with correct thickness. The models of the different tissues were cut on the “Assembly module” using the “Merge/Cut Instances” button. Afterwards, cortical trabecular bone were put together, next, trabecular bone was cut from the cortical bone. In this research, constant thickness values of cortical bone and cartilage were based on previous research work, according to literature cortical bone in the femur has a constant thickness of 1.8 mm and cartilage a constant thickness of 1.5 mm. [29–31].

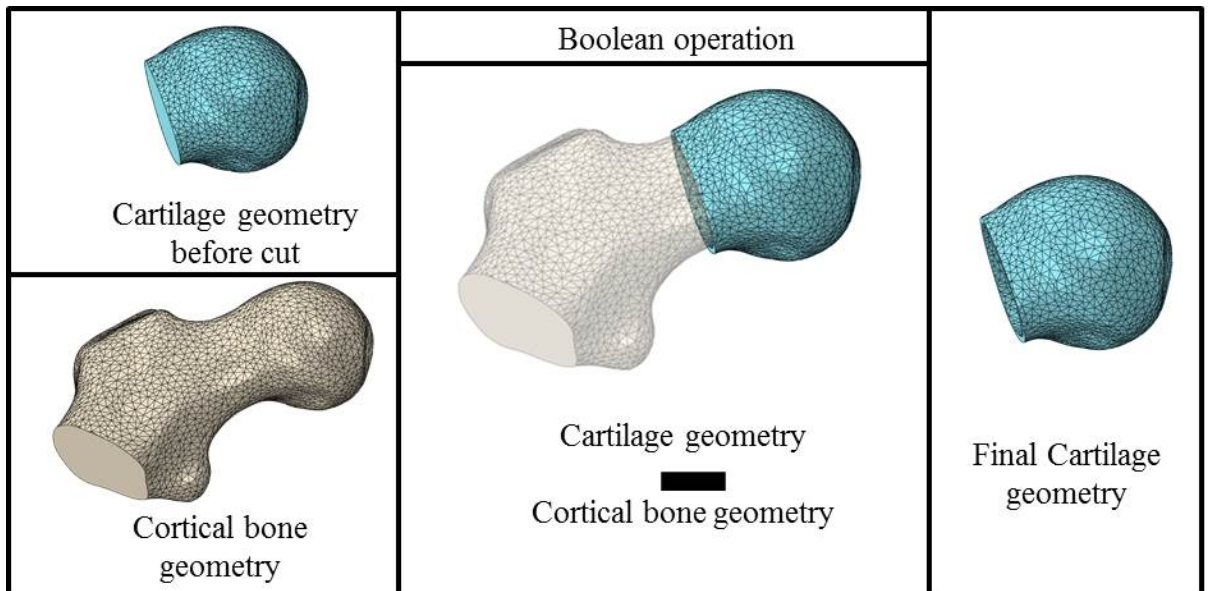


Figure 4.6: Boolean operation to create the cartilage geometry on Abaqus/CAE®.

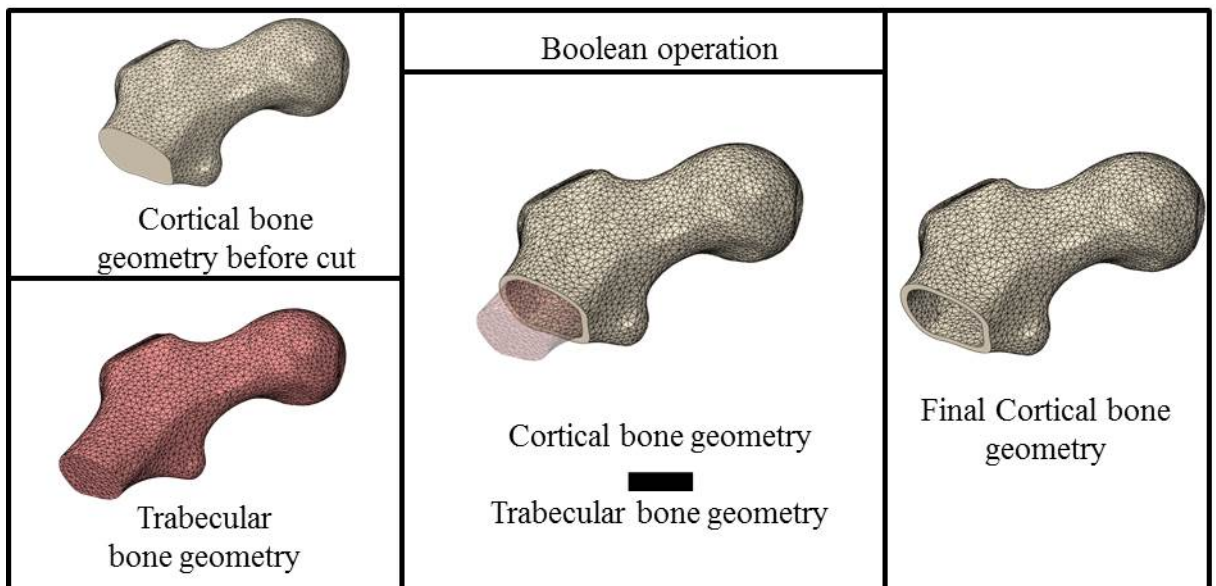


Figure 4.7: Boolean operation to create the cortical geometry on Abaqus/CAE®

On Abaqus/CAE® on the part module of the final cortical bone geometry, a face is created using the inner edges of the hole, on the femur the hole is found in the bottom part of the model

while on the pelvis the hole is found in the upper part of the mode. Afterwards, using the tool “Create Solid” all edges of the cut and the new face are selected to create a new cell in the same part. Figure 4.8 illustrates the process to create a new cell in the same part geometry.

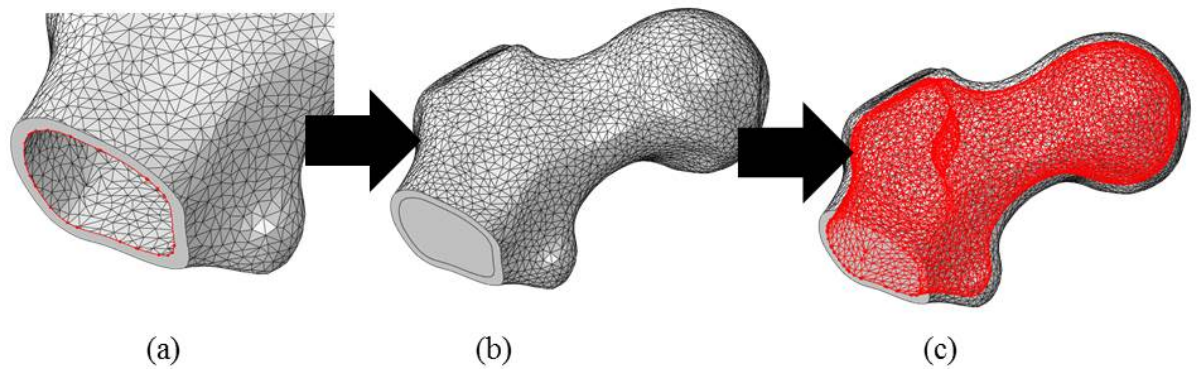


Figure 4.8: Selection of inner edges on the bottom of femur to create a new cell. a)Edges of the hollow at the bottom of the femur part selected. b)New face created. c)Edges to create a new cell selected.

Subsequently, on “Assembly” cartilage, trabecular and cortical bone were assembled to form a complete model. In order to attach cortical and trabecular to cartilage, on the same module the “Merge/Cut Instances” tool was used to attach the cortical and trabecular bone to the cartilage. This operation allows the model to behave as a single part, but with different sections that can be assigned different mechanical properties.

4.2.3 Material properties

The mechanical properties are the material characteristics which define the behaviour of the material when it is exposed to some type of force. In contrast to engineering materials, such as metals, plastics or composites, biological material alter their mechanical properties and morphology in response to external stimuli.

In this research, cartilage, cortical and trabecular bone were assumed to be linearly elastic and isotropic materials. For linear elastic materials the most common properties are the modulus of elasticity and Poisson’s ratio (ν). Mechanical property values were assigned

to each tissue according to literature. Table 4.1 shows the mechanical properties assigned to cartilage, trabecular and cortical bone in this research.[87]

Material	Young's Modulus E (MPa)	Poisson's Ratio(ν)
Cortical bone	17,000	0.3
Trabecular bone	70	0.2
Cartilage	15	0.45

Table 4.1: Young's modulus, poisson's ratio of cartilage, cortical and trabecular bone.

4.2.4 Loading conditions

The body weight and muscles around the hip joint produce a force which acts on the pelvic bone. Generally, only the resultant hip joint force and its directions are determined and applied to the pelvic bone. However, the real loading to the pelvic bone is a distributed load rather than a concentrated load. On Abaqus/CAE[®] to create a distributed force, a kinematic coupling was employed. A kinematic coupling is a constraint which connects a reference point with set of nodes related to the surface of interest, in consequence connected nodes have the same displacement and rotation as the reference point.

In order to apply an adequate distributed force to the pelvic bone a local coordinate system was created. One of the axes coincides with the line of action of the resultant hip joint force. After a kinematic coupling was created, connecting all nodes from the top surface the pelvic bone with the reference point. The total hip joint force was applied to the reference point and transmitted to all the nodes of the surface.

The direction and total force joint applied to the pelvis was calculated based on the anatomical coordinate system and components of joint contact described by Bergmann et al. [88]. Figure 4.9 illustrates Bergmann coordinate system and the respective angles of the hip joint contact components for one-leg-standing position. For this research a constant body weight of 690N was defined for all subjects.

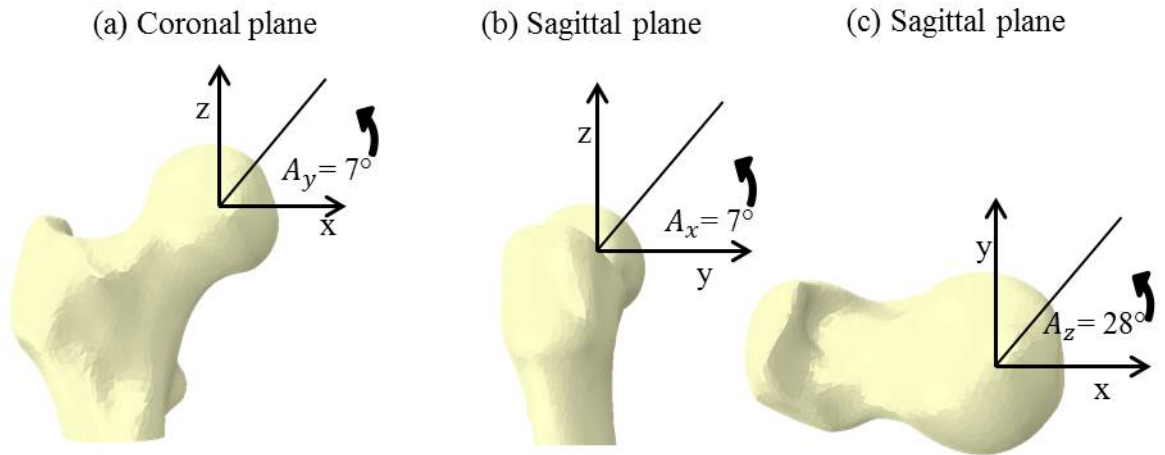


Figure 4.9: Bergmann's coordinate system and angles of the components.

4.2.5 Boundary and contact conditions

Boundary conditions define how the components of a model will interact with each other on experimental and theoretical setups. As it was explained in Chapter 2, the hip joint has an important role on the locomotion of the human body, in consequence other components cause forces that may affect the hip joint. For this reason, it is important to understand the mechanics of the joint and the mechanical effects of its components.

In this research, the analysis performed on hip joints was static on a one-leg-standing position. To correctly recreate this posture the following boundary conditions were applied to the models:

- a) The distal femur was totally fixed.
- b) The pelvic bone was permitted to move only on the direction of the total hip joint force.

The same local coordinate system created to apply the distributed force to the pelvic bone was used to apply the boundary condition (b). The reference point of the kinematic coupling was allowed to move only in the direction of the applied force.

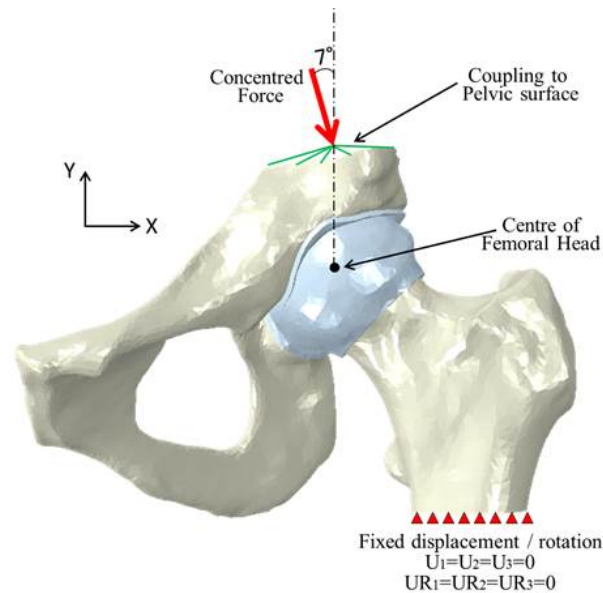


Figure 4.10: Boundary conditions in the coronal plane. The green arrow on the local coordinate system shows the axis where the pelvis is allowed to move.

Part of the analysis of this research was to examine the contact that occurs in the hip joint. For this reason, in order to obtain values and patterns of the contact between the acetabulum and femoral head, contact conditions had to be defined on Abaqus/CAE[®]. A "surface-to-surface" contact interaction was defined because the contact is between two deformable surfaces. The entire surface of both cartilage surfaces was considered in the contact interaction. The contact properties were defined as mechanical contact with tangential behaviour. Furthermore, the surfaces were considered to be frictionless, according to previous work experimental work the static friction coefficient between human cartilage on cartilage is extremely low, approximately 0.06 for a pressure of 2.4 MPa and a temperature of 37°C. [89]

4.2.6 Mesh analysis

Contact area between the femoral head cartilage and acetabulum cartilage patterns and values were analysed on this research, for this reason it was required to have accurate results without using excessive computational resources. The accuracy of results depends on the defined mesh used on the geometries of the hip joint components.

Hip joint geometries were meshed in Abaqus/CAE[®]. Discrete geometries used in the

Finite Element (FE) analysis were very complex, for this reason 4-node linear tetrahedral, also known as “C3D4” (Continuum, 3D, 4 node), elements were used. Figure4.11(a) shows a section of the distal part of a meshed femur geometry and Figure4.11(b) illustrates a “C3D4” element.

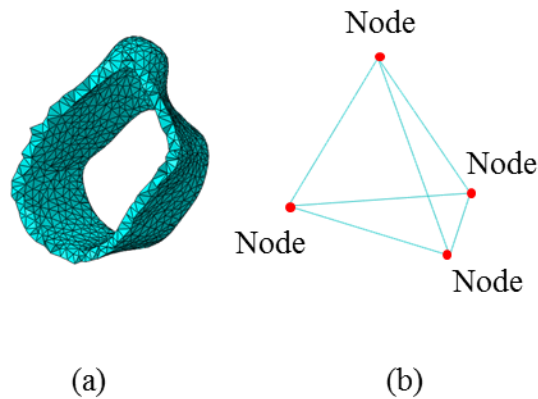


Figure 4.11: (a) Meshed geometry using tetrahedral elements. (b) Tetrahedral element configuration.

The mesh used in cartilage geometries was finer than the mesh used in the bone geometries because the scope of the FE analysis was the contact interaction between the articular cartilages of the hip.

The analysis consisted in comparing contact areas and maximum contact pressures on the acetabulum in normal hips, dysplastic hips and hips with impingements models from three mesh densities. The criterion used for the selection of an appropriate element size was that the results between the different element sizes should not vary more than 1%.

Different mesh densities were achieved by varying the “seed” parameter in the “mesh module” on Abaqus/CAE®. Mesh densities were changed on both cartilages, the femoral head cartilage and acetabulum cartilage.

The mesh density with a “seed” of 1 was chosen, since contact area and contact pressure results from the finer mesh density and the selected mesh density changed by <1.0%. Table 4.2 shows the number of elements and results from different “seed” values. Figure 4.12 shows different sizes of meshes in the femoral head.

Seed	Total number of Elements	Contact area	Contact pressure
3	112,000	573.1 mm ²	7.6 MPa
1	198,000	629.9 mm ²	7.5 MPa
0.8	258,000	633.9 mm ²	7.4 MPa

Table 4.2: Table of mesh densities and their perspective number of elements, contact area and maximum contact pressures

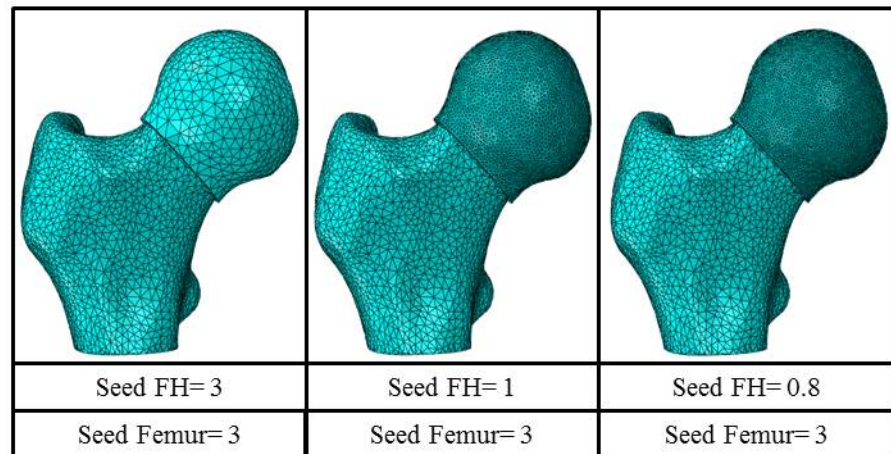


Figure 4.12: Different mesh sizes of the femoral head cartilage.

4.3 Model validation

The model validation of this research was conducted by comparing the results of contact areas and peak contact pressures with previous experimental work and numerical studies under one-leg-standing loading condition from normal and dysplastic hip joints. Anderson et al [31] used a pressure sensitive film to measure contact pressure in a cadaveric subject. Forces from daily routine activities were applied to the hip. The peak contact pressure measured from the experiment was of 10 MPa, and from their FE model they obtained a peak contact pressure of 10.8 MPa with a load of 820N.

Three normal hip joints were selected (N2, N7 and N10) were selected and were subjected to the same loading condition used by Anderson et al. Normal hip joint models predicted

an average peak contact pressure of 9.3 MPa, this value is close to the value obtained by Anderson et al. experimentally (10 MPa) and from their FE analysis (10.8 MPa).

Regarding DDH, Liu et al. [3] performed a finite element analysis on 10 dysplastic hip joints to investigate the influences of using patient specific cartilage model or constant thickness cartilage models on the simulation results. Liu et al.[3] loading conditions were based on Bergmann et al. previous work[88].

This research focuses on the shape of acetabulum and femoral head articular surfaces and its effect on the mechanical behaviour of hip joints from normal patients and patients suffering from DDH and FAI. Chapter 5 describes in detail the procedure undertaken to measure “Sphericity” and the analysis to investigate the effect of the hip joint “Sphericity” on the articular surface mechanical behaviour of normal, FAI and DDH hip joint groups.

Chapter 5

Sphericity analysis normal hip joint group

5.1 Introduction

As mentioned in chapter 3, it is believed that sphericity plays an important role on the mechanical behaviour inside the hip joint. In order to investigate how sphericity of the hip joint affects the contact area and pressure values and patterns on normal hip joints for each hip in the normal group, morphological features were related to sphericity and results from FE analysis. [1, 3, 4]

This chapter describes the procedure to quantify anatomical features and the “Sphericity” on the acetabulum and femoral head surfaces, in particular the general process used to obtain angles that describe the structure of the hip joint, acquisition of the cloud of points of the hip joint articular surfaces, and lastly, obtain the “Sphericity” of acetabulum and femoral head.

In addition, anatomical features to describe the structure of the hip joint include angles used by radiologists to diagnose dysplasia of the hip, such as Centre-Edge, Tonnis and Sharp angles. Additionally, angles measured from 3D models that describe the orientation of the acetabulum and the femoral head are also included.

Also, this chapter presents a description of the analysis undertaken to obtain the typical characteristics of the normal hip joint group based on FE results and morphological features

of the hip joint, including “Sphericity”. This analysis consists of the investigation of the relationship between morphological features, “Sphericity”, contact area and pressure values and patterns. A description of the features that distinguish the normal hip joint group is also presented.

5.2 Computer models development

Ten normal hip joints models were developed to quantify sphericity of articular surfaces of acetabulum and femoral head, and also to analyse contact area and pressure patterns and values when the hip joint is one-leg-standing position. Procedures to develop computer models and details of the finite element analysis are described in Chapter 6.

5.3 “Sphericity” quantification of the acetabulum and femoral head

The following method was designed to assess and quantify “Sphericity” of the femoral head and acetabulum by comparing their natural articular surface to an ideal sphere, which is fitted to their respective surface topologies. To accomplish this, first it was important to properly define the acetabulum and femoral head surfaces. For this purpose anatomical features found in the pelvis and femur were used.

5.3.1 Articular surfaces

Surfaces were defined using Abaqus/CAE[®] tools. Its user interface and tools facilitate the task to create partitions in the model, and obtain coordinate data from desired nodes of the model. The femoral head surface is part of the femur geometrical used for the finite element analysis, and the acetabulum is part of the pelvis geometry. The following methods describes the process to define the articular surfaces of the femoral head and acetabulum for the “Sphericity” quantification.

Femoral Head surface

To define the femoral head articular surface for the “Sphericity” analysis the equator of the femoral head was used. On Abaqus/CAE® in the part module of the cartilage model of the femur, following a line that describes the femoral head equator, as Figure 5.1(a) illustrates, three points were selected, one point on the inferior part, one on the superior anterior part and another point the superior posterior part of the femoral head. Afterwards, a datum plane was defined using these three points. And, finally, a partition cell was created using the datum plane. Figure 5.1(b) shows the final partition of the femoral head cartilage.

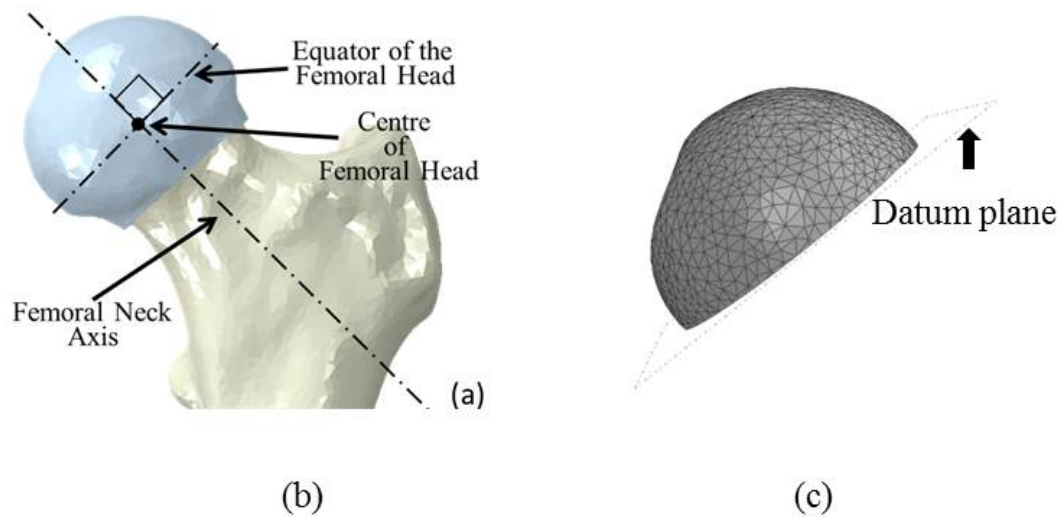
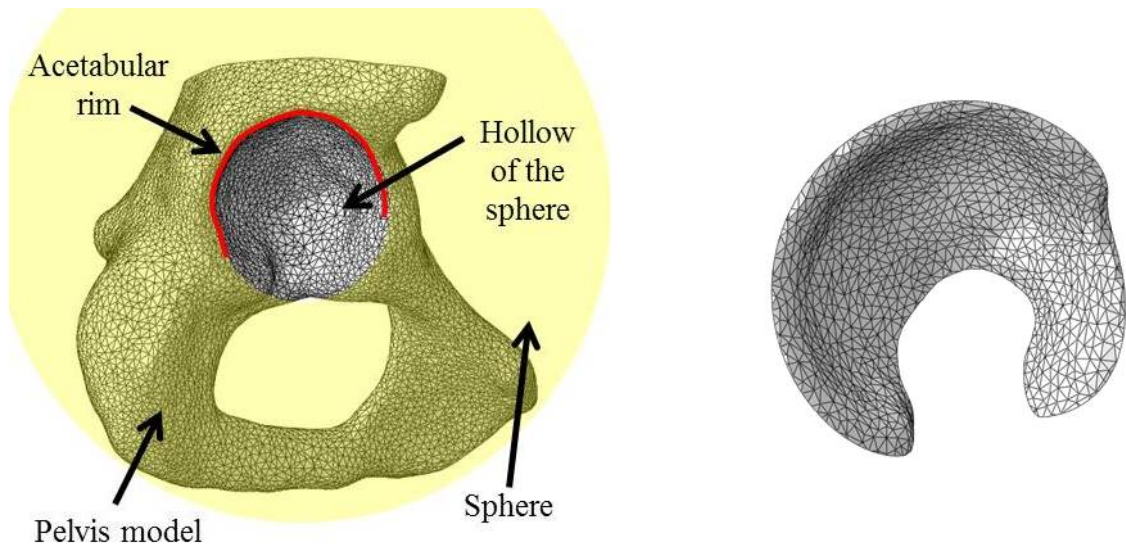


Figure 5.1: Proximal femur structure and epiphyseal line. (a) Proximal femur structure and its name. (b) Concave section formed by the epiphyseal line, arrows show the starting point of the articular surface. (c) Femoral head cartilage surface partition.

Acetabulum surface

Concerning the acetabulum, to define the articular surface the acetabular rim was used. On Abaqus/CAE® in the assembly module, an instance of the cartilage model of the pelvis was created. Subsequently, a hollow sphere was created and fitted in the acetabulum of the pelvis, the diameter of the hollow and position of the sphere were defined that such covered the acetabular rim as Figure 5.2(a) shows. Afterwards, a cut operation was performed subtracting

the hollow sphere from the pelvis model to, finally, obtain the acetabular articular surface. Figure 5.2(b) illustrates the resulting geometry of the articular surface of the acetabulum.



(a) Pelvis model and representation of the hollow sphere. (b) Final geometry of the articular surface of the acetabulum.

Figure 5.2: Definition of the acetabular articular surface.

Once the acetabulum and femoral head surfaces were defined, parts were meshed on Abaqus/CAE[®] and coordinate data of the nodes was obtained, and subsequently, data of the nodes was saved in a spreadsheet file. On the femoral head, nodes from the hollow of the ligament teres attachment were discarded because this section of the femoral head is not in contact with the acetabulum.

5.3.2 Method to create the “Ideal” Sphere of the acetabulum and femoral head

For each hip joint, two “Ideal” spheres were defined, one for the acetabulum and another sphere for the femoral head. Coordinate data of the surfaces was used to define the centre and radius of each of the spheres.

In order to define the “Ideal” sphere centre, a least squares fitting method was employed on the X,Y,Z, data of the surfaces [90], coordinate data was manipulated and processed in

Wolfram Mathematica. Equations to define the centre of “Ideal” sphere [90] are as follows:

$$X = \frac{\left\{ (S_{xx^2} + S_{xy^2} + S_{xz^2})(S_y^2 S_z^2 - S_{yz}^2) + (S_{yx^2} + S_{yy^2} + S_{yz^2})(S_{xz} S_{yz} - S_{xy} S_z^2) \right.}{2 \{ S_x^2 S_y^2 S_z^2 + 2 S_{xy} S_{yz} S_{xz} - S_x^2 S_{yz}^2 - S_{xz}^2 - S_z^2 S_{xy}^2 \}} \left. + (S_{zx^2} + S_{zy^2} + S_{zz^2})(S_{xy} S_{yz} - S_{xz} S_y^2) \right\}} \quad (5.1)$$

$$Y = \frac{\left\{ (S_{xx^2} + S_{xy^2} + S_{xz^2})(S_{xz} S_{yz} - S_{xy} S_z^2) + (S_{yx^2} + S_{yy^2} + S_{yz^2})(S_x^2 S_z^2 - S_{xz}^2) \right.}{2 \{ S_x^2 S_y^2 S_z^2 + 2 S_{xy} S_{yz} S_{xz} - S_x^2 S_{yz}^2 - S_{xz}^2 - S_z^2 S_{xy}^2 \}} \left. + (S_{zx^2} + S_{zy^2} + S_{zz^2})(S_{xy} S_{xz} - S_{yz} S_x^2) \right\}} \quad (5.2)$$

$$Z = \frac{\left\{ (S_{xx^2} + S_{xy^2} + S_{xz^2})(S_{xy} S_{yz} - S_{xy} S_y^2) + (S_{yx^2} + S_{yy^2} + S_{yz^2})(S_{xz} S_{xy} - S_{yz} S_x^2) \right.}{2 \{ S_x^2 S_y^2 S_z^2 + 2 S_{xy} S_{yz} S_{xz} - S_x^2 S_{yz}^2 - S_{xz}^2 - S_z^2 S_{xy}^2 \}} \left. + (S_{zx^2} + S_{zy^2} + S_{zz^2})(S_x^2 S_y^2 - S_{xy}^2) \right\}} \quad (5.3)$$

After the centre coordinates of the “Ideal” sphere were calculated, the radius, r , of the sphere can be calculated. This is accomplished by computing the distance of each node to the centre of the best fitted sphere and calculating the average of the distances, this described by equation 5.4. Figure 5.3 presents a visual representation of this process.

$$r = \sum_{i=1}^n \sqrt{(x_i - X)^2 + (y_i - Y)^2 + (z_i - Z)^2} / n \quad (5.4)$$

Where n is the total number of nodes of the surface.

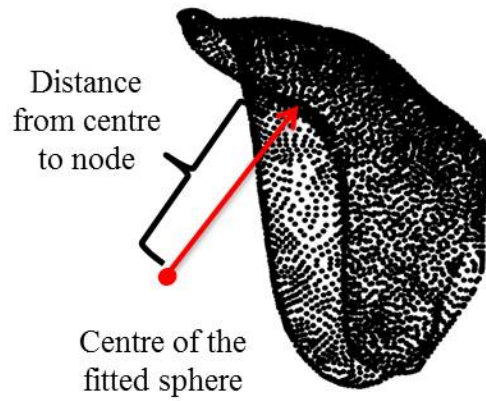


Figure 5.3: Visual representation of the distance of a node to the centre of the “Ideal” sphere.

5.3.3 Sphericity percentage

To assess the “Sphericity”, the natural shape of the acetabulum and femoral head were compared to their corresponding “Ideal” spheres. The comparison is performed by calculating the average of the absolute normalized distance difference between the node distance to the centre of the sphere and the radius of the sphere. The absolute value of the difference distance was used because when calculating the average distance difference of the nodes, negative values cancel positive values resulting in a very small number. Also, the distance difference was normalized by dividing it by the radius of the “ideal” sphere.

The average of the absolute normalized distance difference between the node distance to the centre of the sphere and the radius of the sphere quantifies the “Asphericity” of the acetabulum and femoral head natural shape, in order to present the results in regards of “Sphericity”, the “Asphericity” of the surface was subtracted from one unit, which is the “Sphericity” percentage of the “ideal” sphere. Finally, the “Sphericity” percentage was converted to a 0 to 100 scale. Equation 5.5 calculates the “Sphericity” of the natural shape of the acetabulum and femoral head.

$$Sph = \left(1 - \frac{\sum_{i=1}^{n_T} |d_i - r|}{r \cdot n_T} \right) * 100 \quad (5.5)$$

Where Sph is “Sphericity” percentage, n_T is the total number of nodes, d_i is the distance of

the node to the centre of the ideal sphere, and r is the radius of the ideal sphere.

5.3.4 Average normalised distance

In order to visualize and observe how “Sphericity” is distributed a weighted “Sphericity” of the surface was calculated. In this procedure the acetabulum and femoral head surface were divided into eight equal regions of 45° wide [91], and were labelled with roman numerals, as Figure 5.6 illustrates. Location of the zones and their respective roman numeral are: Superior anterior as I, superior, II, superior posterior, III, lateral posterior, IV, inferior posterior, V, inferior, VI, inferior anterior, VII, lateral anterior, VIII.

Moreover, position of the sections was defined according to anatomical features of the femur and pelvis bone structures and the centre of their respective “ideal” spheres. For the femoral head the orientation of the femoral neck in a the transversal and coronal planes was used, on the acetabulum the orientation of the acetabular notch was used for this purpose.

To measure the orientation of these features, a local coordinate system, with the axes of the CT scan, was set on the centre of the “ideal” spheres of the acetabulum and femoral head. Furthermore, angles located on the anterior quadrants obtain a negative value, in contrast, angles on the posterior quadrant have a positive value.

The femoral head the orientation angle of the femoral neck in the transversal and coronal plane is the angle between the X axis and a line parallel to the femoral neck in half and passes through the centre of the femoral head “ideal” sphere as Figure 5.4.

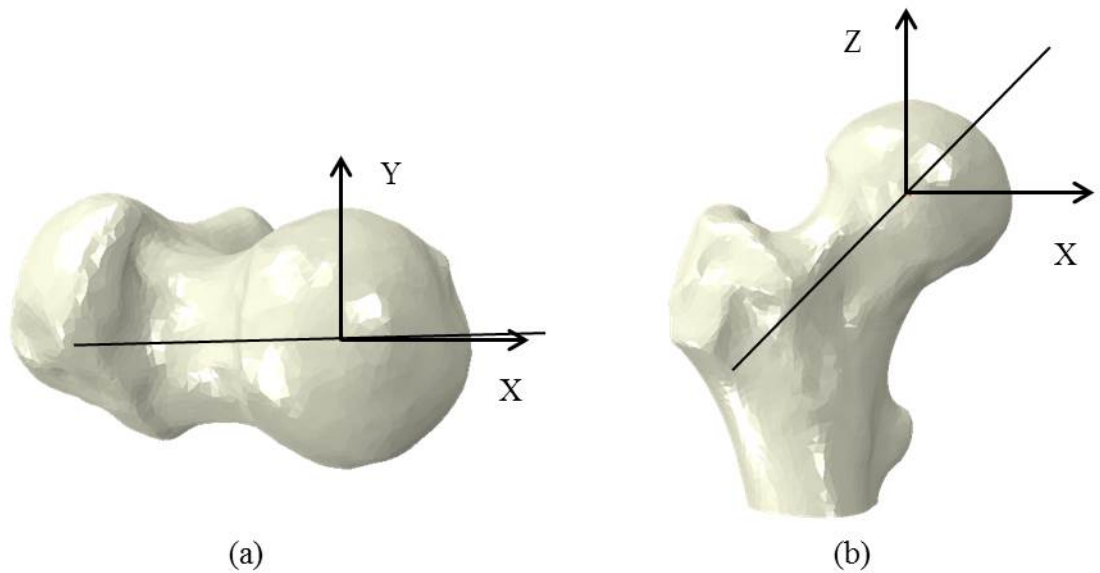


Figure 5.4: Femoral head orientation on the: (a)transversal plane and (b)coronal plane.

The acetabular notch angle orientation is defined by the proximal part of the acetabular surface. On the transversal plane, a line is drawn from the most proximal anterior point (A) of the acetabulum surface to the most proximal posterior point of the surface(P). The acetabular notch angle is the angle between the X axis and line perpendicular to \overline{AP} and contains the centre of the acetabular “ideal” sphere as Figure 5.5 illustrates.

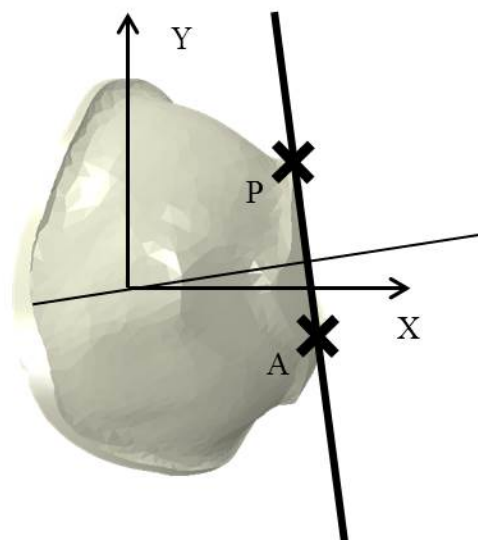


Figure 5.5: Surface sections of the: (a)Acetabulum and (b)Femoral head

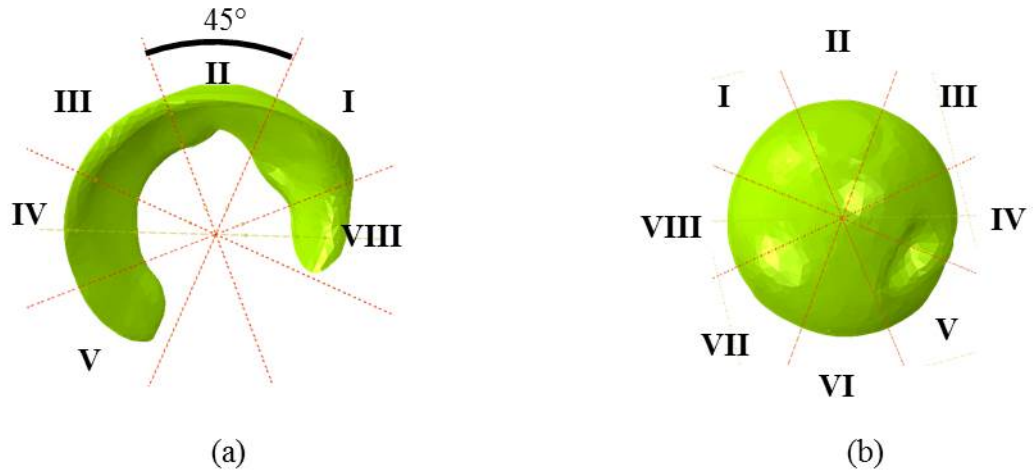


Figure 5.6: Surface sections of the: (a)Acetabulum and (b)Femoral head

The weighted “Sphericity” is calculated using the equation 5.6 where n_s is the number of nodes in the section.

$$ASph_s = \left(\frac{\sum_{i=1}^{n_s} |d_i - r| d_i}{r \cdot n_s} - 1 \right) * \frac{100 \cdot n_s}{n_T} \quad (5.6)$$

The “asphericity”, $ASph_s$, of the obtained sections was calculated with equation 5.7. The average of the node distances of the section to the centre of the “ideal” sphere is calculated. The result is divided by the radius of the “ideal” sphere to obtain a ratio that describes how smaller or bigger the average of the section nodes distance is from the radius of the “ideal” sphere. Subsequently, the ratio is subtracted one unit to get the average “asphericity” of the surface. Finally, the “asphericity” value is multiplied converted to 0 to 100 scale and multiplied by the contribution of the section to the overall surface. The sign of the obtained value was used to make a rough description of the surface section.

$$ASph_s = \left(\frac{\sum_{i=1}^{n_s} d_i}{r \cdot n_s} - 1 \right) * \frac{100 \cdot n_s}{n_T} \quad (5.7)$$

A positive $ASph_s$ value indicates that the average distance of that region is outside the ideal sphere. In contrast, a negative $ASph_s$ value indicates that the average distance of the nodes in that section is inside the ideal sphere. A value of zero indicates that the average

distance is on the radius of the ideal sphere. Position of the nodes and their respective signs are illustrated in Figure 5.7

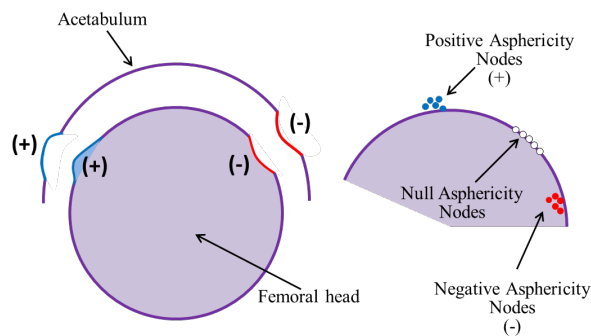


Figure 5.7: Position of the node and sign asphericoty

There are 9 combinations of sections “Asphericity” signs to consider and the effect on the distance between the femoral head and acetabulum as Table 5.1 shows.

Femoral Head Asphericity sign	Acetabulum Asphericity sign	Distance between surfaces
-	-	Congruent
-	0	Widened
-	+	Very Widened
0	-	Narrowed
0	0	Congruent
0	+	Widened
+	-	Very Narrowed
+	0	Narrowed
+	+	Congruent

Table 5.1: “Asphericity” sign of the femoral head and acetabulum and the effect on surface distances.

5.4 Centre-Edge, Tönnis, acetabular and alpha angles

Anatomical angles related to Femoroacetabular Impingement and Dysplasia of the hip were measured from CT scans and X-Rays of 30 subjects. The Centre-Edge (CE), Tönnis, Sharp,

and Alpha angles were measured patients X-Rays. For these procedures, the centre of the femoral head on the X-Ray was defined by the intersection of two perpendicular diameters of a fitted circle in the femoral head[53].

5.5 Results

5.5.1 Table of results

The tables shown in Figures 5.8, 5.9, and 5.10, display anatomical angles and results from the “Sphericity” and finite element analysis from each of the 10 hips in the normal hip joint group. From left to right, the table displays the identification number of the subject, anatomical angles (CE and Tönnis), “Sphericity” of the acetabulum and femoral head total surface and by sections, contact area and peak contact pressure values from one-leg-standing position, and finally an “Asphericity” visualization of the acetabulum and femoral head.

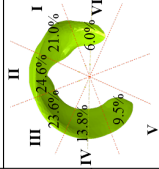
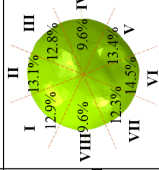
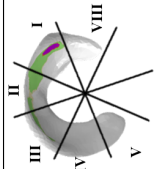
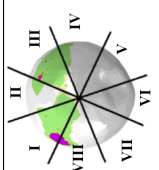
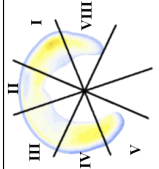
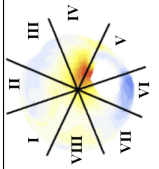
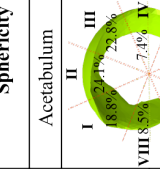
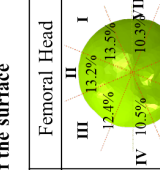
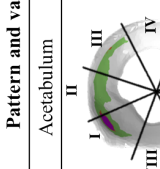
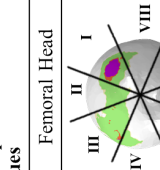
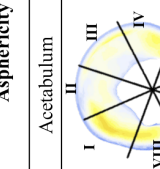
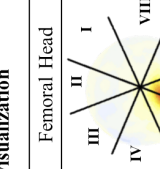
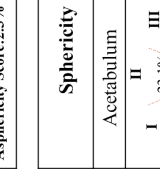
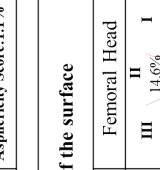
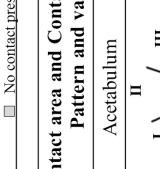
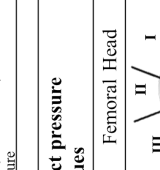
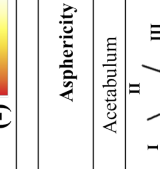
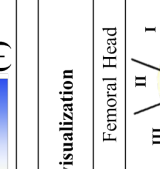
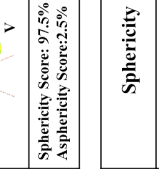
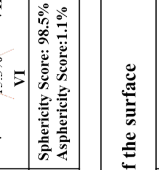
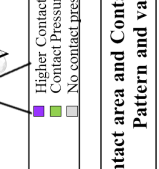
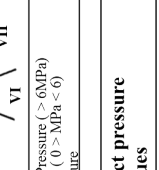
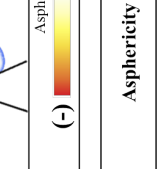
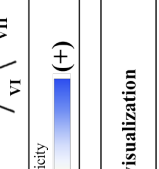
Subject	Angles		Sphericity of the surface				Contact area and Contact pressure Pattern and values				Asphericity visualization			
	CE:	Tomnis:	Acetabulum	Femoral Head	Acetabulum	Femoral Head	Acetabulum	Femoral Head	Acetabulum	Femoral Head	Acetabulum	Femoral Head	Acetabulum	Femoral Head
Normal Right Hip 1	31.3°	5.4°	 I 23.6% II 21.6% III 21.0% IV 13.8% V 9.5% VI 6.0% VII 9.6% VIII 9.6%	 I 13.1% II 12.9% III 12.8% IV 12.8% V 13.4% VI 14.5% VII 13.3% VIII 13.3%	 I II III IV V VI VII VIII	 I II III IV V VI VII VIII	 I II III IV V VI VII VIII	 I II III IV V VI VII VIII						
	Contact Area: 658.0 mm ² Max Contact Pressure: 7.5 MPa Sphericity Score: 98.5% Asphericity Score: 1.5% Higher Contact Pressure (> 6MPa) Contact Pressure (0 > MPa < 6)			Sphericity Score: 98.5% Asphericity Score: 1.5% Sphericity Score: 98.5% Asphericity Score: 1.5%				Higher Contact Pressure (> 6MPa) Contact Pressure (0 > MPa < 6) No contact pressure						
Normal Left Hip 2	34.2°	-0.4°	 I 18.8% II 21.1% III 28.8% IV 7.4% V 16.1% VI 1.6% VII 13.3% VIII 8.5%	 I 13.2% II 13.5% III 13.5% IV 10.3% V 13.3% VI 13.3% VII 13.3% VIII 13.3%	 I II III IV V VI VII VIII	 I II III IV V VI VII VIII	 I II III IV V VI VII VIII	 I II III IV V VI VII VIII						
	Contact Area: 632.0 mm ² Max Contact Pressure: 7.4 MPa Sphericity Score: 97.7% Asphericity Score: 2.3% Higher Contact Pressure (> 6MPa) Contact Pressure (0 > MPa < 6)			Sphericity Score: 97.7% Asphericity Score: 2.3% Sphericity Score: 98.6% Asphericity Score: 1.1%				Higher Contact Pressure (> 6MPa) Contact Pressure (0 > MPa < 6) No contact pressure						
Normal Left Hip 3	31.0°	9.7°	 I 20.4% II 23.1% III 21.3% IV 9.2% V 16.3% VI 16.3% VII 16.3% VIII 7.5%	 I 14.6% II 14.6% III 15.7% IV 8.0% V 10.9% VI 12.8% VII 15.3% VIII 8.6%	 I II III IV V VI VII VIII	 I II III IV V VI VII VIII	 I II III IV V VI VII VIII	 I II III IV V VI VII VIII						
	Contact Area: 724.0 mm ² Max Contact Pressure: 6.5 MPa Sphericity Score: 97.5% Asphericity Score: 2.5% Higher Contact Pressure (> 6MPa) Contact Pressure (0 > MPa < 6)			Sphericity Score: 97.5% Asphericity Score: 2.5% Sphericity Score: 98.5% Asphericity Score: 1.1%				Higher Contact Pressure (> 6MPa) Contact Pressure (0 > MPa < 6) No contact pressure						
Normal Right Hip 4	27.3°	10.0°	 I 23.5% II 24.5% III 19.7% IV 9.6% V 16.3% VI 16.3% VII 16.3% VIII 5.5%	 I 13.4% II 13.4% III 14.2% IV 11.9% V 13.3% VI 13.3% VII 11.2% VIII 11.9%	 I II III IV V VI VII VIII	 I II III IV V VI VII VIII	 I II III IV V VI VII VIII	 I II III IV V VI VII VIII						
	Contact Area: 525.9 mm ² Max Contact Pressure: 14.9 MPa Sphericity Score: 98.1% Asphericity Score: 1.9% Higher Contact Pressure (> 6MPa) Contact Pressure (0 > MPa < 6)			Sphericity Score: 99.0% Asphericity Score: 1.0% Sphericity Score: 98.1% Asphericity Score: 1.9%				Higher Contact Pressure (> 6MPa) Contact Pressure (0 > MPa < 6) No contact pressure						

Figure 5.8: Table of results from subjects N1, N2, N3, and N4

Subject	Angles		Sphericity of the surface		Contact area and Contact pressure Pattern and values			Asphericity visualization		
	CE:	Tonnis:	Acetabulum	Femoral Head	Acetabulum	Femoral Head	Acetabulum	Femoral Head	Acetabulum	Femoral Head
Normal Left Hip 5	37.9°	-3.6°	I 17.1% II 21.4% III 20.3% IV 13.2% V 17.6%	I 13.9% II 14.8% III 9.2% IV 13.7% V 14.9% VI 13.7% VII 14.9%						
	Sphericity Score: 96.6% Asphericity Score: 3.4%		Sphericity Score: 99.2% Asphericity Score: 0.8%		Higher Contact Pressure (> 6MPa) Contact Pressure (0 > MPa < 6) No contact pressure		Higher Contact Pressure (> 6MPa) Contact Pressure (0 > MPa < 6) No contact pressure		Asphericity (-) (+)	
Normal Right Hip 6	33.8°	2.9°	I 22.0% II 22.8% III 16.9% IV 10.5% V 18.1%	I 14.9% II 13.8% III 9.1% IV 11.7% V 14.7%						
	Sphericity Score: 98.1% Asphericity Score: 1.9%		Sphericity Score: 99.2% Asphericity Score: 0.8%		Higher Contact Pressure (> 6MPa) Contact Pressure (0 > MPa < 6) No contact pressure		Higher Contact Pressure (> 6MPa) Contact Pressure (0 > MPa < 6) No contact pressure		Asphericity (-) (+)	
Normal Left Hip 7	37.0°	8.9°	I 21.6% II 21.2% III 18.7% IV 2.8% V 13.4%	I 15.3% II 14.9% III 8.4% IV 12.2% V 14.0% VI 11.6% VII 14.0%						
	Sphericity Score: 96.1% Asphericity Score: 3.9%		Sphericity Score: 99.0% Asphericity Score: 1.2%		Higher Contact Pressure (> 6MPa) Contact Pressure (0 > MPa < 6) No contact pressure		Higher Contact Pressure (> 6MPa) Contact Pressure (0 > MPa < 6) No contact pressure		Asphericity (-) (+)	
Normal Right Hip 8	35.8°	3.2°	I 19.3% II 22.1% III 10% IV 9.8% V 16.1%	I 15.5% II 16.4% III 9.1% IV 14.1% V 12.2%						
	Sphericity Score: 97.5% Asphericity Score: 2.5%		Sphericity Score: 99.1% Asphericity Score: 0.9%		Higher Contact Pressure (> 6MPa) Contact Pressure (0 > MPa < 6) No contact pressure		Higher Contact Pressure (> 6MPa) Contact Pressure (0 > MPa < 6) No contact pressure		Asphericity (-) (+)	

Figure 5.9: Table of results from subjects N5, N6, N7, and N8

Subject	Angles	Sphericity of the surface		Contact area and Contact pressure Pattern and values		Asphericity visualization	
		Acetabulum	Femoral Head	Acetabulum	Femoral Head	Acetabulum	Femoral Head
Normal Left Hip 9	CE: 33.3°						
	Tönnis: -2, 0°	Sphericity Score: 97.0% Asphericity Score: 3.0%		Sphericity Score: 99.0% Asphericity Score: 1.0%		Contact Area: 581.8 mm ² Max Contact Pressure: 7.8 MPa	
Normal Right Hip 10	CE: 36.5°						
	Tönnis: -4, 8°	Sphericity Score: 96.5% Asphericity Score: 3.5%		Sphericity Score: 98.5% Asphericity Score: 1.5%		Contact Area: 581.8 mm ² Max Contact Pressure: 8.2 MPa	

Figure 5.10: Table of results from subjects N9 and N10

5.5.2 Anatomical angles

Centre-Edge, Tönnis, Sharp and Alpha angles were measured from 10 hip joints considered normal. Measurements of anatomical angles are shown in Table 5.2. All subjects angles were normal according to literature. The average of CE angle in the normal hip joint was 33.8° and a range of 27.3° to 37.9°. The range of the Tönnis angle on the normal hip joint group

was from -4.8° to 10.0° . Subject N4 presents the lowest CE Angle and the highest Tönnis angles, its values are in the limit to be considered as normal. In contrast, subject N5 has the largest CE angle (37.9°) and N10 has the lowest Tönnis angle (-4.8°).

Subject	CE angle	Tönnis angle
Normal hip joint 1 (N1)	31.3°	5.4°
Normal hip joint 2 (N2)	34.2°	-0.4°
Normal hip joint 3 (N3)	31.0°	9.7°
Normal hip joint 4 (N4)	27.3°	10.0°
Normal hip joint 5 (N5)	37.9°	-3.6°
Normal hip joint 6 (N6)	33.8°	2.9°
Normal hip joint 7 (N7)	37.0°	8.9°
Normal hip joint 8 (N8)	35.8°	3.2°
Normal hip joint 9 (N9)	33.3°	-2.0°
Normal hip joint 10 (N10)	36.5°	-4.8°
Average	33.8°	2.9°

Table 5.2: Table of anatomical angles of the normal hip joint group

5.5.3 Sphericity percentage

“Sphericity” percentage of the acetabulum and femoral head of the normal hip joint group are shown in table 5.3. Acetabulum sphericity values range from 96.6% to 98.5% with a median of 97.5%. On the other hand, femoral had sphericity values have a range of 98.5% to 99.2%, and a median of 99.0%. In all cases, the femoral head has a greater sphericity percentage than the acetabulum, but the difference magnitude differs from subject to subject. In particular in subject N1, the sphericity of the acetabulum and the sphericity of the femoral head has the same percentage.

Subject	Acetabulum Sphericity	Femoral Head Sphericity	Sphericity Difference
N1	98.5%	98.5%	0.0%
N2	97.7%	98.6%	0.9%
N3	97.5%	98.5%	1.0%
N4	98.1%	99.0%	0.9%
N5	96.6%	99.2%	2.6%
N6	98.1%	99.2%	1.1%
N7	96.1%	99.0%	2.9%
N8	97.5%	99.1%	1.6%
N9	97.0%	99.0%	2.0%
N10	96.5%	98.5%	2.0%
Median	97.4%	98.9%	1.5%

Table 5.3: Table of overall surface “Sphericity” of the normal hip joint group.

Furthermore, a visualisation of the Sphericity values on the femoral head and acetabulum was generated to locate areas of high asphericity, as Figure 5.11 illustrates.

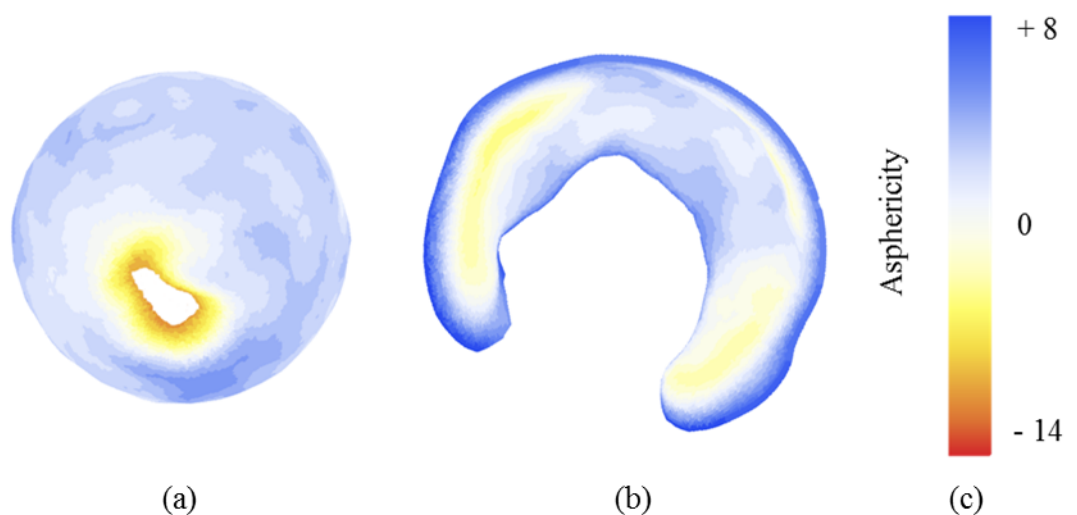


Figure 5.11: Asphericity visualisation of subject N2. (a) Asphericity pattern of the femoral head (b) Asphericity pattern of the acetabulum (c) Asphericity range of the subject.

5.5.4 Asphericity of the sections

Tables 5.4 and 5.5 shows the asphericity location of the eight defined regions on the acetabulum and femoral head from the normal hip joint group. In all cases, section I in the acetabulum presented a negative asphericity. In contrast, section II in the acetabulum presented a positive asphericity, with exception of subject N10 which presented a value of 0.0. Also in nine of ten hips a negative asphericity was located in section IV.

Subject	I	II	III	IV	V	VIII
N1	-	+			-	+
N2	-	+		-		+
N3	-	+		-	-	-
N4	-	+		-		+
N5	-	+	-	-	+	+
N6	-	+	+	-	-	-
N7	-	+	-	-	+	+
N8	-	+		-	-	
N9	-	+	-	-	+	+
N10	-		-	-	+	+

Table 5.4: Table of the sections asphericity signs of the acetabulum from the normal hip joint group.

Subject	I	II	III	IV	V	VI	VII	VIII
N1	-	+	+		-			
N2			+				+	
N3				+		-		+
N4								+
N5								
N6								-
N7					-		-	
N8			+		-			
N9				+				
N10			+	+				+

Table 5.5: Table of the sections asphericity values of the femoral head from the normal hip joint group.

On the femoral head, sections I, II and VI have only one case where its asphericity value is different from zero. The number of femoral head sections with a zero value of asphericity are predominant in comparison with the acetabulum sections.

5.5.5 Contact area and contact pressure

Table 5.6 shows the results of the FE analysis on normal subjects, which include contact area and contact pressure values. Figure 5.12 shows the contact area and contact pressure pattern on the acetabulum and femoral head of an normal hip joint.

Subject	Contact Area	Contact Pressure
N1	658.0 mm ²	7.5 MPa
N2	632.0 mm ²	7.4 MPa
N3	724.0 mm ²	6.5 MPa
N4	525.9mm ²	14.9 MPa
N5	583.9 mm ²	10.7 MPa
N6	605.1 mm ²	8.8 MPa
N7	653.8 mm ²	11.3 MPa
N8	724.2 mm ²	10.9 MPa
N9	581.8 mm ²	7.8 MPa
N10	581.8 mm ²	8.2 MPa
Average	618.6 mm ²	8.5 MPa

Table 5.6: Table of finite element analysis results of the normal hip joint group.

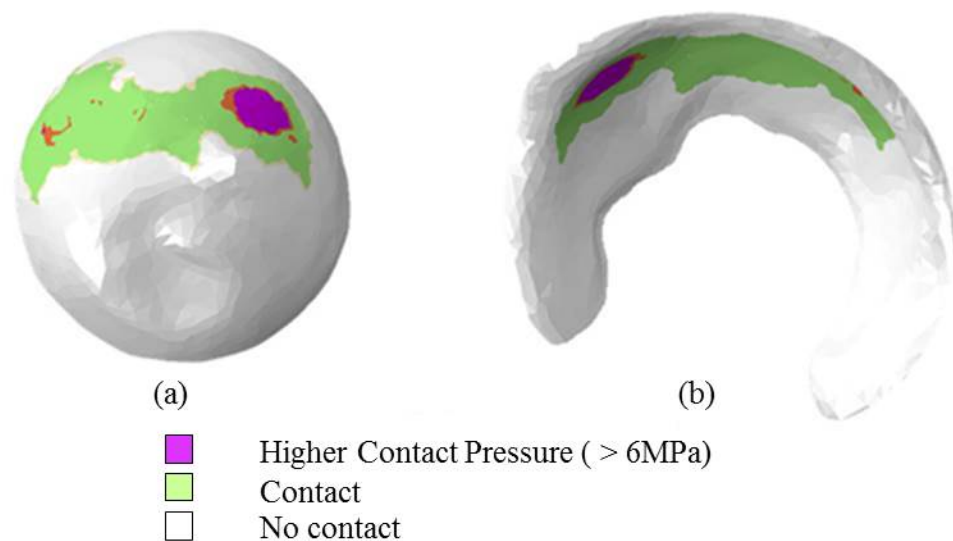


Figure 5.12: Contact pressure distribution of subject N2. (a) Sagittal view of the contact pressure pattern on the femoral head. (b) Sagittal view of the contact pressure pattern on the acetabulum.

The average contact area in the normal hip joint group is 618.6mm² and the average of the peak contact value is of 8.5 MPa. Additionally, Case N8 has the largest contact area in the normal, but it doesn't have the smallest peak contact pressure. On the other hand case N4

has the smallest contact area and the largest peak contact pressure.

In this investigation, peak contact pressures greater than the smallest peak contact pressure value within the hip joints in this study are considered as high contact pressures. In all cases, high contact pressures were located in the superior anterior region (section I) of the acetabulum. Some cases have also a high contact pressure located in the superior posterior region (section III) of the acetabulum.

High contact pressures were located in superior regions where asphericity of the acetabulum was negative, usually found in superior areas. Cases that only had one negative asphericity value in their superior regions of the acetabulum had only one high contact pressure area in the contact area, as Figure 5.13 shows.

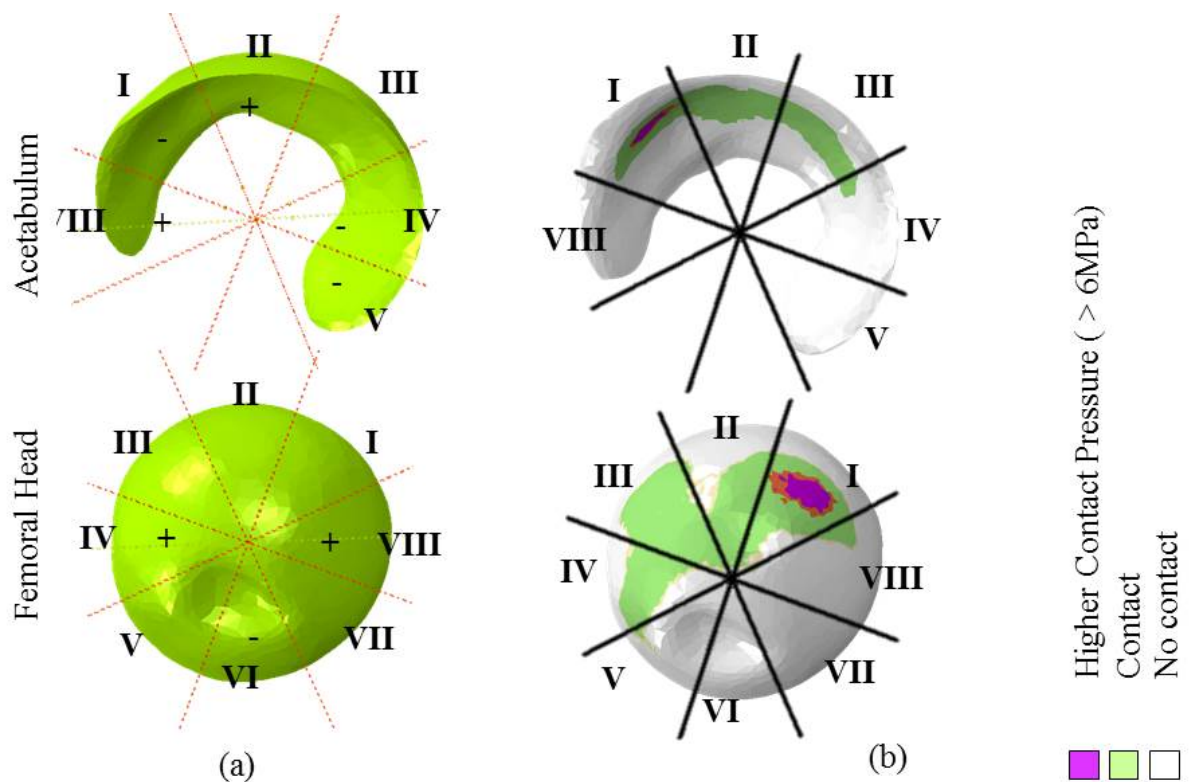


Figure 5.13: (a) Asphericity of the sections on subject N3. (b) Contact pressure distribution on subject N3.

Other subjects in the normal group presented high contact pressures in section III in addition to the high contact pressure in section I. These cases had a negative asphericity in section I and either a negative asphericity in section III of the acetabulum or a positive asphericity in section III of the acetabulum as Figure 5.14 and Figure 5.15 show.

Furthermore, in all cases, contact area pattern and high contact pressure location on the femoral head was slightly different from the acetabulum, because the acetabulum surface diameter is slightly bigger than the femoral head surface diameter.

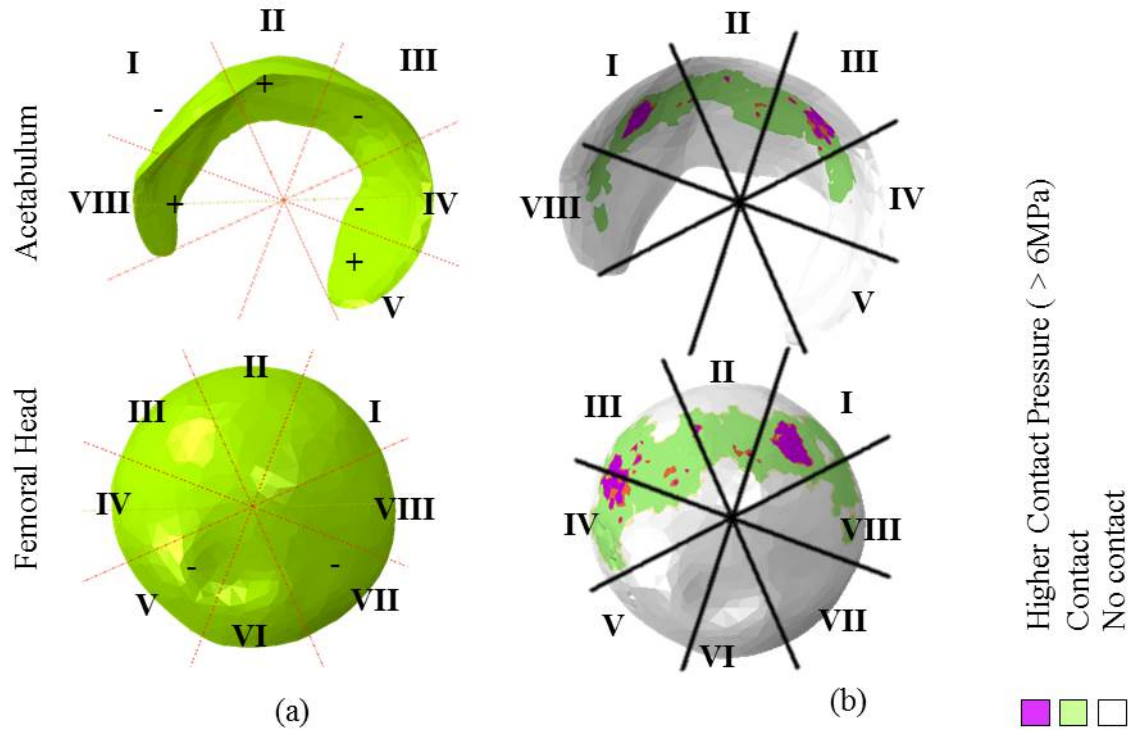


Figure 5.14: (a) Asphericity of the sections on subject N3 femoral head and acetabulum. (b) Contact pressure distribution on subject N3 acetabulum.

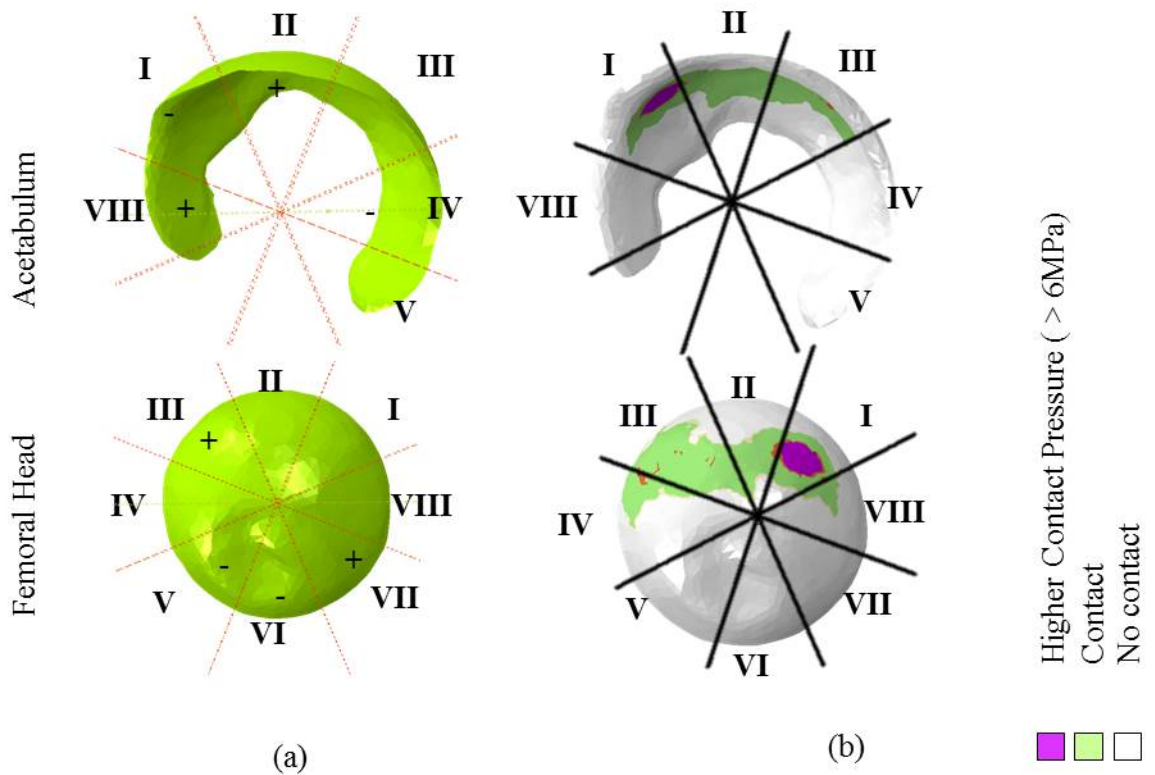


Figure 5.15: (a) Asphericity of the sections on subject N3 acetabulum and femoral head. (b) Contact pressure distribution on subject N3 acetabulum.

5.5.6 Discussion

On the normal hip joint group, peak contact pressures were located in all hips in zone I. Only one subject, N10, presented a peak contact pressure in zone III, in addition to zone I. This is because the femur of this subject is rotated.

CE angle and Tönnis angle were within the normal range (CE: 25° to 40° and Tönnis: -5° to 10°). In particular, N5 Tönnis angle is close to the superior limit of the normal range.

Regarding “Sphericity”, Three subjects had a “Sphericity” percentage lower than 97.0%. The rest of the subjects their acetabulum “Sphericity” ranged from 97.0% to 98.5%. The range of the “Sphericity” of the femoral head in normal hip joints was from 98.5% to 99.2%. This indicates that the femoral head is more spherical than the acetabulum.

In all normal subjects, negative asphericity appears in sections I and IV of the acetabulum. On the other hand, sections of the femoral head were “Spherical”. Also, the location of peak

contact pressures was in the same location of negative “Asphericity” areas in superior sections of the acetabulum. This indicates that the shape of the articular surface affects the contact pattern between the femoral head and acetabulum.

Subject N4 had the highest contact pressure and the lowest CE angle in the normal hip joint group. The range of the contact area was from 525.9 to 724mm², where only two subjects had a contact area greater than 700mm². The range of the peak contact pressure was from 6.5MPa to 13.2MPa.

Chapter 6

Sphericity analysis on hips suffering of Developmental Dysplasia and Femoroacetabular impingement

6.1 Introduction

FAI and Dysplasia of the hip are pathomechanical diseases caused by abnormalities on the bone structures of the hip joint. These abnormalities usually cause damage on the soft tissue surrounding the hip joint and on/or the articular surface of the acetabulum or/and the femoral head. The biomechanical effect of bone abnormalities on the hip joint has been very well investigated and it is believed that damage on soft tissue and articular surface of the acetabulum and femoral head is due to bone deformities.

Permanent medical treatments focus on adjusting the pelvic or femur bone structure to a healthy arrangement to allow the proper movement of the hip joint and to slow the degenerative process of the soft tissue lesion. However, in some cases a new lesion appears in a different location of the articular surface and/or soft tissue of the hip joint. This phenomenon suggests that the articular surface topology is not perfectly spherical and that is related to the bone structure of the hip joint. To investigate if there is any relation between the topology of the hip joint articular surface and pathomechanical diseases, a method to quantify the sphericity of the acetabulum and femoral head was developed and results from

the sphericity analysis were related to anatomical angles and finite element results.

This chapter reports the results from the procedures to measure the anatomical features of the hip joint and to quantify the “Sphericity” on the acetabulum and femoral head surfaces of the pathological hip joint groups. Also, this chapter presents a description of the relationships between the results of the sphericity analysis, anatomical features and FE results. To conclude, a comparison analysis of the results, relations and typical values from the normal and pathological groups is included.

6.2 Computer models development, Sphericity and anatomical angles

Twenty hip joint models, ten suffering from FAI and ten hips suffering from dysplasia, were developed to quantify sphericity of articular surfaces of the hip and to analyse contact area and pressure patterns and values when the hip joint is one-leg-standing position. Also, anatomical angles related to FAI and dysplasia of the hip, such as CE, Sharp, Tönnis and Alpha angles, were assessed and measured from anterior-posterior plain radiographs of the twenty hip joints. Computer models, Sphericity and anatomical angles were constructed, quantified and measured, respectively, using the procedures described in Chapter 5 and 6.

6.3 Femoroacetabular Impingement: Results

6.3.1 Table of results

The tables shown in Figures 6.1, 6.2, and 6.3 display anatomical angles and results from the “Sphericity” and finite element analysis from each of the 10 hips in the FAI hip joint group. From left to right, the table displays the identification number of the subject, anatomical angles (Alpha angles), “Sphericity” of the acetabulum and femoral head total surface and by sections, contact area and peak contact pressure values from one-leg-standing position, and finally an “Asphericity” visualization of the acetabulum and femoral head.

Subject	Angles	Sphericity of the surface		Contact area and Contact pressure Pattern and values		Asphericity visualization	
		Acetabulum	Femoral Head	Acetabulum	Femoral Head	Acetabulum	Femoral Head
FAI Right Hip 1	Alpha: 81.0°						
		Sphericity Score: 97.4% Asphericity Score: 2.6%		Sphericity Score: 97.7% Asphericity Score: 2.3%		Contact Area: 691.7 mm ² Max Contact Pressure: 5.6 MPa	Asphericity (-) to (+)
FAI Right Hip 2	Alpha: 68.0°						
		Sphericity Score: 98.2% Asphericity Score: 1.8%		Sphericity Score: 98.0% Asphericity Score: 2.0%		Contact Area: 808.7 mm ² Max Contact Pressure: 6.1 MPa	Asphericity (-) to (+)
FAI Right Hip 3	Alpha: 72.0°						
		Sphericity Score: 95.4% Asphericity Score: 4.6%		Sphericity Score: 95.5% Asphericity Score: 4.5%		Contact Area: 532.5 mm ² Max Contact Pressure: 8.4 MPa	Asphericity (-) to (+)
FAI Right Hip 4	Alpha: 80.7°						
		Sphericity Score: 95.6% Asphericity Score: 4.4%		Sphericity Score: 98.5% Asphericity Score: 1.5%		Contact Area: 611.2 mm ² Max Contact Pressure: 8.4 MPa	Asphericity (-) to (+)

Figure 6.1: Table of results from subjects FAI1, FAI2, FAI3, and FAI4

Subject	Angles	Sphericity of the surface			Contact area and Contact pressure Pattern and values			Asphericity visualization		
		Acetabulum	Femoral Head	Contact	Acetabulum	Femoral Head	Contact	Acetabulum	Femoral Head	Contact
FAI Left Hip 5	Alpha: 85.8°			Area: 702.1 mm ² Max Contact Pressure: 13.3 MPa						
		Sphericity Score: 97.7% Asphericity Score: 2.3%		Sphericity Score: 99.3% Asphericity Score: 0.7%		Higher Contact Pressure (> 6MPa) Contact Pressure (0 > MPa < 6) No contact pressure		Asphericity (-) (+)		
FAI Right Hip 6	Alpha: 115.2°			Area: 818.9 mm ² Max Contact Pressure: 8.7 MPa						
		Sphericity Score: 96.5% Asphericity Score: 3.5%		Sphericity Score: 97.5% Asphericity Score: 2.5%		Higher Contact Pressure (> 6MPa) Contact Pressure (0 > MPa < 6) No contact pressure		Asphericity (-) (+)		
FAI Left Hip 7	Alpha: 66.7°			Area: 598.4 mm ² Max Contact Pressure: 12.5 MPa						
		Sphericity Score: 97.9% Asphericity Score: 2.1%		Sphericity Score: 98.6% Asphericity Score: 1.4%		Higher Contact Pressure (> 6MPa) Contact Pressure (0 > MPa < 6) No contact pressure		Asphericity (-) (+)		
FAI Right Hip 8	Alpha: 78.8°			Area: 713.2 mm ² Max Contact Pressure: 7.9 MPa						
		Sphericity Score: 96.7% Asphericity Score: 3.3%		Sphericity Score: 98.7% Asphericity Score: 1.3%		Higher Contact Pressure (> 6MPa) Contact Pressure (0 > MPa < 6) No contact pressure		Asphericity (-) (+)		

Figure 6.2: Table of results from subjects FAI5, FAI6, FAI7, and FAI8

Subject	Angles	Sphericity of the surface		Contact area and Contact pressure Pattern and values		Asphericity visualization	
		Acetabulum	Femoral Head	Acetabulum	Femoral Head	Acetabulum	Femoral Head
FAI Left Hip 9	Alpha: 74.3°						
		Sphericity Score: 96.0% Asphericity Score: 4.0%	Sphericity Score: 98.9% Asphericity Score: 1.1%	Contact Area: 541.8 mm ² Max Contact Pressure: 6.9 MPa	Higher Contact Pressure (> 6MPa) Contact Pressure (0 > MPa < 6) No contact pressure.	Asphericity (-) (+)	
FAI Right Hip 10	Alpha: 72.0°						
		Sphericity Score: 94.9% Asphericity Score: 5.1%	Sphericity Score: 98.5% Asphericity Score: 1.5%	Contact Area: 691.7 mm ² Max Contact Pressure: 12.3 MPa	Higher Contact Pressure (> 6MPa) Contact Pressure (0 > MPa < 6) No contact pressure.	Asphericity (-) (+)	

Figure 6.3: Table of results from subjects FAI9 and FAI10

6.3.2 Anatomical Angles

Centre-Edge, Tönnis, Sharp and Alpha angles were measured from 10 hip joints suffering from Femoroacetabular Impingement Cam and Mixed type. Measurements of Alpha angle are shown in table 6.1. All subjects from the FAI hip joint group had an Alpha greater than 55°. The range of the Alpha angle of this group was from 66.7° to 115.2°. Where FAI6 has the

largest angle and FAI7 has the lowest angle. And the average Alpha angle of the FAI group was of 79.5°.

Subject	Alpha Angle
Hip joint with FAI 1 (FAI1)	81.0°
Hip joint with FAI 2 (FAI2)	68.0°
Hip joint with FAI 3 (FAI3)	72.0°
Hip joint with FAI 4 (FAI4)	80.7°
Hip joint with FAI 5 (FAI5)	85.8°
Hip joint with FAI 6 (FAI6)	115.2°
Hip joint with FAI 7 (FAI7)	66.7°
Hip joint with FAI 8 (FAI8)	78.8°
Hip joint with FAI 9 (FAI9)	74.3°
Hip joint with FAI 10 (FAI10)	72.0°
Average	79.5°

Table 6.1: Table of anatomical angles of the FAI hip joint group

6.3.3 Sphericity percentage

“Sphericity” percentage of the acetabulum and femoral head of the femoroacetabular hip joint group are shown in table 6.2.

Acetabulum sphericity values range from 94.9% to 98.2% with a median of 96.6%. On the other hand, femoral had sphericity values have a range of 99.3% to 95.7%, and a median of 98.1%. In all cases, the femoral head has a greater sphericity percentage than the acetabulum, with the exception of subject FAI2, in which the femoral head sphericity is 0.2% smaller than the acetabulum sphericity. Subject FAI10 has the largest sphericity difference between the acetabulum and the femoral head, with a difference value of 3.6%. FAI1, FAI3 and FAI7 had low difference of sphericity between the acetabulum and femoral head, in comparison to the FAI subjects.

Subject	Acetabulum Sphericity	Femoral Head Sphericity	Sphericity Difference
FAI1	97.4%	97.7%	0.3%
FAI2	98.2%	98.0%	-0.2%
FAI3	95.4%	95.5%	0.1%
FAI4	95.6%	98.5%	2.9%
FAI5	97.7%	99.3%	1.6%
FAI6	96.5%	97.5%	1.0%
FAI7	97.9%	98.6%	0.7%
FAI8	96.7%	98.7%	2.0%
FAI9	96.0%	98.9%	2.9%
FAI10	94.9%	98.5%	3.6%
Median	96.6%	98.1%	1.5%

Table 6.2: Table of overall surface “Sphericity” of the Femoroacetabular hip joint group.

A visualisation of the Sphericity values on the femoral head and acetabulum was generated to locate areas of high asphericity, as Figure 6.4 illustrates. In this subject FAI5, a negative asphericity can be observed in the superior and inferior lateral regions of the acetabulum, while the femoral head asphericity is less significant than the acetabulum asphericity.

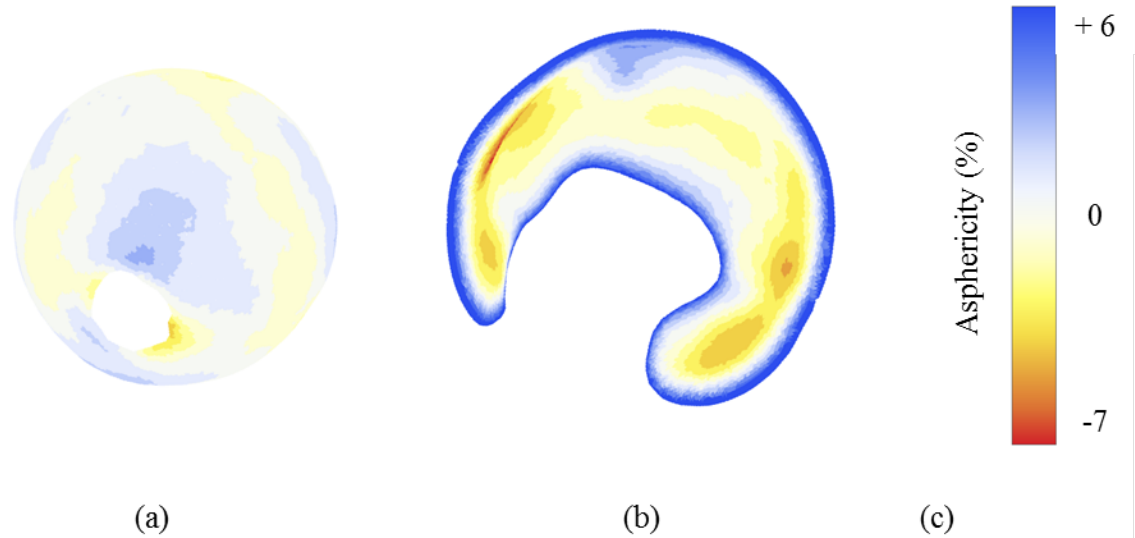


Figure 6.4: Asphericity visualisation of subject FAI5. (a) Asphericity pattern of the femoral head (b) Asphericity pattern of the acetabulum (c) Asphericity range of the subject.

6.3.4 Asphericity of the sections

Tables 6.3 and 6.4 shows the asphericity values of the eight defined regions on the acetabulum and femoral head from the femoroacetabular impingement hip joint group. In all cases, section I in the acetabulum presented a negative asphericity ranging from. On the other hand, section II in the acetabulum presented a positive asphericity, subjects FAI8 and FAI9 reported a 0.0 on this section.

Subject	I	II	III	IV	V	VIII
FAI1	-	+	-	-	+	+
FAI2	-	+				
FAI3	-	+	-	-	+	+
FAI4	-	+		-		+
FAI5	-	+	+	-		
FAI6	-	+	+	-	-	+
FAI7	-	+	+	-	+	-
FAI8	-		-	-	+	
FAI9	-			-	-	
FAI10	-	+	-	-	+	+

Table 6.3: Table of the sections asphericity values of the acetabulum from the femoroacetabular hip joint group.

Femoral heads in the femoroacetabular impingement were diverse in shape, from very "aspherical" to slightly almost "spherical". In this group, the femoral head has "Asphericity" values in sections I, II, and IV.

Subject	I	II	III	IV	V	VI	VII	VIII
FAI1	+	-	-	+	+	-	-	+
FAI2	+	+					+	
FAI3	+	-	-	+	+	-	-	+
FAI4	+			+		-		
FAI5					+			
FAI6	+	-	-	+				-
FAI7		-	+	+		-	+	+
FAI8		-	-	+	-		+	+
FAI9		+						
FAI10		+				+		

Table 6.4: Table of the sections asphericity values of the femoral head from the femoroacetabular hip joint group.

6.3.5 Contact area and contact pressure

Table 6.5 shows the results of the model, which include contact area and contact pressure values of the FAI hip joint group. Figure 6.5 shows the contact area and contact pressure pattern on the acetabulum and femoral head of hip joint suffering from FAI.

The average of the contact area of the FAI hip joint group is 671.0 mm^2 and peak contact pressure average value is of 9.0 MPa . The contact area range from the FAI group was from 532.5 mm^2 to 808.7 mm^2 . And the peak contact pressure was from 5.6 MPa to 12.5 MPa . Subject FAI8 has the largest contact area between the acetabulum and femoral head in the FAI hip joint group and the largest peak contact pressure. On the other hand, FAI3 had the smallest contact area, and FAI2 the smallest peak contact pressure.

Subject	Contact Area	Contact Pressure
FAI1	691.7 mm^2	5.6 MPa
FAI2	808.7 mm^2	6.1 MPa
FAI3	532.5 mm^2	8.4 MPa
FAI4	611.2 mm^2	8.4 MPa
FAI5	702.1 mm^2	13.3 MPa
FAI6	818.9 mm^2	8.7 MPa
FAI7	598.4 mm^2	12.5 MPa
FAI8	713.2 mm^2	7.9 MPa
FAI9	541.8 mm^2	6.9 MPa
FAI10	691.7 mm^2	12.3 MPa
Average	671.0 mm^2	9.0 MPa

Table 6.5: Table of finite element analysis results of the Femoroacetabular hip joint group.

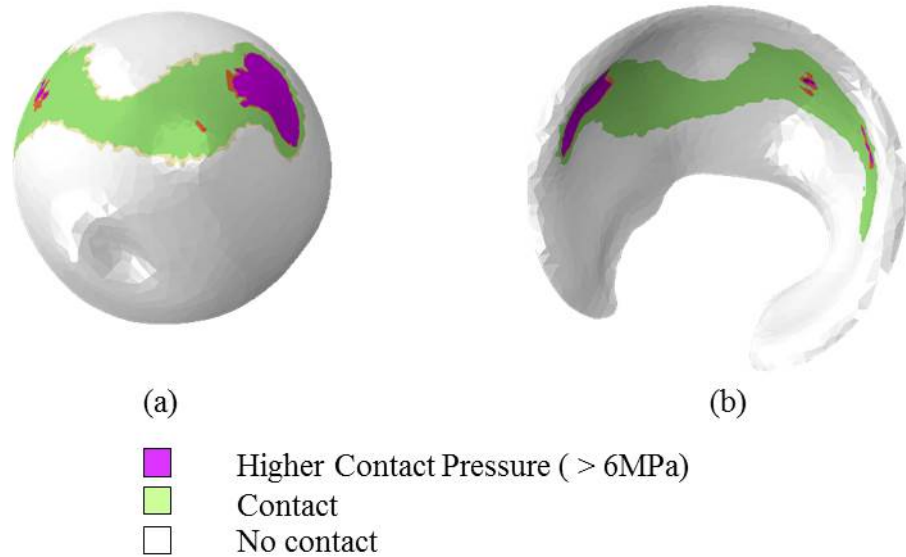


Figure 6.5: Contact pressure distribution of subject FAI5. (a) Sagittal view of the contact pressure pattern on the femoral head. (b) Sagittal view of the contact pressure pattern on the acetabulum.

Two subjects in the FAI hip joint presented small areas of high contact pressure on the superior regions of the acetabulum, nevertheless, acetabulum and femoral head were not “Spherical” as Figure 6.6 shows. Subjects FAI1 and FAI8 correspond to this description. In this cases, location of the contact area and high contact pressures was similar on the acetabula of these cases. On the other hand, contact area and high contact pressure location on the femoral head differed within the subjects. Moreover, negative “asphericity” of acetabulum coincided with the location of the small areas of high contact pressures, however, effects of the femoral “asphericity” was not observed.

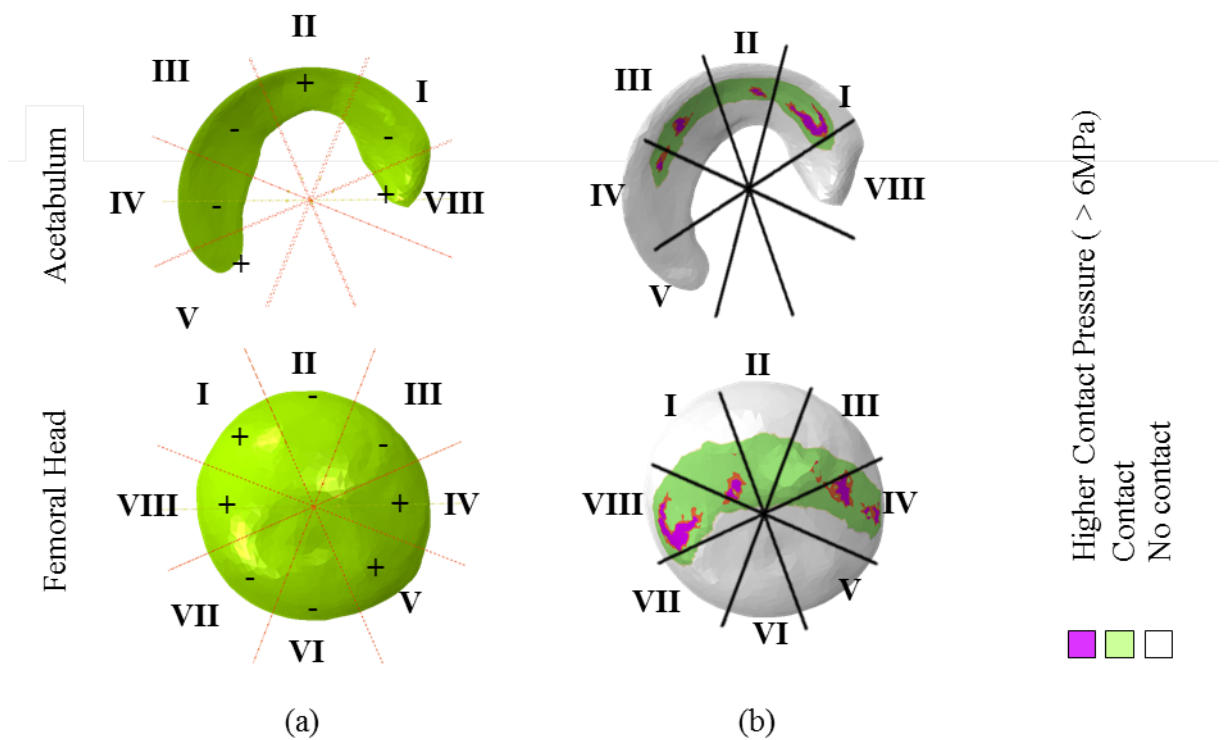


Figure 6.6: (a) Asphericity of the sections on subject FAI1 femoral head and acetabulum. (b) Contact pressure distribution on subject FAI1 acetabulum.

Subject FAI4 showed two high contact pressure areas, as Figure 6.7 shows. Contact area on the acetabulum was present on the superior regions, high contact pressures areas were located posterior and anterior. In this case, the contact area high contact pressure areas locations in the femoral were different from the acetabulum, contact area was located on lateral and superior regions. Moreover, high contact pressures were located on sections VIII and III, as for the acetabulum high contact areas were on I and III. Also, negative “asphericity” of acetabulum coincided with the location of high contact pressures areas, however, effects of the femoral “asphericity” was not observed.

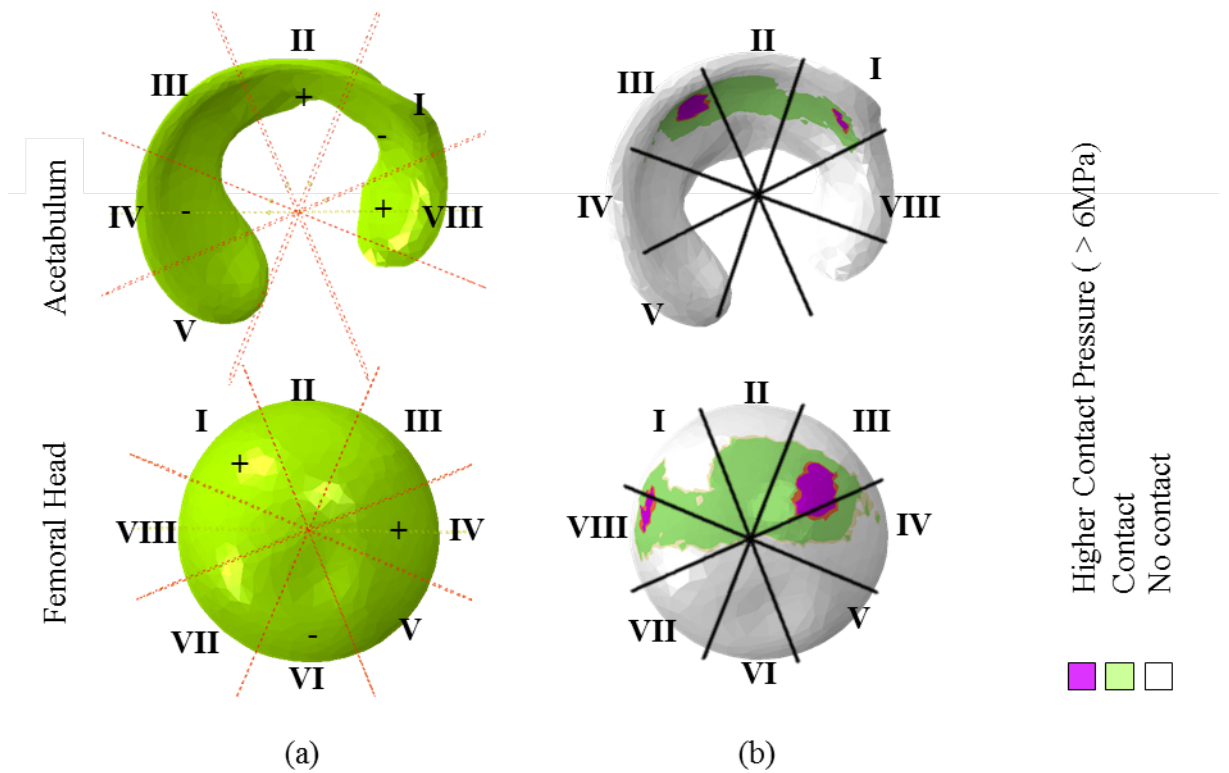


Figure 6.7: (a) Asphericity of the sections on subject FAI4 femoral head and acetabulum. (b) Contact pressure distribution on subject FAI4 acetabulum.

Subjects FAI9 and FAI10 showed high contact pressure values slightly close to the acetabular rim. Contact area on the acetabulum and femoral head was located on superior regions as Figure 6.8 illustrates. On the acetabulum, contact area was slightly on the acetabular rim. Also, negative “asphericity” of acetabulum coincided with the location of high contact pressures areas and positive “asphericity” of the femoral head moderately affects the contact distribution between the femoral head and acetabulum.

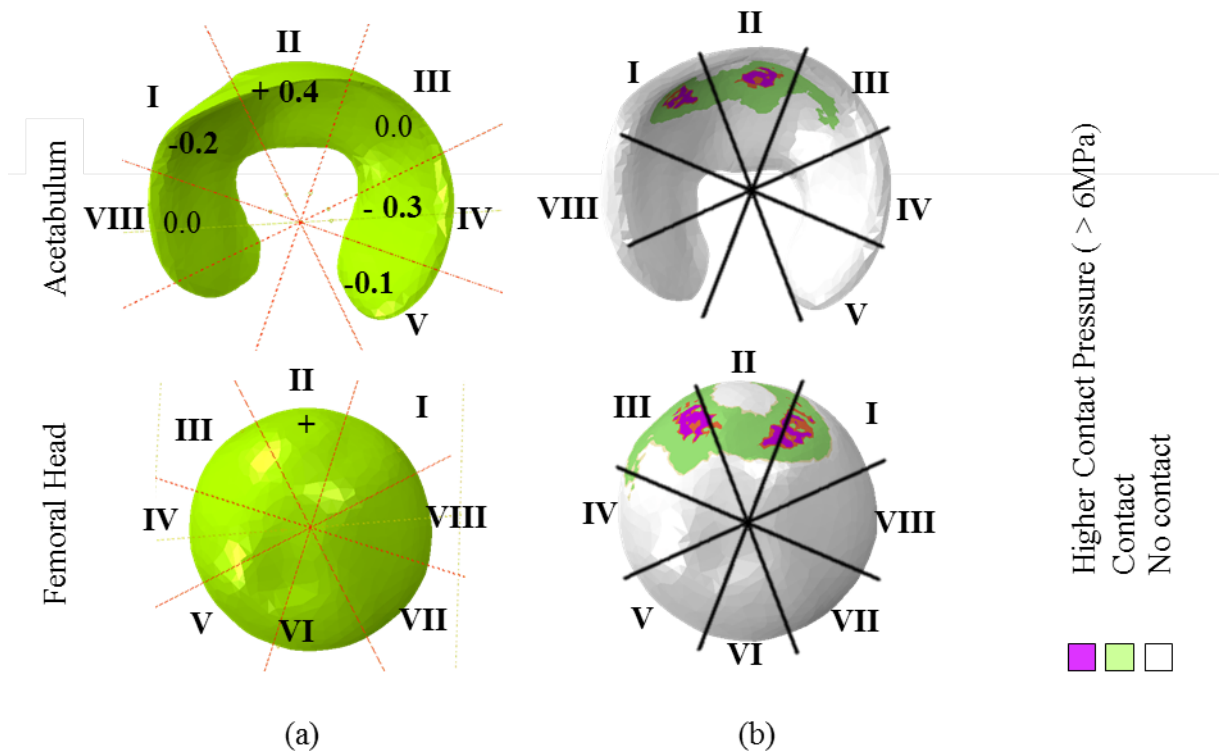


Figure 6.8: (a) Asphericity of the sections on subject FAI9 femoral head and acetabulum. (b) Contact pressure distribution on subject FAI9 acetabulum.

A number of subjects showed a high contact area very close to the acetabular rim. Location of the high contact pressure are was located on the superior anterior part of the acetabulum and femoral head, as Figure 6.8 shows. Negative “asphericity” on superior regions of acetabulum coincided with the location of high contact pressures areas. As for the femoral head positive values of “asphericity” on superior regions matched with the location of high contact pressures areas. Cases under this description are FAI2, FAI5, FAI6 and FAI7.

Additionally, on three of four of these cases, FAI2, FAI5 and FAI7, a small negative “Asphericity” was observed between sections IV and V, on the acetabulum as Figure 6.10 illustrates.

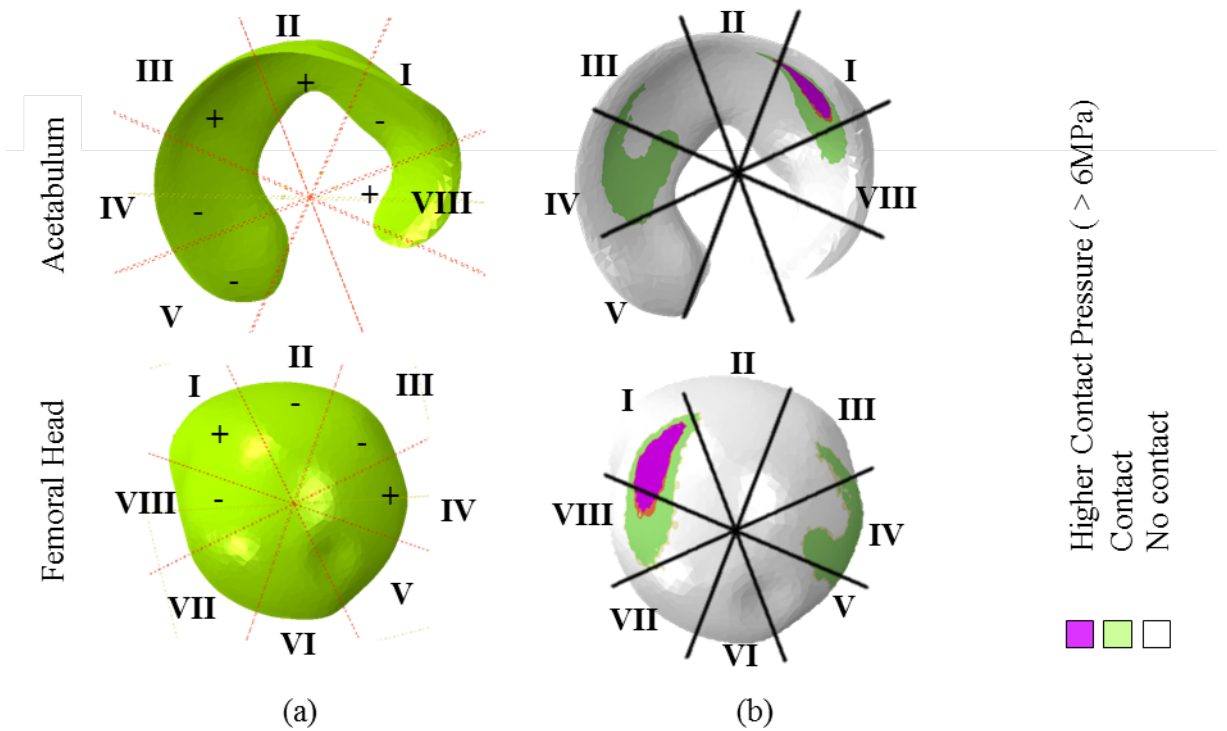


Figure 6.9: (a) Asphericity of the sections on subject FAI6 femoral head and acetabulum. (b) Contact pressure distribution on subject FAI6 acetabulum.

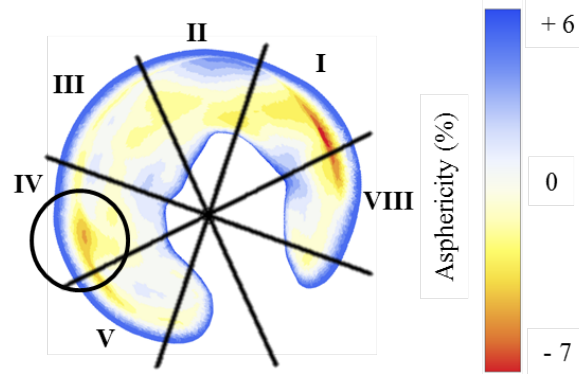


Figure 6.10: Posterior asphericity on the acetabular rim of subject FAI2.

Subject FAI3 showed two high contact pressure areas, as Figure 6.11. Contact area on the acetabulum was present on the superior regions and negative “asphericity” of acetabulum coincided with the location of high contact pressures areas. Contact area location on the femoral head highly disagreed with contact area location of the acetabulum.

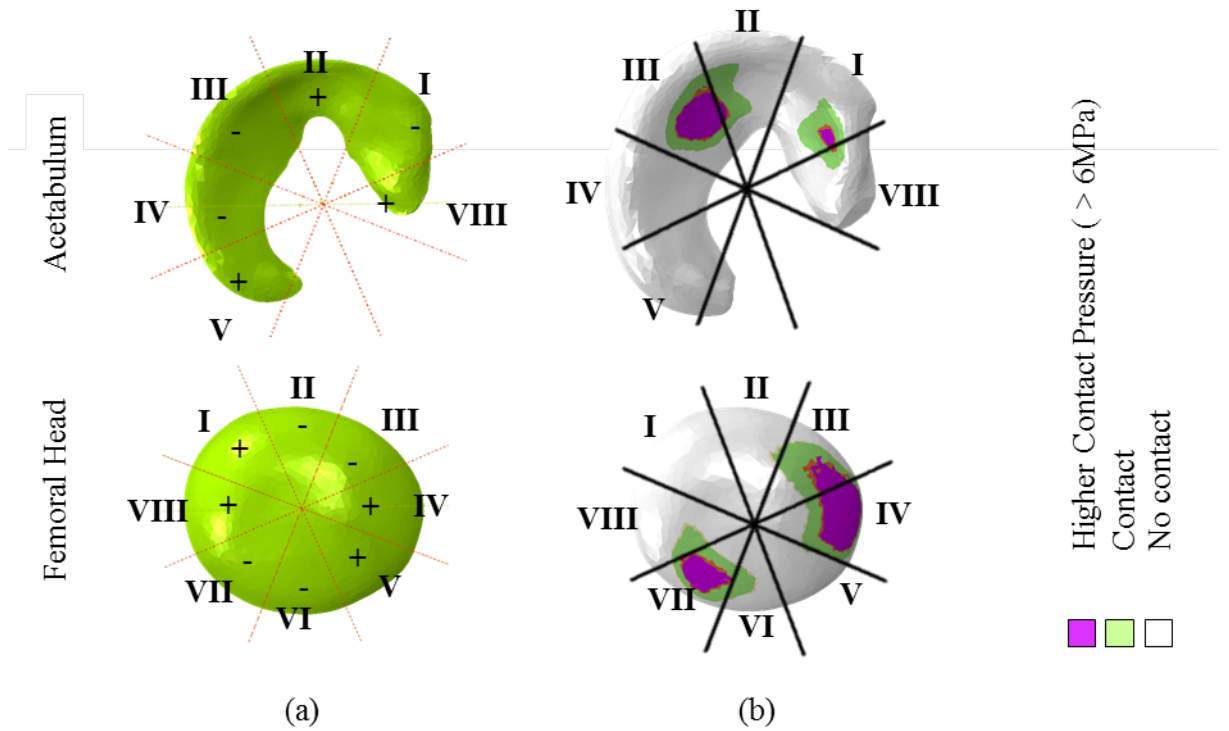


Figure 6.11: (a) Asphericity of the sections on subject FAI3 femoral head and acetabulum. (b) Contact pressure distribution on subject FAI3 acetabulum.

6.3.6 Discussion

Peak contact pressure was found in section I in five of the ten hips joints with cam-type impingement. One subject, FAI9, had its peak contact pressure in section II because of an abnormal femoral head. FAI1 and FAI2 had two peak contact pressures located in zone I and III, FAI2 because of the bone abnormality on the femoral head and FAI1 because of an abnormal shape of the femoral head and acetabulum. In subject FAI3, due to an abnormal shape of the acetabulum the peak contact pressure was observed in section III. Finally, subject FAI4 displayed a peak contact pressure in section III because its femur is rotated.

The contact area range in FAI hip joint group was from 632.5 to 808.7 mm² with an average of 671.0 mm². Contact areas above 700mm² are produced by the bone abnormality on the femoral head.

The “Sphericity” of the femoral head had a wider range in comparison to normal and DDH group. In the FAI group the shape of the femoral and acetabulum were variable as well.

Subjects FAI1, FAI3, FAI6 and FAI10 had an acetabulum and femoral head with a oval shape, the remaining hips were similar to those found in the normal hip joint group.

In a number cases, the acetabulum on the FAI group presented a small negative sphericity area in the opposite side of the antero superior region, this asphericity is like due to the effect of impingement. In other cases, the femoral head had two positive asphericity areas usually found in opposing sides giving to the femoral head and oval-like shape.

6.4 Developmental Dysplasia of the Hip: Results

6.4.1 Table of results

The tables shown in Figures 6.12, 6.13, and 6.14 display anatomical angles and results from the “Sphericity” and finite element analysis from each of the 10 hips in the DDH hip joint group. From left to right, the table displays the identification number of the subject, anatomical angles (CE, Tönnis, and Sharp angles), “Sphericity” of the acetabulum and femoral head total surface and by sections, contact area and peak contact pressure values from one-leg-standing position, and finally an “Asphericity” visualization of the acetabulum and femoral head.

Subject	Angles			Sphericity of the surface				Contact area and Contact pressure Pattern and values			Asphericity visualization		
	CE:	Tomnis:	Sharp:	Acetabulum	Femoral Head			Contact	Acetabulum	Femoral Head	Acetabulum	Femoral Head	
DDH Right Hip 1	21.4°	9.4°	44.7°		I: 19.6%, II: 21.2%, III: 18.6%, IV: 9.7%, V: 13.9%	I: 14.1%, II: 15.0%, III: 12.6%, IV: 12.8%, V: 14.1%, VI: 10.5%, VII: 12.8%, VIII: 12.5%	Area: 482.7 mm ²						Asphericity (-) (+)
				Sphericity Score: 98.5% Asphericity Score: 1.5%			Max Contact Pressure: 7.0 MPa	Higher Contact Pressure (> 6MPa) Contact Pressure (0 > MPa < 6) No contact pressure					
				Sphericity Score: 98.6% Asphericity Score: 1.4%									
DDH Left Hip 2	23.0°	13.4°	40.5°		I: 22.1%, II: 27.7%, III: 18.5%, IV: 11.4%, V: 13.0%	I: 12.5%, II: 12.6%, III: 11.1%, IV: 12.0%, V: 12.7%, VI: 12.9%, VII: 12.0%, VIII: 12.0%	Area: 707.0 mm ²						Asphericity (-) (+)
				Sphericity Score: 96.7% Asphericity Score: 2.5%			Max Contact Pressure: 9.7 MPa	Higher Contact Pressure (> 6MPa) Contact Pressure (0 > MPa < 6) No contact pressure					
				Sphericity Score: 99.0% Asphericity Score: 1.0%									
DDH Left Hip 3	10.1°	24.0°	50.7°		I: 18.5%, II: 21.3%, III: 20.2%, VIII: 10.2%, IV: 9.0%, V: 15.3%	I: 12.5%, II: 13.6%, III: 12.2%, IV: 14.5%, V: 11.0%, VI: 11.5%, VII: 10.9%, VIII: 10.9%	Area: 450.2 mm ²						Asphericity (-) (+)
				Sphericity Score: 97.5% Asphericity Score: 2.5%			Max Contact Pressure: 9.9 MPa	Higher Contact Pressure (> 6MPa) Contact Pressure (0 > MPa < 6) No contact pressure					
				Sphericity Score: 97.5% Asphericity Score: 2.2%									
DDH Left Hip 4	16.8°	11.4°	58.7°		I: 20.3%, II: 23.1%, III: 19.1%, VIII: 8.5%, IV: 11.0%, V: 13.6%	I: 16.5%, II: 14.9%, III: 8.5%, IV: 11.4%, V: 13.2%, VI: 9.5%, VII: 7.9%, VIII: 16.3%	Area: 525.9 mm ²						Asphericity (-) (+)
				Sphericity Score: 95.6% Asphericity Score: 4.4%			Max Contact Pressure: 14.9 MPa	Higher Contact Pressure (> 6MPa) Contact Pressure (0 > MPa < 6) No contact pressure					
				Sphericity Score: 98.2% Asphericity Score: 1.8%									

Figure 6.12: Table of results from subjects DDH1, DDH2, DDH3, and DDH4

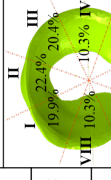
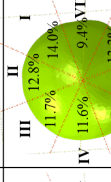
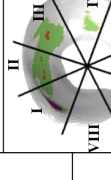
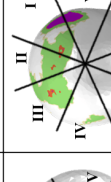
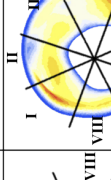
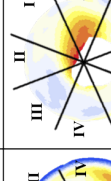
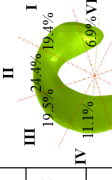
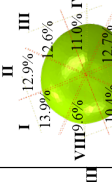
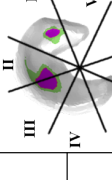
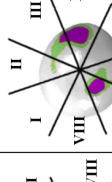
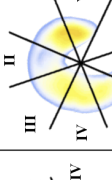
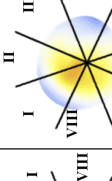
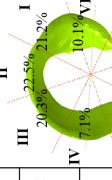
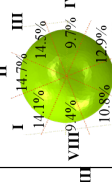
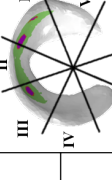
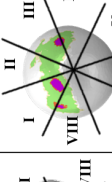
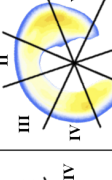
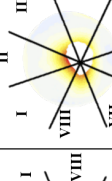
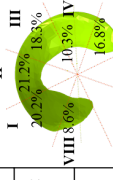
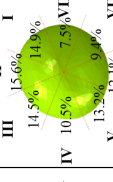
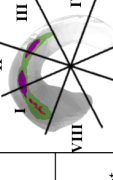
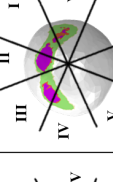
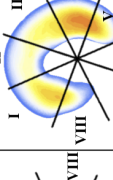

Subject	Angles			Sphericity of the surface				Contact area and Contact pressure Pattern and values				Asphericity visualization				
	CE:	Tonnis:	Sharp:	Acetabulum	Femoral Head	Acetabulum	Femoral Head	Contact Area:	Acetabulum	Femoral Head	Acetabulum	Femoral Head	Asphericity	Acetabulum	Femoral Head	
DDH Left Hip 5	30.1°	6.4°	41.1°	 I 19.9% II 22.4% III 20.4% IV 10.3% V 14.6% VI 11.5% VII 13.3% VIII 14.7%	 I 12.8% II 11.7% III 14.0% IV 11.6% V 9.4% VI 13.3% VII 14.7% VIII 14.0%	575.3 mm ²	 I II III IV V VI VII VIII	 I II III IV V VI VII VIII	15.0 MPa	 I II III IV V VI VII VIII	 I II III IV V VI VII VIII	(-)	(+)			
	Sphericity Score: 97.9% Asphericity Score: 2.1%				Sphericity Score: 99.0% Asphericity Score: 1.0%				Higher Contact Pressure (> 6MPa) Contact Pressure (0 > MPa < 6) No contact pressure				Asphericity			
	Max Contact Pressure: 15.0 MPa				Max Contact Pressure: 15.0 MPa											
DDH Right Hip 6	14.6°	20.6°	50.3°	 I 19.8% II 24.4% III 19.4% IV 11.1% V 14.6% VI 11.1% VII 6.9% VIII 14.6%	 I 12.9% II 13.9% III 12.6% IV 11.0% V 12.7% VI 10.4% VII 12.5% VIII 12.7%	430.8 mm ²	 I II III IV V VI VII VIII	 I II III IV V VI VII VIII	12.3 MPa	 I II III IV V VI VII VIII	 I II III IV V VI VII VIII	(-)	(+)			
	Sphericity Score: 95.9% Asphericity Score: 4.1%				Sphericity Score: 95.7% Asphericity Score: 4.3%				Higher Contact Pressure (> 6MPa) Contact Pressure (0 > MPa < 6) No contact pressure				Asphericity			
	Max Contact Pressure: 12.3 MPa				Max Contact Pressure: 12.3 MPa											
DDH Right Hip 7	22.6°	10.0°	42.8°	 I 20.8% II 22.5% III 21.2% IV 7.1% V 15.8% VI 10.1% VII 10.1% VIII 15.8%	 I 14.4% II 14.7% III 14.5% IV 9.7% V 10.8% VI 12.7% VII 12.7% VIII 15.9%	663.1 mm ²	 I II III IV V VI VII VIII	 I II III IV V VI VII VIII	7.4 MPa	 I II III IV V VI VII VIII	 I II III IV V VI VII VIII	(-)	(+)			
	Sphericity Score: 97.0% Asphericity Score: 3.0%				Sphericity Score: 98.8% Asphericity Score: 1.2%				Higher Contact Pressure (> 6MPa) Contact Pressure (0 > MPa < 6) No contact pressure				Asphericity			
	Max Contact Pressure: 7.4 MPa				Max Contact Pressure: 7.4 MPa											
DDH Left Hip 8	6.6°	22.6°	49.2°	 I 20.2% II 12.2% III 18.3% IV 10.3% V 16.8% VI 8.6% VII 10.3% VIII 16.8%	 I 15.6% II 14.5% III 14.0% IV 7.5% V 13.2% VI 12.1% VII 9.8% VIII 12.1%	443.6 mm ²	 I II III IV V VI VII VIII	 I II III IV V VI VII VIII	11.7 MPa	 I II III IV V VI VII VIII	 I II III IV V VI VII VIII	(-)	(+)			
	Sphericity Score: 95.4% Asphericity Score: 4.6%				Sphericity Score: 97.7% Asphericity Score: 2.3%				Higher Contact Pressure (> 6MPa) Contact Pressure (0 > MPa < 6) No contact pressure				Asphericity			
	Max Contact Pressure: 11.7 MPa				Max Contact Pressure: 11.7 MPa											

Figure 6.13: Table of results from subjects DDH5, DDH6, DDH7, and DDH8

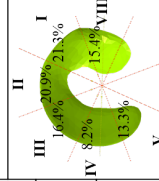
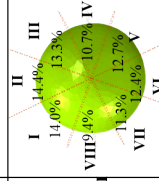




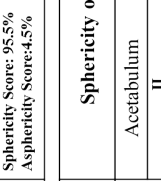
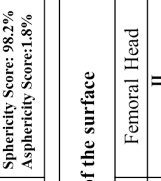
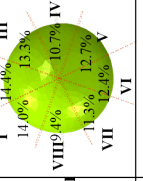
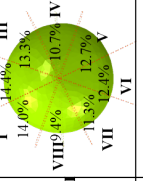
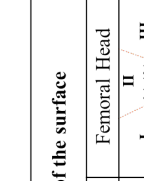
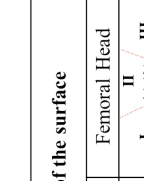
Subject	Angles			Sphericity of the surface		Contact area and Contact pressure Pattern and values		Asphericity visualization		
	CE:	Tönnis:	Sharp:	Acetabulum	Femoral Head	Acetabulum	Femoral Head	Acetabulum	Femoral Head	
DDH Right Hip 9	11.9°	12.1°	48.1°	 I 16.8% II 20.9% III 21.3% IV 8.2% V 13.3% VI 15.4% VII 15.4% VIII 15.4%	 I 14.0% II 14.4% III 13.3% IV 10.7% V 12.7% VI 12.4% VII 11.3% VIII 14.4%	 I II III IV V VI VII VIII	 I II III IV V VI VII VIII	 I II III IV V VI VII VIII	 I II III IV V VI VII VIII	
	Contact Area: 581.8 mm ²		Sphericity Score: 95.5% Asphericity Score: 4.5%		Sphericity Score: 98.2% Asphericity Score: 1.8%		Higher Contact Pressure (> 6MPa) Contact Pressure (0 > MPa < 6) No contact pressure		Asphericity (+)	
	Max Contact Pressure: 7.8 MPa									
DDH Right Hip 10	22.0°	11.9°	42.9°	 I 19.8% II 22.3% III 19.8% IV 7.0% V 12.6% VI 13.3% VII 13.3% VIII 13.3%	 I 14.3% II 14.4% III 13.3% IV 10.8% V 11.9% VI 13.2% VII 11.1% VIII 14.4%	 I II III IV V VI VII VIII	 I II III IV V VI VII VIII	 I II III IV V VI VII VIII	 I II III IV V VI VII VIII	
	Contact Area: 666.4 mm ²		Sphericity Score: 96.0% Asphericity Score: 4.0%		Sphericity Score: 98.4% Asphericity Score: 1.6%		Higher Contact Pressure (> 6MPa) Contact Pressure (0 > MPa < 6) No contact pressure		Asphericity (+)	
	Max Contact Pressure: 7.8 MPa									

Figure 6.14: Table of results from subjects DDH9 and DDH10

6.4.2 Anatomical Angles

Centre-Edge, Tönnis, Sharp and Alpha angles were measured from 10 hip joints suffering from Developmental Dysplasia of the hip. Measurements of anatomical angles are shown in table 6.6. In almost all subjects CE angle was less than 25 degrees which is considered as abnormal according to literature. Subject DHH5 has CE angle considered as normal,

however its Sharp angle is out of the range considered as healthy. Tönnis angle was within the healthy range in three subjects, DDH1, DDH 5 and DDH7. The remaining cases reported a Tönnis angles in the dysplastic range. As for the Sharp angle all cases were greater than 40°, considered as dysplastic.

The average CE angle of the DDH group was of 17.9° with a range from 11.9° to 30.1°, Tönnis angle had a range of 24.0° to 9.4° and average value of 14.2°. Finally, the average angle for the DDH group was of 46.9° with a range of 40.5° to 50.7°.

Subject	CE angle	Tönnis angle	Sharp Angle
Hip joint with DDH 1 (DDH1)	21.4°	9.4°	44.7°
Hip joint with DDH 2 (DDH2)	23.0°	13.4°	40.5°
Hip joint with DDH 3 (DDH3)	10.1°	24°	50.7°
Hip joint with DDH 4 (DDH4)	16.8°	11.4°	58.7°
Hip joint with DDH 5 (DDH5)	30.1°	6.4°	41.1°
Hip joint with DDH 6 (DDH6)	14.6°	20.6°	50.3°
Hip joint with DDH 7 (DDH7)	22.6°	10.0°	42.8°
Hip joint with DDH 8 (DDH8)	6.6°	22.6°	49.2°
Hip joint with DDH 9 (DDH9)	11.9°	12.1°	48.1°
Hip joint with DDH 10 (DDH10)	22°	11.9°	42.9°
Average	17.9°	14.2°	46.9°

Table 6.6: Table of anatomical angles of the DDH hip joint group

6.4.3 Sphericity percentage

“Sphericity” percentage of the acetabulum and femoral head of the dysplastic hip joint group are shown in Table 6.7.

Acetabulum sphericity values range from 95.4% to 98.5% with a median of 96.4%. On the other hand, femoral had sphericity values have a range of 99.0% to 95.7%, and a median of 98.3%. In all cases, the femoral head has a greater sphericity percentage than the acetabulum, with the exception of subject DDH5, in which the femoral head sphericity is 0.2% less spherical than the acetabulum. Subject DDH4 has the largest difference between

the acetabulum and femoral head sphericity.

Subject	Acetabulum Sphericity	Femoral Head Sphericity	Sphericity Difference
DDH1	98.5%	98.6%	0.1%
DDH2	96.7%	98.9%	2.2%
DDH3	97.5%	97.5%	0%
DDH4	95.6%	98.2%	2.6%
DDH5	97.9%	99.0%	1.1%
DDH6	95.9%	95.7%	-0.2%
DDH7	97.0%	98.4%	1.4%
DDH8	95.4%	97.7%	2.3%
DDH9	95.5%	98.2%	2.7%
DDH10	96.0%	98.4%	2.4%
Average	96.6%	98.1%	1.5%

Table 6.7: Table of overall surface “Sphericity” of the normal hip joint group.

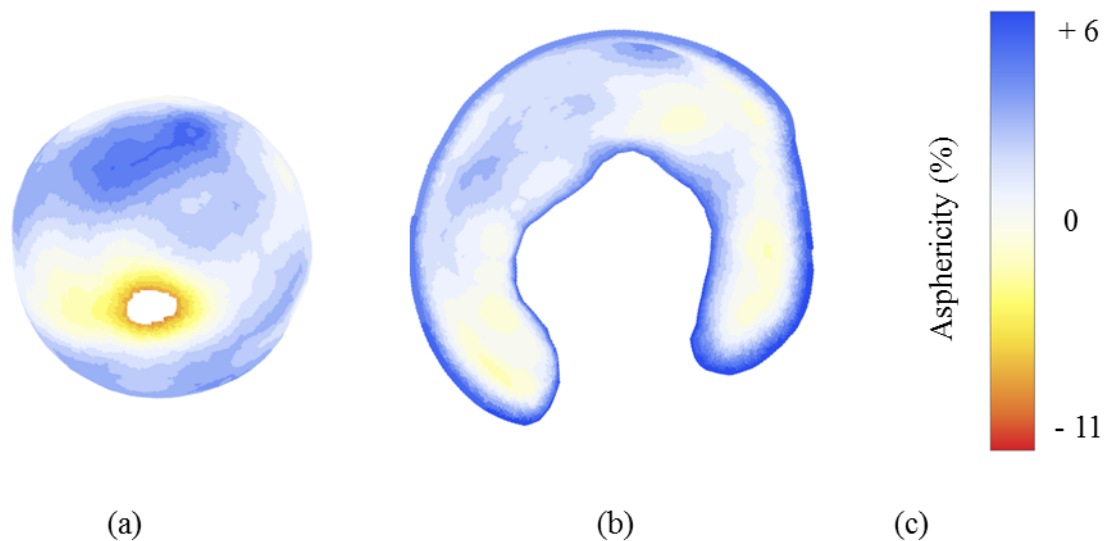


Figure 6.15: Asphericity visualisation of subject DDH1. (a) Asphericity pattern of the femoral head (b) Asphericity pattern of the acetabulum (c) Asphericity range of the subject.

A visualisation of the Sphericity values on the femoral head and acetabulum was generated to locate areas of high asphericity, as Figure 6.15 illustrates. In this subject

DDH1, a positive asphericity can be observed in the superior region of the femoral head. On the acetabulum three negative asphericity regions can be located, on the inferior right/left and superior regions of the acetabulum.

6.4.4 Asphericity of the sections

Tables 6.8 and 6.9 shows the asphericity values of the eight defined regions on the acetabulum and femoral head from the dysplastic hip joint group. In all cases, section I in the acetabulum presented a negative asphericity. In contrast, section II in the acetabulum presented a positive asphericity in all cases.

Subject	I	II	III	IV	V	VIII
DDH1	-	+		-		
DDH2	-	+	+	-		+
DDH3	-	+	-	-	+	
DDH4	-	+	+			+
DDH5	-	+	+	-		+
DDH6	-	+	-	-	+	
DDH7	-	+	+	-	+	+
DDH8	-	+	-	-		+
DDH9	-	+	+	-		+
DDH10	-	+	-	-		+

Table 6.8: Table of the sections asphericity values of the acetabulum from the dysplastic hip joint group.

Subject	I	II	III	IV	V	VI	VII	VIII
DDH1	+		+					-
DDH2			+		-	+		
DDH3		-		+	-	-	+	+
DDH4	+	-	-	-	-		+	
DDH5	+							
DDH6	+	-	-	+	+	-	-	+
DDH7	+		+		-			
DDH8								
DDH9	+		-	+	+	-	-	
DDH10	+		-				+	

Table 6.9: Table of the sections asphericity values of the femoral head from the dysplastic hip joint group.

On the femoral heads subjects DDH5 and DDH8 have the most “Spherical” femoral heads, DDH8 has no “asphericity” values while DDH5 has an “asphericity” in the anterior superior section (I). The remaining subjects have more than three sections with “asphericity” values. Subject DDH6 reports “asphericity” in all sections of the femoral head, and also the largest “asphericity” value, a positive and negative “asphericity” in sections II and IV, respectively.

6.4.5 Contact area and contact pressure

Table 6.10 shows the results of the FE analysis on the Dysplastic hip joint group, which include contact area and contact pressure values. Figure 6.16 shows the contact area and contact pressure pattern on the acetabulum and femoral head of a dysplastic hip joint.

Subject	Contact Area	Contact Pressure
DDH1	482.7 mm ²	7.0 MPa
DDH2	707.0 mm ²	9.7 MPa
DDH3	450.2 mm ²	9.9 MPa
DDH4	525.9mm ²	14.9 MPa
DDH5	575.3 mm ²	15.0 MPa
DDH6	430.8 mm ²	12.3 MPa
DDH7	663.1 mm ²	7.4 MPa
DDH8	443.6 mm ²	11.7 MPa
DDH9	581.8 mm ²	7.8 MPa
DDH10	666.4 mm ²	7.8 MPa
Median	550.6 mm ²	9.8 MPa

Table 6.10: Table of finite element analysis results of the normal hip joint group.

The average of the contact area of the dysplastic hip joint group is 550.6 mm² and peak contact pressure average value is of 9.8 MPa. Range of the contact area in the DDH group is from 430.8 mm² to 707.0mm², and the peak contact range is from 7.0 MPa to 15.0 MPa. Subject DDH2 has the largest contact area in the dysplastic group, but it doesn't have the largest peak contact pressure. Subject DDH5 has the largest contact peak pressure, but it doesn't have the smallest contact area.

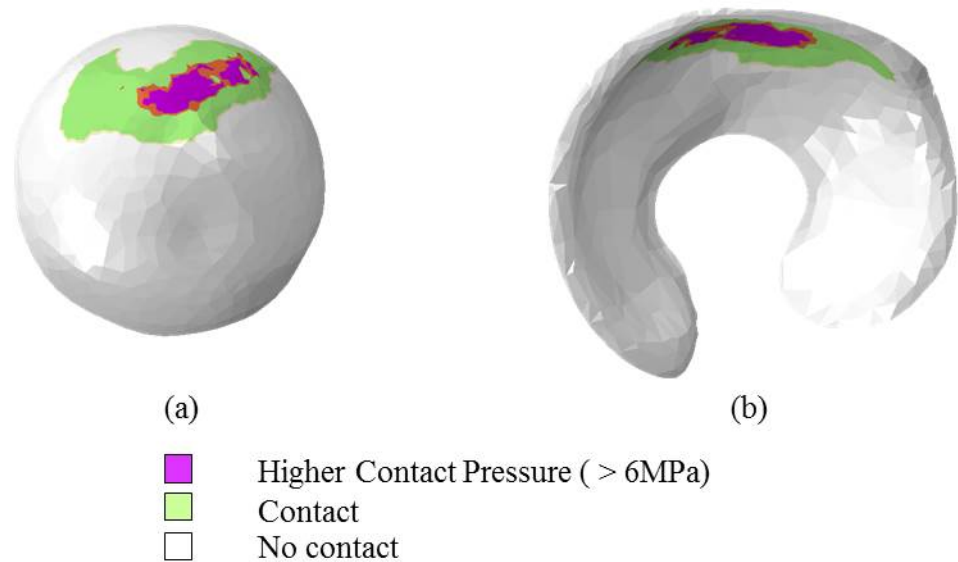


Figure 6.16: Contact pressure distribution of subject DDH1. (a) Sagittal view of the contact pressure pattern on the femoral head. (b) Sagittal view of the contact pressure pattern on the acetabulum.

In all cases, high contact pressures were located in the superior anterior region (section D) of the acetabulum, with exception of subject DDH1. This subject shows high contact pressures in the superior section of the acetabulum as Figure 6.17 illustrates. In this case, the femoral head presents a large positive “asphericity” on the superior part as it can be observed in Figure 6.15. By comparing the “asphericity” and contact pressure distribution, in this case, it can be deduced that the femoral head sphericity has a larger role on the biomechanical behavior of the hip joint. The acetabulum in this case had the highest acetabulum sphericity percentage in the dysplastic hip joint group.

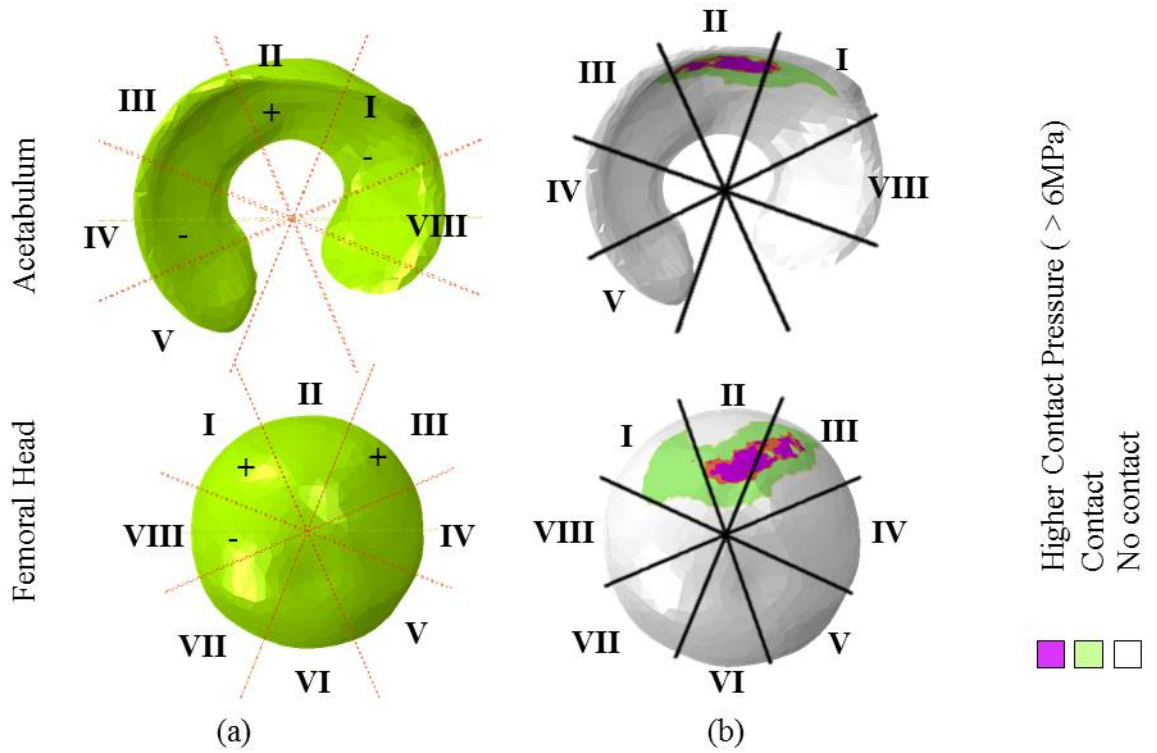


Figure 6.17: (a) Asphericity of the sections on subject DDH1 femoral head and acetabulum. (b) Contact pressure distribution on subject N3 acetabulum.

Subjects in the dysplastic group presented high contact pressures in section III in addition to the high contact pressure in section I. These cases had a negative asphericity in section I and either a negative asphericity in section III, also the femoral head presented a positive sphericity in the lateral sections (IV and VIII) and it was not “spherical”. Moreover, contact area distribution has a discontinuity in section II of the acetabulum, and contact area of the femoral head is not in the same sections as the contact area of the acetabulum is as Figure 6.18 illustrates. Subjects DDH3, DDH4, DDH6 and DDH10 fall under this category.

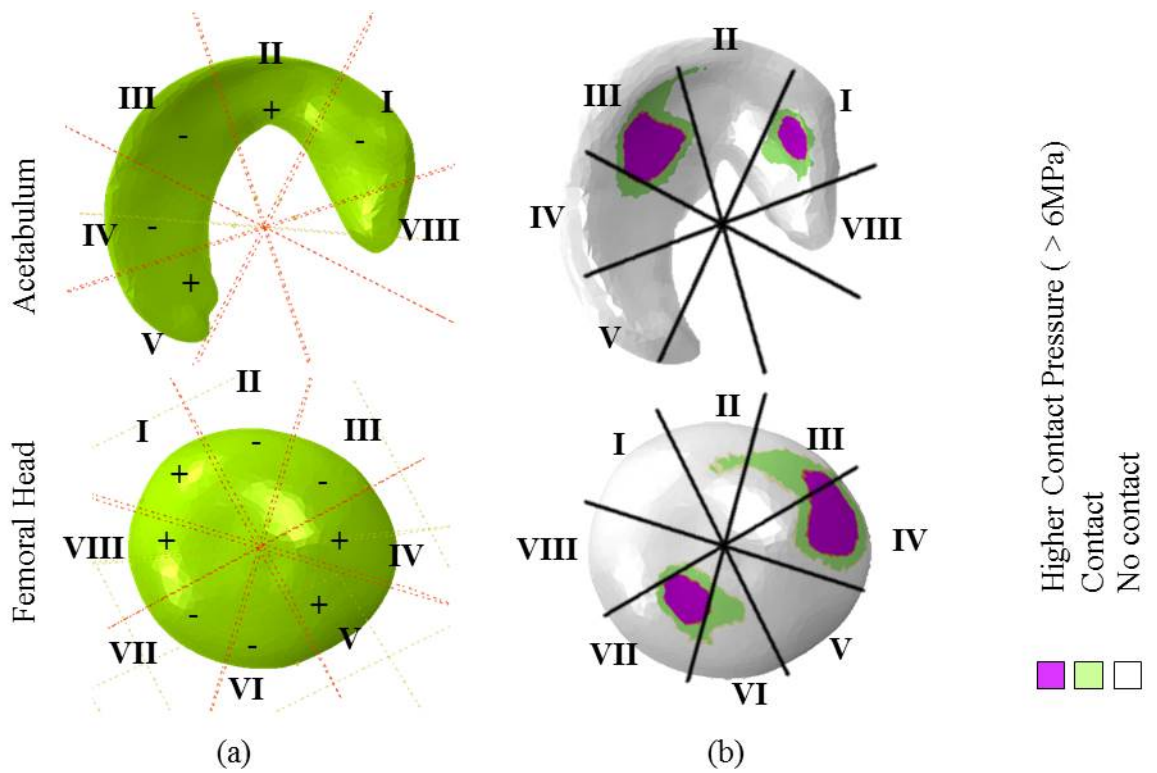


Figure 6.18: (a) Asphericity of the sections on subject DDH6 femoral head and acetabulum. (b) Contact pressure distribution on subject N3 acetabulum.

Other subjects in the dysplastic group presented more than two high contact pressures in superior sections of the acetabulum. These cases had a negative asphericity in section I and III of the acetabulum. In these cases, the femoral head presented a positive asphericity in its superior sections. Also, contact area of the femoral head is not in the same sections as the contact area of the acetabulum is as Figure 6.19 illustrates. Subjects DDH2, DDH5, DDH7, DDH8 and DDH9 fall under this description.

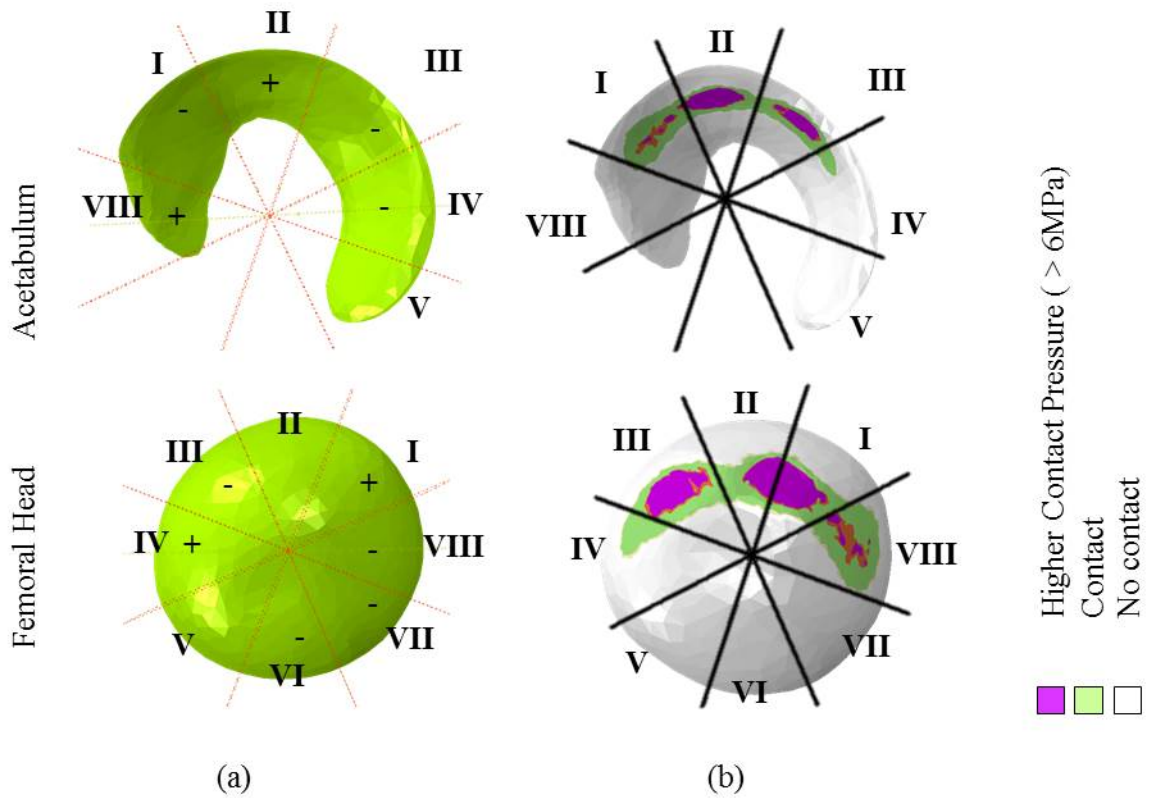


Figure 6.19: (a) Asphericity of the sections on subject DDH8 femoral head and acetabulum. (b) Contact pressure distribution on subject N3 acetabulum.

Additionally, in all cases contact area in section I of the acetabulum was close to the acetabular rim. Cases where a contact discontinuity was present in section II of the acetabulum, contact area in section III was also close to the acetabular rim.

6.4.6 Discussion

In two hips (DDH6 and DDH7) the location of the peak contact pressure in the femoral head was not in the same section as in the acetabulum, this is because of the abnormal shape of the hip joint components. In 5 subjects peak contact pressures were location in zone I (DDH2, DHH3, DDH5, DDH9 and DDH10). In the other five hips the location varied. In two hips peak contact pressure was located in zone II due to an abnormal femoral head (DDH1 and DDH8). In two hips peak contact pressure was found in zone I and III produced by the abnormal shape of the femoral head and acetabulum (DDH4 and DDH6). In subject DDH7 the peack contact pressure is located between zone I and II caused by an abnormal acetabulum.

Eight of ten hips had a CE angle lower than considered as normal (DDH1, DDH3, DDH4, DDH6, DDH7, DDH8, DDH9 and DDH10). DDH2 had Tönnis and Sharp angles not within the normal range, and in subject DDH5 only the sharp angle was not in the normal range.

Seven hips of ten had contact area in the range of 400mm² and 500mm². Only three hips had a contact area greater than 600mm².

Six of ten acetabula in the DDH hip joint group (DDH1, DDH2, DDH3, DDH4, DDH5 and DDH10) had negative asphericity areas in section I and IV. Similar to acetabula of the normal hip joint group.

In two of 10 femoral head, positive asphericity was located in one section. In other three femoral heads two areas of positive asphericity were found making the femoral head have an oval shape.

In addition, negative asphericity on superior regions of the acetabulum coincided with peak contact pressures on the acetabulum. On the femoral head, asphericity sections with a positive sign on superior regions coincided with high contact pressures. However, location and distribution of the contact area on the femoral head and acetabulum from the dysplastic hip joint group was different and less consistent within subjects than the normal group, this is likely due to different pelvis structures typical of each group.

Chapter 7

Conclusions

This chapter presents the main conclusions, limitations and future work of this research. The conclusions presented are based on sphericity analysis, FE analysis and quantitative analysis performed on 30 hip joint models, 10 asymptomatic hip joints .

7.1 Conclusions: Normal hip joints

- The femoral head is more “Spherical” than the acetabulum.
- The femoral head in the hip joint group is almost 100% spherical.
- In all subjects, the maximum contact pressure was found in section I.
- The location of the maximum contact pressure on the acetabulum was the same as the location of negative asphericity on the acetabulum.
- The effect of the femoral head “asphericity” was minimal because of its high percentage of sphericity.

7.2 Conclusions: Hips joints with cam-type Impingement

- The femoral head is more “Spherical” than the acetabulum.

- “Sphericity” percent average of the acetabulum and femoral head was lower than the sphericity of the acetabula and femoral head of the normal hip joint group. But the range of “Sphericity” was wider than the range of the two other groups.
- A number of hips had similar shape and “Sphericity” percentage as those found in the DDH group.
- The average of the peak contact pressure and contact area average was similar of the FAI hip joint group was similar to the average values of the normal hip joint group.
- The location of the maximum contact pressure was different within the subjects because of the “Sphericity” and anatomical morphology of each subject.
- In a few hip joints suffering from Cam-type impingement a small negative asphericity area was found in inferior/lateral posterior side of the acetabulum, on the opposite side where the abnormal growth of the femoral head is.

7.3 Conclusions: Dysplastic hip joints

- The femoral head is more “Spherical” than the acetabulum.
- “Sphericity” percent average of the acetabulum and femoral head was lower than the sphericity of the acetabula and femoral head of the normal hip joint group.
- DDH group had the lowest average contact area and the highest peak contact pressure average of the three groups.
- The location of the peak contact was different within the subjects because of the “Sphericity” and anatomical morphology of the hip joint components of each subject.

7.4 Overall

- The femoral head shape usually is very close to a sphere and it is more spherical than the acetabulum.

- Sphericity differences between the acetabulum and femoral head is related to peak contact pressures.
- Asphericity visualization showed that the most negative aspherical sections on the acetabulum were on the anterior superior and posterior inferior.
- High contact pressures were usually found on the superior anterior region of the acetabulum.
- On the acetabulum, high contact pressure areas coincide with negative asphericity in superior regions.
- On normal hip joints, positive asphericity of the femoral head coincides with high contact pressure areas in superior regions.
- On pathologic hip joints, contact area location on the femoral head was different from the acetabulum contact area location.
- The interaction of asphericity of the acetabulum and femoral head affects the articular contact.
- Asphericity visualization of the articular surfaces asphericity gives an overview of the topology of the acetabulum and femoral head.
- Dysplastic and FAI groups showed a lower sphericity percentage on the acetabulum and femoral head than the normal group.
- Visualization of the asphericity of the femoral head and acetabulum suggests that the topology of the articular surfaces is related to contact behaviour of the hip joints.

7.5 Limitations

This investigation only includes the study of contact between the acetabulum and femoral head on one-leg-standing position and its relationship with anatomical features and sphericity of the hip joint.

Despite the limitations, sphericity analysis demonstrated a relationship between the biomechanical behaviour of the hip joint, structure and sphericity of the hip joint.

7.6 Future work

The results presented have demonstrated a relationship between normal and pathologic hip joints and sphericity of the hip. Further analysis of the effect of sphericity should include more data about the patient, such as symptoms and location of the soft tissue damage. Also, sphericity analysis can be implemented as a tool to help surgeons on-pre operative procedures.

Bibliography

1. Russell, M. E., Shivanna, K. H. & Grosland, N. M. Cartilage contact pressure elevations in dysplastic hips: a chronic overload model. *J Orthop Surg Res* **1**, 6–6 (2006).
2. Anderson, A. E., Ellis, B. J. & Maas, S. A. Effects of idealized joint geometry on finite element predictions of cartilage contact stresses in the hip. *J Biomech* **43**, 1351–1357 (2010).
3. Liu, L., Ecker, T. M., Schumann, S., Siebenrock, K.-A. & Zheng, G. Evaluation of constant thickness cartilage models vs. Patient specific cartilage models for an optimized computed-assisted planning of periacetabular osteotomy. *PLOS ONE* **11**, e0146452 (2016).
4. Gu, D.-Y., Dai, K.-R., Hu, F. & Chen, Y.-z. The shape of the acetabular cartilage surface and its role in hip joint contact stress. *IEEE*, 3934–3937 (2010).
5. Sankar, W. N. & Neuberg, C. O. Femoral head sphericity in untreated developmental dislocation of the hip. *Pediatr Orthop* **30**, 558–561 (2010).
6. Gu, D., Chen, Y., Dai, K., Zhang, S. & Yuan, J. The shape of the acetabular cartilage surface: A geometric morphometric study using three-dimensional scanning. *Med Eng Phys* **30**, 1024–1031 (2007).
7. Cowin, S. & Doty, S. *Tissue Mechanics* (Springer Science+Business Media, LLC., 2007).
8. BM, N. & W., H. *Biomechanics of the musculo-skeletal system* (John Wiley and Sons, 2003).
9. Marieb, E. & Hoehn, K. *Human anatomy and physiology seventh* (Pearson Education, Inc., 2006).

10. Margareta, N. & H., F. V. *Basic Biomechanics of the Musculoskeletal System* fourth (Lippincott Williams & Wilkins, 2012).
11. Abernathy, B., Hanrahan, S., Kippers, V., Mackinnon, L. & Pandey, M. *The Biophysical Foundations Human Movement* second (Human kinetics, 2005).
12. Kent M. Van de Graaff & Fox, S. I. *Concepts of human anatomy and physiology* 5th (McGraw-Hill, 1999).
13. Palastanga, N., Field, D. & Soames, R. *Anatomy and Human movement, structure and function.* fourth (Butterworth-Heinemann, 2002).
14. Cael, C. *Functional Anatomy* (Lippincott Williams & Wilkins, 2010).
15. Drake, R., W, V. & AW, M. *Gray's anatomy for students* 2nd ed. (Churchill Livingstone, 2004).
16. Peterson, D. & Bronzino, J. *Biomechanics, principles and applications* (CRC Press, 2008).
17. Rogers, A. *Textbook of Anatomy* (Churchill Livingstone, 1992).
18. Abraham, P. H., Spratt, J. D., Loukas, M. & Hutchings, R. T. *Clinical atlas of human anatomy* (Elsevier Health Sciences UK, 2013).
19. Hamill, J., Knutzen, K. M. & Derrick, T. R. *Biomechanical basis of human movement* Fourth (Wolters Kluwer, 2015).
20. Gosling, J. A., Harris, P. F., Humpherson, J. R., Whitmore, I. & Willan, P. L. T. *Human anatomy, colour Atlas and Textbook* (Elsevier Health Sciences UK, 2008).
21. McCarthy, J. J., Scoles, P. V. & McEwen., G. D. Developmental Dysplasia of the hip (DDH). *Curr Orthop* **19**, 223–230 (2005).
22. Netter, F. H. *Atlas of the human anatomy* (Elsevier Health Sciences, 2014).
23. Saladin, K. S. *Human Anatomy* (Mc Graw Hill, 2008).
24. Inman, V. Functional aspects of the abductor muscles of the hip. *J Bone J Surg* (1947).
25. Thompson, J. *Netter's Concise Atlas of Orthopaedics Anatomy* first (Elsevier, 2002).
26. Nather, A. *Bone Grafts and Bone substitutes. Basic Science and Clinical Applications* first (World Scientific Publishing, 2005).
27. Gross, J., Fetto, J. & Rosen, E. *Musculoskeletal Examination* third (Wiley-Blackwell, 2009).

28. Gupta, H. & Zioupos, P. Fracture of bone tissue: The 'hows' and the 'whys'. *Med Eng Phys* **30**, 1209–1226 (2008).
29. Peters, C. L., Erickson, J. A. & Anderson, L. P.-C. Hip-Perseving surgery: Understanding complex pathomorphology. *J Bone J Surg* **91**, 42 (2009).
30. Phillips, A. T. M., Pankaj, P., Howie, C., Usmani, A. & Simpson, A. Finite element modelling of the pelvis: Inclusion of muscular and ligamentous boundary conditions. *Med Eng Phys* **29**, 739–748 (2007).
31. Anderson, A. E., Ellis, B. J. & Maas, S. A. Validation of Finite Element Prediction of Cartilage Contact Pressure in the Human Hip Joint. *J Biomech Eng* **130** (2008).
32. Rizzo, D. *Delmar's Fundamentals of Anatomy and Physiology* first (Thomson Learning, 2001).
33. VC, M. & R, H. *Basic orthopaedic biomechanics and mechano-bilogy* (Lippencott Williams and Wilkins, 2005).
34. Calais-Germain, B. *Anatomy of movement* first (Eastland Press, Inc., 2007).
35. Clohisy, J. C., Carlisle, J. C. & Beaulé, P. E. A systematic approach to the plain radiographic evaluation of the young adult hip. *J Bone Joint Surg* **90**, 47–66 (2008).
36. Li, B., Lu, H. & Cai, W. Computer Aided Diagnosis and Treatment Planning for Developmental Dysplasia of the Hip. *PROC SPIE* **5744**, 781–788 (2005).
37. Lee, C. B., Mata-Fink, A., Millis, M. B. & Kim, Y.-J. Demographic Differences in Adolescent-diagnosed and Adult-diagnosed Acetabular Dysplasia Compared With Infantile Developmental Dysplasia. *Pediatr Orthop* **33**, 107–111 (2013).
38. Dezateux, C. & Rosendahl, K. Developmental Dysplasia of the Hip. *The Lancet* **369**, 1541–1552 (2007).
39. Dooley, P. J. Femoroacetabular impingement syndrome: Nonarthritic hip pain in young adults. *Can Fam Physician* **54**, 42–47 (2008).
40. Ganz, R. *et al.* Femoroacetabular Impingement: A Cause for Osteoarthritis of the Hip. *Clin Orthop Relat Res* **417**, 112–120 (2003).
41. Crockarell, J. R., Trousdale, R. T. & Guyton, J. L. The anterior centre-edge angle. A cadaver study. *J Bone Joint Surg* **82**, 532–534 (2000).

42. Croft, P., Cooper, C. & Wickham, C. Osteoarthritis of the hip and acetabular dysplasia. *Ann Rheum Dis* **5744**, 781–788 (1991).
43. Sewell, M. D., Rosendahl, K. & Eastwood, D. M. Developmental dysplasia of the hip. *BMJ* **339**, 1242–1248 (2009).
44. Kyun, L. Y. & Chung, C. Y. Measuring acetabular dysplasia in plain radiographs. *Arch Orthop Trauma Surg* **131**, 1219–1226 (2011).
45. D., M. P. & Redfern, R. C. The prevalence of dislocation in developmental dysplasia of the hip in britain over the past thousand years. *J Pediatr Orthop* **27**, 890–892 (2007).
46. Loder, R. T. & Skopelja, E. N. The Epidemiology and Demographics of Hip Dysplasia. *ISRN Orthop* **2011** (2011).
47. Beck, M., Kalhor, M., Leunig, M. & Ganz, R. Hip morphology influences the pattern of damage to the acetabular cartilage. *J Bone Joint Sur* **87**, 1012–1018 (2005).
48. Sharpe, P., Mulpuri, K., Chan, A. & Cundy, P. J. Differences in risk factors between early and late diagnosed developmental dysplasia of the hip. *Arch Dis Child Fetal Neonatal Ed* **91**, F158–F162 (2005).
49. Johnsen, K., Goll, R. & Reikeras, O. Acetabular dysplasia as an aetiological factor in development of hip osteoarthritis. *Int Orthop* **33**, 653–657 (2008).
50. Atweh, L. A. & Kan, J. H. Multimodality Imaging of developmental dysplasia of the hip. *Pediatr Radiol* **43**, 166–171 (2013).
51. Fredensborg, N. The CE angle of normal hips. *Acta Orthop Scand* **47**, 403–405 (1976).
52. Engesaeter, I. O., Laborie, L. B., Lehma, T. G. & Sera, F. Radiological findings for hip dysplasia at skeletal maturity. Validation of digital and manual measurements techniques. *Skeletal Radiol* **41**, 775–785 (2012).
53. Schofer, M. D., Pressel, T. & Heyse, T. J. Radiological determination of the anatomic hip centre from pelvic landmarks. *Acta Orthop Belg* **76**, 479–485 (2010).
54. Chosa, E., Tajima, N. & Nagatsuru, Y. Evaluation of acetabular coverage of the femoral head with anteroposterior and false profile radiographs of hip joint. *J Orthop Sci* **2**, 378–390 (1997).
55. Gold, S. L., Burgue, A. J. & Potter, H. G. MRI of cartilage: Joint Morphology, strycture and composition. *Clin Orthop Relat Res* **470**, 3321–3331 (2012).

56. Turgeon, T. R., Phillips, W. & Kantor, S. R. The role of acetabular and femoral osteotomies in reconstructive surgery of the hip. *Clin Orthop Relat Res* **441**, 188–199 (2005).
57. Jaber, F. M. & Parvizi, J. Hip pain in young adults: Femoroacetabular Impingement. *J Arthroplasty* **22**, 37–42 (2007).
58. Ganz, R., Leunig, M., Leunig-Ganz, K. & Harris, W. H. The Etiology of Osteoarthritis of the Hip. *Clin Orthop Relat Res* **466**, 264–272 (2008).
59. Ito, K., Leunig, M. & Ganz, R. Histopathologic Features of the Acetabular Labrum in Femoroacetabular Impingement. *Clin Orthop Relat Res* **429**, 262–271 (2004).
60. Kassarian, A., Brisson, M. & Palmer, W. E. Femoroacetabular Impingement. *Eur J Radiol* **63**, 29–35 (2007).
61. Mardones, R., Barrientos, V., Nemptala, F., Tomic, A. & Salineros, M. Femoroacetabular impingement as a cause of inguinal pain. *Rev Med Chile* **138**, 102–108 (2010).
62. Leunig, M., Robertson, W. J. & Ganz, R. Femoroacetabular Impingement: Diagnosis and Management, Including Open Surgical Technique. *Oper Tech Sports Med* **15**, 178–188 (2007).
63. Leunig, M., Beck, M., Dora, C. & Ganz, R. Femoroacetabular Impingement: Etiology and surgical concept. *Oper Tech Orthop* **15**, 247–255 (2005).
64. Philippon, M., Schenker, M. & Kuppersmith, K. B. D. Femoroacetabular impingement in 45 professional athletes: associated pathologies and return to sport following arthroscopic decompression. *Knee Surg Sports Traumatol Arthroscopy* **15**, 908–914 (2007).
65. Fadul, D. A. & Carrino, J. A. Imaging of Femoroacetabular Impingement. *J Bone Joint Surg* **91**, 138 (2009).
66. Chegini, S., Beck, M. & Ferguson, S. J. The Effects of Impingement and Dysplasia on Stress Distributions in the Hip Joint during Sitting and Walking: A Finite Element Analysis. *J Orthop Res* **27**, 195–201 (2007).
67. Pauwels, F. Der Schenkelhalsbruch: ein mechanisches Problem. *BJS* **23**, 874–874 (1936).

68. Tannast, M., Siebenrock, K. A. & Anderson, S. E. Femoroacetabular Impingement Radiographic Diagnosis - What the radiologist should know. *AJR Am J Roentgenol* **188**, 1540–1552 (2006).
69. Tannast, M., D. Goricki, M. B., Murphy, S. & Siebenrock, K. A. Hip damage occurs at the zone of femoroacetabular impingement. *Clin Orthop Relat Res* **466**, 273–280 (2008).
70. Konan, S., Rayan, F., Meermans, G., Witt, J. & Haddad, F. S. Validation of the classification system for acetabular chondral lesions identified at arthroscopy in patients with femoroacetabular impingement. *J bone Joint Surg* **93**, 332–336 (2010).
71. Wisniewski, S. J. & Grogg, B. Femoroacetabular Impingement. An overlooked cause of hip pain. *Am J Phys Med Rehabil* **85**, 546–549 (2006).
72. Skinner, H. & P., M. *Current diagnosis and treatment in orthopaedics* second (Mc Graw-Hill Companies, Inc., 2006).
73. Sink, E. L., Gralla, J., Ryba, A. & Dayton, M. Clinical presentation of femoroacetabular impingement in Adolescents. *J Pediatr Orthop* **28**, 806–811 (2008).
74. Philippon, M. J., Maxwell, R. B., Johnston, T. L. & Schenker, M. Clinical presentation of femoroacetabular impingement. *Knee Surg Sports Traumatol Arthrosc* **15**, 1041–1047 (2007).
75. Barton, C., Matias, J. S., Kawan, S. R. & Paul, E. B. Validity of the Alpha Angle Measurement on Plain Radiographs in the Evaluation of Cam-type Femoroacetabular Impingement. *Clin Orthop Relat Res* **469**, 464–469 (2010).
76. Laborie, L., Lehmann, T., Engesaeter, I. & Rosendahl, K. Prevalence of Radiographic Findings Thought to Be Associated with Femoroacetabular Impingement in a Population-based Cohort of 2081 Healthy Young Adults. *Musculoskeletal Imaging* **260**, 494–502 (2011).
77. Laborie, L., Lehman, T. & Engaeseter, I. The alpha angle in cam-type femoroacetabular impingement. *J Bone Joint Surg* **96-B**, 449–454 (2013).
78. Dudda, M., Albers, C., Mamisch, T. C., Werlen, S. & Beck, M. Do Normal Radiographs Exclude Asphericity of the Femoral Head-Neck Junction? *Clin Orthop Relat Res* **467**, 651–659 (2009).

79. Pogliacomi, F., Stark, A. & Wallensten, R. Periacetabular osteotomy: Good pain relief in symptomatic hip dysplasia, 32 patients followed for 4 years. *Acta Orthop* **76**, 67–74 (2005).
80. Wyss, T. F., Clark, J. M. & Weishaupt, D. Correlation between internal rotation and bony anatomy in the hip. *Clin Orthop Relat Res* **460**, 152–158 (2007).
81. Li, B. *et al.* Computer aided diagnosis and treatment planning for developmental dysplasia of the hip. *SPIE* **5744**, 781–788 (2005).
82. Beaulé, P. E., Zaragoza, E. & Motamedi, K. Three-dimensional computed tomography of the hip in the assessment of femoroacetabular impingement. *J Orthop Res* **23**, 1286–1292 (2005).
83. Armiger, R. S., Arman, M. & Lepisto, J. Evaluation of a computerized measurement technique for joint alignment before and during periacetabular osteotomy. *Comput Aided Surg* **12**, 215–224 (2007).
84. Chen, H.-Y., Xin, L. & Hong-Bing, L. Application of Segmentation and Measurement in the Treatment of Developmental Dysplasia of the Hip. *IEEE*, 989–991 (2007).
85. Tan, S., Yao, J., Yao, L., Summers, R. M. & Ward, M. M. Acetabular rim and surface segmentation for hip surgery planning and dysplasia evaluation. *Proc SPIE* **6918**, (2008).
86. Simpleware. Reference Guide. ScanIP, +ScanFE, +ScanCAD. *Version 3.2* (2010).
87. Li, W., Abram, F. & Beaudoin, G. Human hip joint cartilage: MRI quantitative thickness and volume measurements discriminating acetabulum and femoral head. *IEEE* **55**, 2731–2740 (2008).
88. Bergmann, G., Deuretzbacher, G., Heller, M. & Graichen, F. Hip contact forces and gait patterns from routine activities. *J Biomech* **34(1)**, 859–871 (2001).
89. Merkhara, Y., S., S. & I., E. A rational human joint friction test using a human cartilage-on-cartilage arrangement. *Tribol Lett* **22**, 29–36 (2006).
90. Umbach, D. & Jones, K. N. A few methods for fitting circles to data. *IEEE* **56**, 1881–1885 (2003).
91. Fuji, M., Nakashima, Y., Jinguishi, S. & Yamamoto, T. Intraarticular findings in symptomatic developmental dysplasia of the hip. *J Pediatr Orthop* **29**, 9–13 (2009).